Notch3 Signaling Promotes Adhesion and Tumor Progression in a Murine Epithelial Ovarian Cancer Model

Jessica C. Price

Submitted in partial fulfillment of the

requirements for the degree of

Doctor of Philosophy

under the Executive Committee

of the Graduate School of Arts and Sciences

COLUMBIA UNIVERSITY

2017

ABSTRACT

Notch3 Signaling Promotes Adhesion and Tumor Progression in a Murine Epithelial Ovarian Cancer Model

Jessica C. Price

Ovarian cancer is the 5th leading cause of cancer death in women in the United States and is the most fatal gynecological malignancy. High grade serous ovarian cancer (HGSC) is the most common and deadly type of ovarian cancer largely due to the rapid metastasis throughout the peritoneum (abdominal cavity wall and organ lining). Metastatic spread of ovarian cancer usually occurs before diagnosis and can lead to bowel obstruction, organ failure, ascites, cachexia, infection and sepsis, and pulmonary embolism all causing death. Current methods to detect early stage ovarian cancer do not increase overall survival. A better understanding of the metastatic ability of ovarian cancers and the mechanism of cancer cell dissemination are critical to the development of new treatments for this devastating disease. In particular, investigation of pathways that affect early metastasis may indicate treatments that will lower disease burden and may suggest biomarkers of recurrent and/or chemotherapy resistant disease.

Notch3 expression correlates with worse prognosis, chemotherapy resistance, and increased tumorigenic cell behaviors in HGSC. Here, we demonstrate that Notch3 acts to promote early stages of metastasis in a model of HGSC using the murine ID8 IP2 ovarian surface epithelial cell line. ID8 IP2 cells have little to no endogenous Notch3 expression and model metastatic disease when introduced intraperitoneally. We investigated the role of Notch3 by ectopically expressing the intracellular domain of murine Notch3 to induce constitutive Notch3 signaling in ID8 IP2 cells and verified Notch signal activation by target gene assessment. Induction of Notch3 signaling in ID8 IP2 reduced survival and accelerated disease burden, as measured by ascites accumulation, after intraperitoneal introduction of cells into nude mice. We interrogated downstream targets in Notch3 activated cells by RNA-Seq and found that Notch3 induced a significant enrichment of adhesion and extracellular matrix pathways. Notch3 active cells showed increased ITGA1 expression and increased adhesion on collagens I and IV *in vitro*, suggesting that increased adhesion to collagen-rich peritoneal surfaces drives the observed increase in tumor burden. Notch3 active cells showed reduced migration on surfaces coated with multiple types of extracellular matrix

and no detectable increase in invasion through extracellular matrix, indicating that Notch3 effects may be specific to the initial adhesion of tumor cells and not the later stages of metastasis.

These results demonstrate that Notch3 upregulates the expression of specific adhesion genes in ovarian cancer cells and this promotes increased attachment to the collagen-rich extracellular matrix. The implications of this study are that oncogenic Notch signal activation, as documented in human disease, may promote dissemination and metastasis of primary and/or recurrent HGSC by increasing attachment to the peritoneal lining.

TABLE OF CONTENTS

LIST OF FIGURES AND TABLES

ACKNOWLEDGEMENTS

I would like to thank my thesis advisor Dr. Jan Kitajewski for inviting me into his lab and providing me the opportunity to complete this investigation and train as a scientist. I appreciate the opportunity and know that through this experience I have developed into a better and more independent investigator.

I am grateful to my thesis committee for their direction and advice over the past few years, and for helping me achieve success in my project. Thank you to all the members of my committee, Dr. Darrell Yamashiro, Dr. Peter Canoll, Dr. Swarnali Acharyya, and Dr. Jason Wright. I have truly benefitted from all your knowledge, guidance, and support. Thank you, Dr. Yamashiro, for being my chair, and counseling me during my training. I am also grateful to Dr. Lora Hedrick-Ellenson for giving her time and effort to participate in my defense.

I am indebted to Dr. Elham Azizi for working on this project with me by completing all of the RNA-Seq data analysis in this work and for helping me to understand it. I really value all the time and effort she put into this project, and am grateful for many answered questions along the way. Her kindness and understanding was appreciated, and I could not have done this work without her.

I would also like to thank Dr. Jill Slack-Davis for graciously providing us with the ID8 IP2 cell line with which I completed these experiments.

I would like to recognize my colleagues from the Kitajewski laboratory for all their advice, assistance, and commiseration. I would like to acknowledge Dr. Naiche Adler for her mentorship and for advising me on writing this work. I would also like to give a special thank you to James Herts for communicating my data to me so I could finish writing this thesis while far away from the laboratory. Thank you to Valeria Borisenko for her kindness and support, and helping me start to learn mouse work.

I appreciate both of my programs for allowing me to be a student at Columbia and complete my work. Thank you to the Columbia University MD/PhD Program, and the Integrated Program in Cellular Molecular and Biomedical Studies. A special thank you to Jeffrey Brandt and Zaia Sivo for their friendship and helping me along the way.

I would like to acknowledge the financial support I have received from the National Institutes of Health National Cancer Institute award F31 CA19289.

I would also like to give a warm and special thanks to my first P.I. and still mentor Dr. Daphne Bell. She introduced me to my love and esteem of research and I would not have become a scientist without her. She is a wonderful mentor to me and has continued to advise me through my thesis journey even though I am no longer in her laboratory, and I will always be beholden to her.

Lastly, but most of all, I would like to thank my family, extended family, and friends. I could not have finished without them and their constant love and support. I owe them all for listening to me, and encouraging me to keep moving forward through this process. Their support is never ending and I appreciate all of them being there through my failures and accomplishments. I could not have survived without them. I would like to thank Lisa, Amina, Rima, Rosa, and Steph for all their love. Thank you to Sonya. I would not have even attempted research, applied to this program, or believed I could do any of this without her. Thank you to my Dad for always being proud and supportive of me. And most importantly, thank you to my mother. Words cannot express my gratefulness for all the sacrifices she has made to get me to where I am today. She has been my comfort in difficult times, and her love, support, compassion, and faith in me has kept me going. I attribute any success I have achieved to her.

CHAPTER 1

INTRODUCTION

Ovarian Cancer

Ovarian cancer is the deadliest gynecologic malignancy. It is expected that in 2017 ovarian cancer will be the 5th leading cause of cancer death in women in the United States, with an estimated 22,400 new cases and 14,080 deaths in the current year (Siegel et al., 2017). Worldwide, ovarian cancer is the 8th leading cause of death in women, with an estimated 238,700 new cases and 151,900 deaths each year (Torre et al., 2015).

The most common subtype of ovarian cancer is high grade serous ovarian cancer (HGSC), described in detail later in this introduction. Standard treatment for HGSC includes surgical cytoreduction (removal of macroscopic tumors) and combination chemotherapy with platinum (a DNA damaging agent) and taxane (a microtubule inhibitor) (Matulonis et al., 2016, Bowtell et al., 2015). HGSC recurs in over 80% of cases that were initially disseminated beyond the pelvis and 20-30% of HGSC cases will recur in less than 6 months (Matulonis et al., 2016, Berns and Bowtell, 2012). Recurrent tumors are also chemotherapy resistant in 80-90% of cases (Bowtell et al., 2015). Once disease recurs there is no standard therapy, although many other treatments and therapy combinations have been attempted (Matulonis et al., 2016). For example, chemotherapy drugs other than platinum and taxane agents, angiogenesis inhibitors, PARP inhibitors, and immunotherapy have been tested, but few treatments increase overall survival (Matulonis et al., 2016). Treatment is similar for other subtypes of ovarian cancer; however, other subtypes are more likely to be detected while still confined to the pelvis and treatments may include the use of other chemotherapeutics, or therapy based on tumor specific genetic alterations (Cont et al., 2015). Because of the potential for earlier stage of diagnosis, survival can be much higher for the other, less common, subtypes of epithelial ovarian cancer (Cont et al., 2015).

Ovarian cancer is so deadly because it is often detected after metastasis throughout the peritoneum, and because it is likely to become resistant to chemotherapy and recur. Approximately 70-75% of cancers are discovered after dissemination of disease (Naora and Montell, 2005, Barbolina et al., 2009). Ovarian cancers are often initially diagnosed in late stages of development due to rapid dissemination of

tumors and the fact that most patients experience no symptoms, or non-specific symptoms such as fatigue and gastrointestinal discomfort (Matulonis et al., 2016). When detected at late stages, the 5-year survival rate is only 25%-30% (Matulonis et al., 2016, Cho and Shih Ie, 2009).

Unfortunately, early detection measures such as transvaginal ultrasound and screening for CA-125, a tumor marker in blood serum, have not shown any effect on mortality rates (Matulonis et al., 2016, Cho and Shih Ie, 2009, Fathalla, 2013). It has been suggested that, because of the rapid dissemination exhibited by ovarian cancers, focus should be on detecting and treating low volume disease, when tumors are still less than 1cm and relatively sparse, and early detection of recurrence (Cho and Shih Ie, 2009, Kurman et al., 2008).

HGSC metastasizes by forming direct extensions to adjacent organs and by transport of exfoliated cells in the peritoneal fluid to new sites on the peritoneal lining (Barbolina et al., 2009, Naora and Montell, 2005). Non-adherent tumor cells are vulnerable to anoikis, or apoptosis triggered by detachment from extracellular matrix, but survive transport via supportive signals from the surrounding peritoneal fluid or by forming spheroids where adjacent cells can signal through adhesion molecules (Naora and Montell, 2005). Metastases form when tumor cells adhere to new sites on the peritoneal lining, which consists of a single layer of mesothelial cells over collagen-rich extracellular matrix and other stroma (Barbolina et al., 2009). Ovarian cancer is thought to preferentially attach to sites where the mesothelial layer is disrupted and extracellular matrix is exposed (Sodek et al., 2012). Once tumor cells adhere, they further reduce the integrity of the peritoneal mesothelial layer via interaction with the surrounding matrix and stroma that trigger mesothelial contraction, metalloprotease expression, and other signaling through cytokines and growth factors which leads to increased invasion, motility, and further growth of metastases (Barbolina et al., 2009, Rosen et al., 2009).

Ovarian cancers often cause dramatic increases in the amount of peritoneal fluid, called ascites, which can result from tumor cell blockage of lymph nodes and/or an increase in vascular leakage in the tumors or adjacent tissues of the peritoneum (Naora and Montell, 2005, Barbolina et al., 2009). Ascites accumulation can increase the normal peritoneal fluid volume (less than 20mL) to volumes often over 500mL, and can exceed 2L (Barbolina et al., 2009). Ascites accumulation is correlated with worse prognosis (Barbolina et al., 2009, Puls et al., 1996), possibly because ascites can contain many molecules that

support tumor growth and dissemination, including growth factors, extracellular matrix, proteolytic enzymes, and inflammatory signals (Barbolina et al., 2009).

Most ovarian cancers are epithelial in origin (Matulonis et al., 2016). Non-epithelial ovarian cancers, which generally derive from germ cells or sex cord stromal cells, comprise about 10-15% of ovarian cancers and will not be discussed in detail here (Boussios et al., 2016).

Epithelial ovarian cancer encompasses tumors from several tissues of origin with similar clinical presentation and reproductive tract derivation; it is a collection of diseases that are histologically and molecularly distinct, but share the ability to disseminate in the pelvis (Vaughan et al., 2011, Matulonis et al., 2016). There are 4 histological subtypes of epithelial ovarian cancer: serous, endometrioid, clear cell, and mucinous (Berns and Bowtell, 2012, Cho and Shih Ie, 2009). Some of these are further categorized by high and low grade, describing the extent of differentiation (Cho and Shih Ie, 2009). Based on histological subtype and grade, epithelial ovarian tumors are separated into two groups, Types I and II (Shih Ie and Kurman, 2004). Type I and Type II tumors are molecularly distinct, showing activation or loss of different genes and pathways (Shih Ie and Kurman, 2004). For example, Type I tumors are more likely to have alterations in genes and pathways like *KRAS*, *BRAF*, and *ARID1A*, while Type II tumors are likely to have alterations in *TP53, BRCA1/2*, and *CCNE1* (Nik et al., 2014, Berns and Bowtell, 2012). Type I tumors are low grade, have lower malignant potential, and are more likely to initially be platinum insensitive because their lack of alteration in DNA damage repair pathways; Type I tumors, however, respond better to treatment because these tumors are more likely to be detected at low stage, giving patients with these tumors higher survival rates (Bowtell, 2010, Cont et al., 2015). Type I tumors usually include low grade serous, low grade endometrioid, clear cell, and mucinous subtypes (Cho and Shih Ie, 2009, Nik et al., 2014). Type II tumors are more likely to be aggressive and arise rapidly (Bowtell, 2010, Cho and Shih Ie, 2009, Nik et al., 2014). Type II tumors are generally high grade serous, high grade endometrioid, clear cell, or undifferentiated/ mixed mesodermal tumors (Cho and Shih Ie, 2009). HGSC is the most common subtype, comprising ~75% of all ovarian cancers, and this subtype will be the focus of our experiments and discussion (Nik et al., 2014).

HGSC is characterized by a specific molecular signature. Almost all HGSC have TP53 loss or mutation and approximately half present with alterations in homologous recombination repair genes

(Bowtell et al., 2015, Cancer Genome Atlas Research, 2011, Ahmed et al., 2010). These alterations in tumor suppressors that affect DNA repair can lead to copy number changes in other genes that increase the progression of HGSC (Bowtell, 2010). Histologically, HGSC display atypical nuclei with high numbers of mitoses and papillary or solid growth with slit-like spaces (Cho and Shih Ie, 2009).

Originally it was believed that all ovarian cancers derive from the ovarian surface epithelium (OSE), or ovarian cysts lined with OSE (Nik et al., 2014). However, it is currently believed that ovarian cancers can derive from several sources. For example, mucinous cancers are believed to originate from the gastrointestinal tract or endocervix, while endometrioid and clear cell tumors may derive from endometriosis (Wiegand et al., 2010, Fukunaga et al., 1997, Cho and Shih Ie, 2009, Tenti et al., 1992). The tissue of origin of HGSC is currently under debate, and HGSC has been suggested to derive from either the ovary, the fallopian tube/oviduct, or from endosalpingiosis, which is ectopic tissue outside the reproductive tract that resembles the fallopian epithelium (Nik et al., 2014).

The historical assumption of an OSE origin of HGSC was based on observations such as correlation of incidence with ovulation, presence of tumors in the ovary, and presence of malignant tumors with benign ovarian cysts, indicating this may be their origin (Fathalla, 2013, Fathalla, 1971, Finn and Javert, 1949, Dubeau, 2008, Dubeau and Drapkin, 2013). OSE cells express both epithelial and mesenchymal markers and characteristics, suggesting a level of plasticity amenable to the development of cancer (Naora and Montell, 2005, Barbolina et al., 2009). Ovulation and inflammation associated with ovulation are linked to development of ovarian cancer, indicating a critical role for the ovary; however, some data suggests that fallopian epithelium becomes trapped in the ovary and ovarian cysts during ovulation and later becomes tumorigenic in the inflammatory- and hormone-rich environment of the ovary (Rosen et al., 2009, Fathalla, 2013, Dubeau and Drapkin, 2013).

More recent data suggests a fallopian origin of HGSC. Tumors are thought to arise from fallopian secretory cells, which are unable to repair double strand breaks and thus are particularly susceptible to DNA damage and tumorigenic progression (Bowtell, 2010). Primary serous lesions (known as serous tubal intraepithelial carcinoma, or STIC) are often found in the fallopian epithelium, but not ovarian epithelium, of BRCA1/2 positive patients undergoing prophylactic removal of the ovaries and fallopian tube (salpingo-oophorectomy), suggesting that fallopian lesions may be the primary origin of HGSC in some women (Piek

et al., 2001, Nik et al., 2014). Müllerian-specific Hox genes and Pax8 are expressed or overexpressed in some HGSC, suggesting genesis from Müllerian-derived tissue such as the fallopian tube and not the ovary (Cheng et al., 2005, Bowtell et al., 2015, Cheung et al., 2011, Laury et al., 2011). However, OSE may upregulate Müllerian markers during tumorigenic progression (Dubeau and Drapkin, 2013, Resta et al., 1993).

Contradicting both of these theories, some women who undergo prophylactic salpingo-oophorectomy still develop HGSC, indicating that at least some HGSC originate from non-fallopian epithelium (Dubeau and Drapkin, 2013, Dubeau, 2008). This has led to yet a third hypothetical tissue of origin: endosalpingiosis, which is ectopic fallopian epithelium from developmental remnants or retrograde sloughing/menstruation (Kurman et al., 2011, Dubeau and Drapkin, 2013). Furthermore, some ovarian cancers are histologically mixed, and fallopian epithelium only gives rise to serous cancers (Dubeau and Drapkin, 2013).

Given the substantial uncertainty in the literature, for the purposes of this thesis we will consider HGSC as one disease that may originate in any of these manners, but which are unified by their ability to develop disseminated disease with ascites accumulation, HGSC histology, and a HGSC molecular signature (Dubeau, 2008).

The Notch signaling pathway

The first known mutation of a Notch gene was discovered in *Drosophila melanogaster* almost a century ago and the gene was named for its resulting phenotype, abnormal notches in the border of the fly wing (Mohr, 1919). Since then, much has been discovered about the mechanisms of the Notch signaling pathway and the roles of Notch genes in directing development and disease progression.

In mammals, Notch signaling occurs via four Notch genes, Notch1, Notch2, Notch3, and Notch4, which act as receptors, and five ligands Delta-like1 (Dll1), Dll3, Dll4, Jagged1, and Jagged2 (Borggrefe and Oswald, 2009, Hori et al., 2013, Radtke et al., 2005). The Notch genes and their ligands are single pass transmembrane proteins (Capaccione and Pine, 2013, Mumm and Kopan, 2000). The Notch proteins generally consist of an extracellular domain (N-terminus) containing a varying number of EGF-like repeats and an intracellular domain containing a RBPjκ association module (RAM) domain, two nuclear localization sequences (NLS), six Ankyrin repeats (ANK), a transactivation domain (TAD), and a proline, glutamate,

serine, threonine rich (PEST) domain at the C-terminus (Capaccione and Pine, 2013, Kopan and Ilagan, 2009, Ehebauer et al., 2005). After translation, Notch is processed in the Golgi apparatus by a furin-convertase cleavage at site 1 (S1) and the two peptides then form a heterodimer held together by a calcium-coordinated non-covalent bond (Mumm and Kopan, 2000, Capaccione and Pine, 2013, Hori et al., 2013). Notch can be further processed by glycosylation, glucosylation, or fucosylation and shuttled to the cell membrane (Hori et al., 2013, Mumm and Kopan, 2000). Notch ligands also consist of an extracellular domain of EGF-like repeats and contain a DSL (Delta/Serrate/LAG-2) domain necessary for Notch interaction, but ligands have only a small intracellular domain with no TAD and do not undergo S1 cleavage (Kangsamaksin et al., 2015, Hori et al., 2013).

Canonical Notch signaling activation requires direct contact between Notch and a ligand expressed in neighboring cells (Capaccione and Pine, 2013). Notch then undergoes a conformational change that allows for a second cleavage event at S2 by an ADAM/TACE (tumor necrosis factor α converting enzyme, part of the A Disintegrin And Metalloproteinase family) protein (Capaccione and Pine, 2013, Mumm and Kopan, 2000). This is immediately followed by cleavage at site S3 by a γ-secretase complex containing a presenilin catalytic domain (Capaccione and Pine, 2013, Mumm and Kopan, 2000, Bellavia et al., 2008, Borggrefe and Oswald, 2009). The S3 cleavage occurs at the intracellular border of the transmembrane domain and releases the Notch intracellular domain from the membrane, which then translocates to the nucleus to effect gene expression. Nuclear localized Notch intracellular domain binds the CSL (CBF-1/RBP-Jκ, Suppressor of hairless, and Lag-1) transcriptional repressor complex and causes a conformational change that allows CSL to release its co-repressors, and instead bind Mastermind-like (MAML) and other co-activator proteins to form a transcriptional activator complex (Capaccione and Pine, 2013, Bellavia et al., 2008, Borggrefe and Oswald, 2009) (Figure 1.1). Thus, when freed from the membrane, the Notch intracellular domain converts repressor complexes to activator complexes and induces downstream target gene expression. Some well-established canonical targets induced directly by Notch signaling include HES (human hairy and enhancer of split) genes, HEY (hairy/enhancer of split related with YRPW motif) genes, and NRARP (Notch regulated Ankyrin repeat protein) (Capaccione and Pine, 2013).

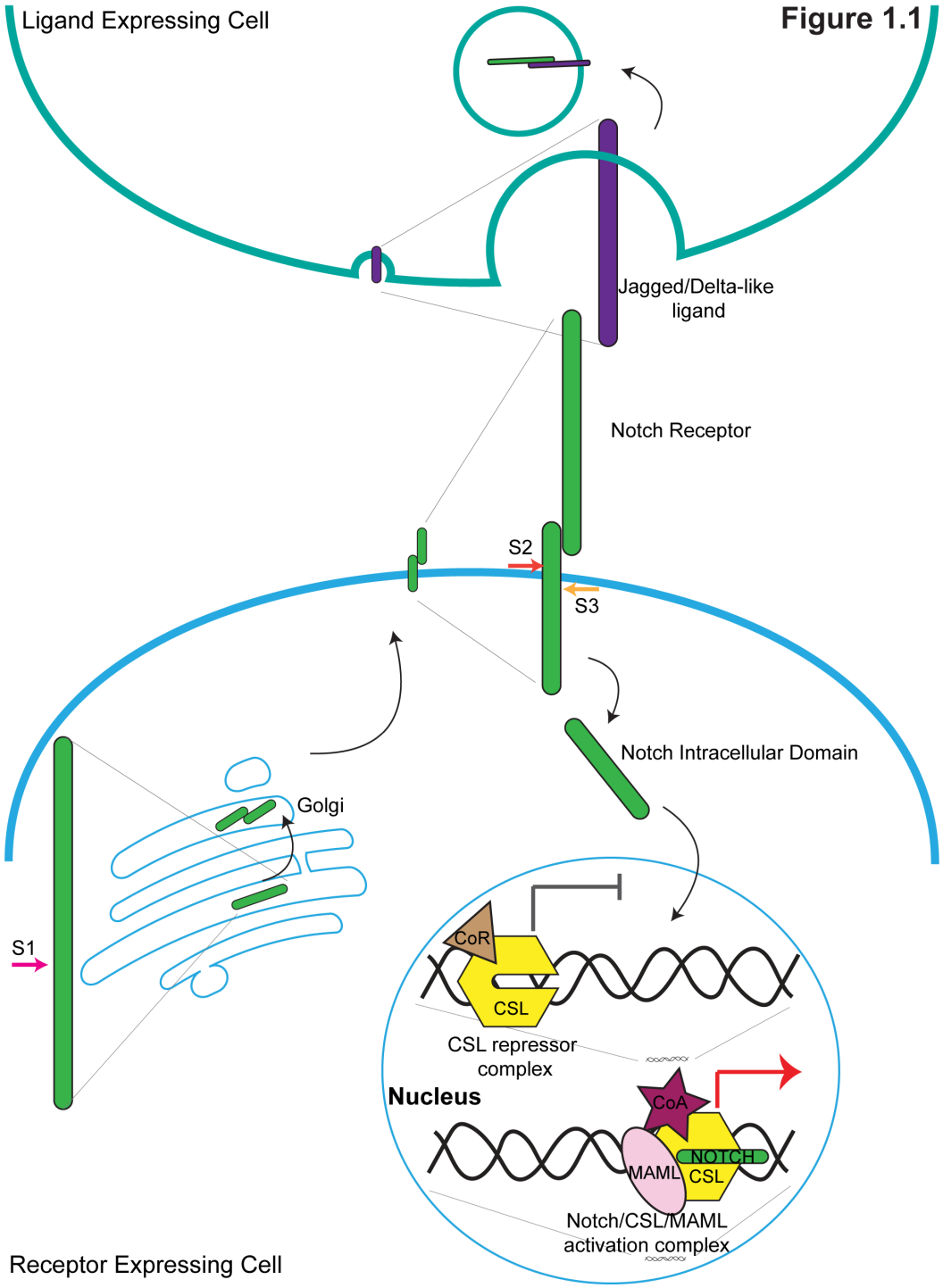

Figure1.1 Canonical Notch receptor signaling leads to the activation of gene transcription. This figure illustrates the Notch signaling pathway. Notch goes through 3 cleavage events, the first to create a heterodimer which becomes localized to the cell membrane. Subsequent cleavage events are triggered by ligand binding, which causes a conformational change to expose the S2 cleavage site for ADAM/TACE. S3 cleavage is completed by γ-secretase, releasing the Notch intracellular domain to translocate to the nucleus. Once in the nucleus, the intracellular domain of Notch converts the CSL transcriptional repressor complex into a transcriptional activator complex which initiates transcriptional activation.

Notch signaling is modulated by multiple negative regulatory mechanisms. Notch signaling is downregulated by E3 ubiquitin ligases such as FBXW7 that direct Notch receptor degradation, endocytosis and endosomes that regulate Notch presence on the cell surface, and the C-terminal PEST domain that regulates protein stability and degradation (Mumm and Kopan, 2000, Bellavia et al., 2008, Hori et al., 2013). Notch interactions with ligands expressed on the same cell, rather than neighboring cells, often results in inhibition of Notch signaling (Hori et al., 2013). Canonical Notch pathway targets, such as NRARP, are involved in negative regulation of Notch signaling (Borggrefe and Oswald, 2009). Conversely, Notch signaling can be either enhanced or suppressed by addition of various post-translational side chains by the Fringe family and other glucosyltransferases (Kopan and Ilagan, 2009).

Notch proteins can also engage in non-canonical signaling, which is independent of CSL complex activation or DSL domain containing ligands (Mumm and Kopan, 2000, Hori et al., 2013, Ayaz and Osborne, 2014). Non-canonical signaling is not restricted to the nucleus, and often occurs in the cytoplasm; it can even occur in the mitochondrial or cell membrane (Andersen et al., 2012, Ayaz and Osborne, 2014). Notch can act through modulation of kinase signaling (Mumm and Kopan, 2000, Ayaz and Osborne, 2014). Notch has been shown to affect NF-κB, PI3K/AKT/mTOR, Wnt/β-catenin, and HIF1α signaling pathways independent of CSL in immune cells and particular cancers (Ayaz and Osborne, 2014, Andersen et al., 2012).

Notch genes were first identified as being critical in embryonic development, in particular for the differentiation of cell types. Notch signaling often determines the cell fate of adjacent cells, and is best known for its ability to mediate either lateral inhibition or lateral induction of cell types (Mumm and Kopan, 2000, Hori et al., 2013, Borggrefe and Oswald, 2009). More recently, Notch signaling has been shown to be a causative or contributing factor for the development of many cancers. Notch receptors were first shown to be oncogenic in T-cell acute lymphoblastic leukemia (Capaccione and Pine, 2013). Since then, Notch and members of the Notch pathway have been shown to be oncogenic in acute myelogenous leukemia, non-small cell lung carcinoma, colorectal cancer, pancreatic cancer, melanoma, breast tumors, and others (Ntziachristos et al., 2014, Capaccione and Pine, 2013). Notch signaling can maintain cancer stem cells, induce proliferation, assist epithelial to mesenchymal transition, increase cancer cell motility, increase tumor angiogenesis, resist apoptosis and anoikis, and confer chemotherapy resistance (Capaccione and Pine,

2013, Takebe et al., 2014, Radtke and Raj, 2003, Ayaz and Osborne, 2014). Notch often works with other dysregulated pathways within the cell, such as RAS, to enhance tumorigenesis (Radtke and Raj, 2003). Conversely, Notch signaling has also been implicated as a tumor suppressive, particularly in certain squamous cell carcinomas where Notch is thought to drive terminal differentiation and therefore exit from the cell cycle (Nowell and Radtke, 2017, Ntziachristos et al., 2014, Radtke and Raj, 2003). Notch signaling can contribute to cancer development both through canonical and non-canonical signaling methods (Ayaz and Osborne, 2014).

Our focus for this thesis will be on Notch3. Compared to Notch1 and Notch2, Notch3 has fewer EGF-like repeats in its extracellular domain (34 as opposed to 36) and a shortened C-terminal intracellular domain, which may result in differences in activation of downstream signaling (Lardelli et al., 1994, Bellavia et al., 2008). For example, the change in the TAD may lead to a preference for NOTCH3 to CSL binding sites near zinc finger promoters (Ong et al., 2006). Notch3 can undergo different conformational changes than other Notch receptors and also differentially recruits co-activators (Bellavia et al., 2008). Notch3 appears to share many of the canonical transcriptional targets as other Notch genes, but shows different preferences for strongest induction (Beatus et al., 1999, Shimizu et al., 2002). For example, Hes1 is strongly upregulated by Notch1, but not Notch3 (Beatus et al., 1999, Beatus et al., 2001). Notch3 in particular has been implicated in cancers such as non-small cell lung carcinoma, breast cancer, T-cell leukemia, and ovarian cancer (Capaccione and Pine, 2013, Bellavia et al., 2008, Ayaz and Osborne, 2014, Ntziachristos et al., 2014). In cancer, it has also been shown that Notch3 has a preference for interaction with Jagged ligands (Bellavia et al., 2008, Choi et al., 2008, Chen et al., 2010, Steg et al., 2011, Hu et al., 2014).

The role of Notch3 signaling in high grade serous ovarian cancer

Ovarian cancer is correlated with high levels of Notch3 signaling in ovarian tumors, specifically in HGSC cases and derived cell lines. Unbiased screening of almost 500 HGSC tumors (Cancer Genome Atlas Research, 2011) demonstrated that the Notch3 pathway was altered in 22% of HGSC samples assessed. Most of these alterations are predicted to activate signaling, including copy number amplification, predicted activating mutations, and upregulation of mRNA expression compared to diploid tumors. The most frequent alterations of the Notch pathway were in *NOTCH3* itself, but other parts of the Notch pathway were altered at lower frequency, including the *JAGGED1 and JAGGED2* ligand genes and Notch activation

complex genes *MAML1,MAML2, MAML3*, and *RBPJκ* (*CSL*) (Cancer Genome Atlas Research, 2011). Re-analysis of a modified version of the TCGA dataset including additional tumors showed that over half of HGSC samples also harbor deletions of *WWP2*, which targets NOTCH3 (but no other Notch genes) for endocytosis and degradation, and these *WWP2* mutations correlate with increased Notch3 expression (Jung et al., 2014).

Additional studies have confirmed that mutations predicted to increase Notch3 signaling occur at high frequency in serous ovarian cancers. *NOTCH3* was found to have an increase in copy number in serous ovarian cancer in several independent studies, and the increased copy number correlated with higher levels of NOTCH3 protein (Lu et al., 2004, Nakayama et al., 2007, Park et al., 2006b, Shih Ie et al., 2011). *NOTCH3* transcripts were elevated in high grade serous cancers when compared with benign tumor levels, and NOTCH3 protein levels are upregulated in ovarian cancer patient samples (Jung et al., 2010, Liu et al., 2016, Park et al., 2010). Increases in NOTCH3 protein correlated with worse prognosis; patients with high levels of NOTCH3 showed shorter overall survival, higher grade and stage tumors, increased ascites accumulation, and increased recurrence (Jung et al., 2010, Liu et al., 2016, Park et al., 2010). Reanalysis of the original TCGA data determined that patients with *NOTCH3* alterations demonstrated poorer overall survival as well (Hu et al., 2014).

Jagged1 is the major Notch ligand found in HGSC. At the RNA level, Jagged1 is the most highly expressed Notch ligand in HGSC derived cell lines when compared to non-tumorigenic ovarian surface epithelial cell lines (Choi et al., 2008). NOTCH3 expressing tumors show high levels of JAGGED1 protein expression (Choi et al., 2008). JAGGED1 expression correlates with expression of NOTCH3 in HGSC, and endocytosis associated with Jagged1 can activate Notch3 signaling in an ovarian cancer cell line (Hu et al., 2014). Notch3 can regulate Jagged1 expression and the receptor/ligand pair act in a positive regulatory loop in ovarian cancer cells (Chen et al., 2010). JAGGED1 is also expressed in cells in the peritoneal environment, suggesting that it may participate in tumor-peritoneal interactions (Choi et al., 2008, Steg et al., 2011).

Notch3 levels also correlate with tumorigenic phenotypes in ovarian cancer cell lines. Proliferation, viability, cell cycle arrest, and apoptosis have all been linked to Notch3 activity in ovarian cancer, indicating a role for Notch3 in tumor growth (Hu et al., 2014, Park et al., 2006b, Zhang et al., 2012, Zhang et al.,

2015). Notch3 inhibition reduced proliferation and induced apoptosis, indicating that Notch3 is a critical cell survival factor in some ovarian cancers. Notch3 signaling also upregulates other tumorigenic behaviors, such as epithelial to mesenchymal cell transition and resistance to anoikis (Gupta et al., 2013, Hu et al., 2014, Brown et al., 2015).

Lastly, Notch3 has a role in both platinum and taxane chemotherapy resistance. Patient samples with elevated Notch3 transcripts or protein are significantly more likely to become resistant or refractory to chemotherapy (Park et al., 2010, Rahman et al., 2012, Jung et al., 2010). *In vitro,* high levels of NOTCH3 have been correlated with increased ovarian cancer cell viability in the presence of platinum chemotherapy, and Notch inhibition during platinum treatment has been shown to reduce viability and increase apoptosis (Park et al., 2010, Rahman et al., 2012, Gupta et al., 2013, McAuliffe et al., 2012). NOTCH3 expressing ovarian cancer lines implanted into mouse hosts respond to combination platinum chemotherapy and Notch inhibition better than platinum therapy alone (Hu et al., 2014, McAuliffe et al., 2012, Shah et al., 2013). Combination therapy using taxane and several different methods of Notch3 inhibition has also proven effective at reducing tumor burden or cell viability (Groeneweg et al., 2014a, Hu et al., 2014, Kang et al., 2015, Jeong et al., 2017).

It is not currently known whether the mechanisms of increased growth, viability, anoikis resistance, and chemotherapy resistance are related to canonical, non-canonical, or both types of Notch3 signaling. There is some evidence that Notch3 may act in a non-canonical pathway through Wnt/βcatenin signaling in ovarian cancer (Chen et al., 2010) or other pathways (Ayaz and Osborne, 2014).

Previous studies thus implicate Notch3 signaling as critical in ovarian cancer development and progression. However, the mechanism by which Notch3 signaling affects metastasis and cancer development remains to be elucidated. Analysis of Notch3 pathway activation and its effects in an ovarian cancer model will provide insights into the causal relationship of Notch3 and ovarian tumorigenesis, the downstream targets that drive the greater lethality of Notch3 expressing tumors, and the mechanisms of ovarian cancer progression.

CHAPTER 2

MATERIALS AND METHODS

Cell culture

The Peo1 human ovarian cancer cell line was obtained from Dr. Andrea Califano's laboratory at Columbia University. Cells were cultured in RPMI with 10% FBS, 2mM sodium pyruvate, and 1% penicillin-streptomycin. This line was then lentivirally infected with a reporter via a FUW vector with firefly luciferase, mCherry, and puromycin resistance genes.

The OVCAR5 human ovarian cancer cell line was acquired from the Dr. Tian-Li Wang laboratory at Johns-Hopkins University and were cultured in RPMI with 10% FBS and 1% penicillin-streptomycin. OVCAR5 was lentivirally infected with virus generated from a FUW plasmid containing firefly luciferase, mCherry, and puromycin resistance to follow tumors *in vivo*.

The ID8 line, along with ID8 luciferase and ID8 GFP, were obtained from the Dr. Katherine Roby laboratory at the University of Kansas Medical Center. Cells were cultured in DMEM 10% fetal bovine serum (FBS) 1% insulin, transferrin, sodium selenite (Sigma I1884), and 1% penicillin-streptomycin.

The ID8 IP2 line was from our collaborators in the Dr. Jill Slack-Davis laboratory at University of Virginia. The ID8 IP2 cell line was lentivirally infected with a FUW firefly luciferase and mCherry construct. The ID8 IP2 luciferase cell line was lentivirally infected with Notch3 intracellular domain (pCCL Notch3 intracellular domain-HA IRES-GFP, Notch3IC) or control vector (pCCL multiple cloning site only, Control). ID8 IP2 lines were cultured in DMEM 10% FBS 1% insulin, transferrin, sodium selenite (Sigma-Aldrich I3146), and 1% penicillin-streptomycin. 5 total sets of lentivirally infected ID8 IP2 luc Notch3IC activated and control line biological replicates were generated.

Ovarian cancer lines OVCAR3, A2780, and SKOV3-IP1 were obtained from the Dr. Joanna Burdette laboratory at University of Illinois at Chicago (originally from ATCC), the Dr. Tian-Li Wang laboratory at Johns-Hopkins University, and the Dr. Olga Razorenova laboratory at University of California, Irvine respectively. Lines were cultured in RPMI 1640 10% FBS 1% penicillin-streptomycin.

All cultured cells were incubated at 37°C in 5% CO_2.

Peo1 luciferase modeling *in vivo*

Peo1 luciferase ovarian cancer cells were injected intraperitoneally in female NCR nu/nu athymic mice. A total of 5 mice were injected with $1.0x10^7$ cells in phosphate buffered saline each. Mice were between 5-7 weeks old at the time of injection. Mice were evaluated weekly for mass, circumference, and by bioluminescent imaging. Mice were injected with 100µL of 30mg/mL luciferin (XenoLight D-Luciferin, Perkin Elmer) intraperitoneally, anesthetized with isoflurane, and imaged at 10 minutes post injection with the IVIS Spectrum *in vivo* imaging system (Perkin Elmer). Mice were also dissected at endpoint to visually assess for the presence or lack of tumors. The Columbia University Institutional Animal Care and Use Committee approved all animal experiments.

OVCAR5 luciferase modeling *in vivo*

OVCAR5 luciferase were injected intraperitoneally in 10-week-old female NCR nu/nu athymic mice. 5 mice were each injected with $2.5x10^6$ cells in sterile phosphate buffered saline. Mice were evaluated weekly for mass, circumference, and by bioluminescent imaging. Mice were injected with 100µL of 30mg/mL luciferin (XenoLight D-Luciferin, Perkin Elmer) intraperitoneally, anesthetized with isoflurane, and imaged at 10 minutes post injection with the IVIS Spectrum *in vivo* imaging system (Perkin Elmer). Mice were also dissected at endpoint to visually assess for the presence or lack of tumors. The Columbia University Institutional Animal Care and Use Committee approved all animal experiments.

ID8 luciferase modeling *in vivo*

ID8 luciferase were injected either intraperitoneally or subcutaneously into 5- to 7-week-old female NCR nu/nu mice. Each injection consisted of $5x10^6$ cells in phosphate buffered saline. Intraperitoneally injected mice were evaluated weekly for mass and by bioluminescent imaging. Subcutaneously injected mice were evaluated weekly by mass, caliper measurements of tumors, and bioluminescent imaging. Bioluminescent imaging of mice was performed by intraperitoneal injection with 100µL of 30mg/mL luciferin (XenoLight D-Luciferin, Perkin Elmer), anesthetization with isoflurane, and imaging at 10 minutes post injection with the IVIS Spectrum *in vivo* imaging system (Perkin Elmer). Mice were also dissected at endpoint to visually assess for the presence or lack of tumors. For intraperitoneal injected mice, we also collected peritoneal wall and intestinal tissue with tumors to evaluate histology.

A second experiment with the ID8 luciferase cell line was completed by intraperitoneally injecting a second cohort of 4 NCR nu/nu mice and a cohort of 4 C57BL/6 mice. Mice were injected with $4x10^6$ cells

in phosphate buffered saline per mouse. All mice were between 5-7 weeks of age at the time of injection. Mice were assessed weekly for mass and by bioluminescent imaging. Imaging was completed with the same protocol as the previous ID8 luciferase experiment. C57BL/6 mice only were either shaved or fur was removed by depilatory cream on the abdomen prior to imaging. C57BL/6 mice were sacrificed at day 43 due to lack of bioluminescent signal, and mice were dissected and visually assessed for presence of tumor burden. NCR nu/nu mice were sacrificed between days 98 and 111.

The Columbia University Institutional Animal Care and Use Committee approved all animal experiments.

ID8 IP2 luciferase modeling *in vivo*

ID8 IP2 luciferase cells were injected intraperitoneally into either NCR nu/nu or C57BL/6 mice. All mice were injected with $2x10^6$ cells in phosphate buffered saline. C57BL/6 mice were injected at 13-16 weeks of age and sacrificed in the 9th week post tumor injection on day 65. NCR nu/nu mice were injected at 16-18 weeks of age and were sacrifice in the 7th week post injection of tumor cells at day 46. Mass and bioluminescent imaging of tumor burden was assessed weekly. At endpoint, mice were dissected and bioluminescent imaging of the peritoneal wall tumor burden was assessed as well. Live bioluminescent imaging of mice was performed by intraperitoneal injection with 100μL of 30mg/mL luciferin (XenoLight D-Luciferin, Perkin Elmer), anesthetization with isoflurane, and imaging at 10 minutes post injection with the IVIS Spectrum *in vivo* imaging system (Perkin Elmer). Fur from the abdomen of C57BL/6 mice was either shaved or removed by depilatory cream prior to live imaging. Imaging at time of sacrifice was accomplished by addition of 100 μL of 30mg/mL luciferin mixed with 400 μL of phosphate buffered saline directly to the peritoneal wall and diaphragm tissue. Measurements were captured at 5 min post addition of luciferin. Dissected tissue from nude mice was also sectioned and assessed for histology.

A second cohort of C57BL/6 female mice was injected at 7 weeks of age with $2x10^6$ ID8 IP2 luciferase cells in phosphate buffered saline. Mice were sacrificed at either 10 or 15 weeks post injection. In addition to measures completed on previously assessed ID8 IP2 luciferase injected mice, these mice were also weekly evaluated for circumference, and the volume of ascites was measured at the time of sacrifice.

The Columbia University Institutional Animal Care and Use Committee approved all animal experiments.

ID8 IP3 luciferase modeling *in vivo*

ID8 IP3 tumors were generated by collecting peritoneal wall with tumors and ascites containing tumors from C57BL/6 mouse #10 of the second cohort of C57BL/6 mice injected with $2x10^6$ ID8 IP2 luciferase cells. This mouse was chosen for tumor harvest based on the high presence of luminescent signal at the time of sacrifice compared to similar treated mice. The peritoneal wall tissue was enzymatically digested with collagenase IV, hyaluronidase V, and DNase I at 37°C. Red blood cells were then lysed, and cells were collected by centrifugation and passage through a 70 μm cell strainer. Ascites was subjected to red blood cell lysis and cells were collected in the same manner. Resulting cells were subjected to fluorescent activated cell sorting (FACS) for mCherry, which should be present in the tumor cells based on the FUW luciferase mCherry puromycin resistance construct lentivirally infected into the ID8 IP2 luc cell line that generated the tumors. FACS cells were then cultured *in vitro* under puromycin selection, which should select for cells with the firefly luciferase reporter. Cells were assessed *in vitro* for mCherry expression via fluorescent microscopy, and with reagents from the Promega Dual-Luciferase® Reporter Assay System for positive luciferase presence to confirm reporter activity in cells before injection.

C57BL/6 mice were injected intraperitoneally with $2x10^6$ ID8 IP3 cells either from peritoneal tumor cells, or ascites tumor cells in phosphate buffered saline. 4 mice were injected with each line for a total of 8 mice. Mice were assessed weekly for mass, circumference, and by bioluminescent imaging for the first 9 weeks post tumor injection. Imaging was performed by intraperitoneal injection of mice with 100μL of 30mg/mL luciferin (XenoLight D-Luciferin, Perkin Elmer), anesthetization with isoflurane, imaging at 10 minutes post injection with the IVIS Spectrum *in vivo* imaging system (Perkin Elmer). Abdominal fur of mice was removed via shaving or depilatory cream prior to imaging. Mice were sacrificed between 10 and 17 weeks post injection based on visible ascites accumulation and signs of illness. Mice that did not accumulate ascites were sacrificed at 17 weeks. At the time of sacrifice mice were dissected and assessed visually for the presence or absence of tumors.

The Columbia University Institutional Animal Care and Use Committee approved all animal experiments.

Histology

Tissue from mice was collected at time of dissection and was snap frozen in optimal cutting tissue compound (Tissue-Tek® O.C.T.). Samples were then sectioned at 5 μm and mounted on slides. Hematoxylin and eosin (H&E) staining was performed on frozen sections. Permount mounting media was added to slides and sections were covered with glass coverslips.

Immunofluorescent staining for vasculature of ID8 luciferase tumors was completed with antibody to CD31 (rat anti mouse CD31, BD Biosciences 553370) at 1:100 in blocking buffer, followed by secondary antibody donkey anti rat 594 (Donkey anti-Rat IgG Highly Cross-Adsorbed Secondary Antibody Alexa Fluor 594, ThermoFisher A-21209) at 1:1000. Vasculature stain on frozen sections of ID8 IP2 luciferase tumor sections was completed with a rat anti endomucin primary antibody (Endomucin Antibody V.7C7 IgG2a, Santa Cruz sc-65495) diluted to 1:500 in blocking buffer. The same secondary antibody, donkey anti rat 594 at a 1:000 dilution, was used. Vectashield mounting medium with DAPI (H-1200, Vector Laboratories) was added to stained sections and covered in glass coverslips.

Images were acquired on a Nikon Eclipse E800 Fluorescence Microscope with Nikon High-Resolution Digital Camera DXM 1200. Images were taken in Microsoft Image Pro Plus Morphometric Software 4.5. Photos were then modified in ImageJ (NIH) (Schneider et al., 2012).

Lentiviral infection

Lentiviral infection was completed by first transfecting 293T packaging cells with virus components, and then using produced virus to infect target cancer cells. Calcium phosphate transfection was completed by adding 3μg of envelope plasmid pVSVG, 5μg of packaging plasmid pRRE, 2.5μg of splicing regulator pRSV-Rev, and pCCL empty vector or vector with the gene of interest (FUW mCherry luciferase, pCCL HA tagged *Notch3* intracellular domain, or pCCL GFP) to 2.5M $CaCl_2$ and 2X HBS. Transfected cells were allowed to sit overnight at 37°C in 5% CO_2, and then the media was changed to the media preferred by the target cancer cell. This conditioned media was collected from transfected 293T cells and 0.45μm filtered to collect virus while removing other unwanted components such as contaminating 293T cells. Virus was then added to target cancer cells overnight at 37°C in 5% CO_2. Target cells were infected twice and then switched to complete target cell media without virus. Target cells were fluorescently imaged to confirm

successful infection, and lysates were subjected to western blot to confirm protein production for the gene of interest (see immunoblotting).

Retroviral infection

Retroviral infection was completed by first transfecting GP2-293 packaging cells with viral components, and then using produced virus to infect target cancer cells. Calcium phosphate transfection of GP2-293 was conducted with 10µg of envelope plasmid pVSVG and 10µg of pQCXIN vector either alone or with the gene of interest (full length *Notch3* tagged with HA, or EGFP) with 2.5M $CaCl_2$ and 2XHBS for 6 hours. 293T were then cultured overnight in target medium at 37°C in 5% CO_2. To infect cells, media from GP2-293 was removed and 0.45µm filtered to collect virus, and was subsequently added to target cells with 8µg/mL of polybrene overnight at 37°C in 5% CO_2. Infection was completed twice on cells. Cells were then selected with G418 (Sigma G8168-10ML).

Immunoblotting

Western blot was performed on 15µg of cell lysates subjected to SDS-PAGE electrophoresis. Lysates were run in an 8% gel and subsequently blotted to nitrocellulose membrane. Notch3 antibody (Santa Cruz Biotechnology Inc., sc-5593) according to the manufacturer is a rabbit polyclonal antibody targeted to amino acids 2107-2240 of mouse Notch 3. α-Tubulin antibody (Sigma-Aldrich, T6074) is a mouse monoclonal antibody. HA tag antibody (Cell Signaling Technology C29F4) is a rabbit monoclonal antibody. Secondary IgG horseradish peroxidase conjugated antibodies include goat anti-rabbit (Sigma-Aldrich, A6154), and sheep anti-mouse (GE Healthcare Life Sciences, NA931VS). Enhanced chemiluminescence was used to detect secondary antibodies (Thermo Scientific™, SuperSignal™ West Femto Chemiluminescent Substrate, or GE Healthcare Life Sciences, Amersham ECL).

Semiquantitative reverse transcriptase polymerase chain reaction (RT-PCR)

RNA was extracted using the RNeasy Mini Kit (QIAGEN, 74104), and cDNA was generated using Verso™ cDNA synthesis Kit (Thermo Scientific™, AB1453A). 1 unit of Maxima Hot Start Taq polymerase (ThermoFisher Scientific) was added per reaction to a final concentration of 1X PCR buffer, 1.5mM $MgCl_2$, 0.2mM dNTPs, and 0.2 µM of each primer for each gene were mixed in molecular grade water. 150ng of cDNA template was added to each reaction. Thermal cycler cycle conditions were as follows: 94°C 4min, 35 cycles of 94°C 45sec, 60°C 1min, 72°C 1min, and 72°C 5min followed by 4C. Primer sequences are

listed in the appendix. (Specifications for Platinum Taq (ThermoFisher Scientific) were used, but Maxima Hot Start Taq was substituted.)

Reverse transcriptase quantitative polymerase chain reaction (RT-qPCR)

RNA was extracted using the RNeasy Mini Kit (QIAGEN, 74104), and cDNA was generated using Verso™ cDNA synthesis Kit (Thermo Scientific™, AB1453A). Relative mRNA expression was determined by assessing generated cDNA for Notch3, Hes1, Hey1 and HeyL on a Life Technologies ABI ViiA7™ Real-Time PCR system using ABsolute Blue qPCR SYBR Green ROX (Thermo Scientific™, AB4163A) reagent. All 5 lentiviral infected sets of ID8 IP2 luc lines was assessed. Mean threshold cycle numbers (Ct) were determined for each gene and compared to the mean Ct of beta actin. The fold change compared to control was calculated according to the formula $2^{(-\Delta\Delta Ct)}$ comparing the Notch3IC and Control Ct normalized to beta actin Ct. Results were graphed in GraphPad Prism 7 software. Primer sequences are listed in the appendix.

Proliferation

Proliferation/ viability assays were performed by seeding 2500 cells per well in a 24 well plate and assessing the number of viable cells at 48 hours with WST-8 (Dojindo Molecular Technologies) absorbance readings at 450nm. 450nm readings were compared to readings of a standard curve generated from like cells. 5 separate experiments were performed with 3 replicates of both Notch3IC and Control. One matched set of lentiviral infected ID8 IP2 luc was assessed (Set #1). Graphs and statistical analysis were generated in GraphPad Prism 7.

Experiments with FACS Notch3IC and Control, were completed with the same procedure. All data points from two experiments of sextuplicate plates were analyzed.

Colony formation in soft agar

Colony-forming plates were prepared by layering 0.75% agar in media, 0.75% agar and $2x10^4$ cells, 0.75% agar in media, and complete media in a 24 well plate in the listed order (see cell culture). Cells were incubated at 37°C in 5% CO_2 for 3 weeks, changing media layer every other day. At 3 weeks, plates were stained with MTT at 37°C in 5% CO_2 for 3 hours followed by washing with phosphate-buffered saline. Five 5X photos per well were taken and the number of colonies and area of colonies were evaluated with ImageJ (NIH) software (Schneider et al., 2012). 4-6 wells were evaluated for each of 3 experiments conducted on

one matched ID8 IP2 luciferase line set (Set #1). Graphs and statistics were generated with GraphPad Prism 7.

Cisplatinum therapy dose response

ID8 IP2 luciferase Notch3IC and Control lines were seeded at 2000 cells per well in a 96 well plate and were left to attach overnight at 37°C and 5% CO_2. Cells were subsequently subjected to cisplatinum doses of 0μM (DMSO vehicle alone at 16μM), 2μM, 4μM, 8μM, or 16μM for 48 hours at 37°C and 5% CO_2. Cisplatinum was obtained from Sigma-Aldrich (P4394-100MG), and dissolved in DMSO at 10mM concentration. Cisplatinum was then diluted to 1mM in complete media (see cell culture), prior to each experiment before making dilutions for cell treatment. After 48 hours, cells were treated at a final concentration of 10μg/mL fluorescein diacetate (FDA) and 0.1% eosin Y in complete media for 20min at room temperature in the dark. The FDA fluorescently stains viable cells by being converted to fluorescein by cellular esterases, while the eosin Y quenches fluorescence in cells that are not viable (Keshelava et al., 2005). Cells were then assessed on the DIMSCAN, an imager that measures fluorescence staining live cells. 4 separate experiments were completed on ID8 IP2 luc Notch3IC and Control from Set #1.

ID8 IP2 luciferase Notch3IC and Control *in vivo* model

In vivo implants in NCR-nu/nu athymic mice were performed via intraperitoneal injection with $2x10^6$ ID8 IP2 luciferase Notch3IC or Control tumor cells in phosphate buffered saline. Implants were performed in 6 to 8-week-old female mice. A total of 76 mice were injected, and the 69 which developed tumor burden were assessed. Mice were assessed weekly via circumference measurement and IVIS Spectrum In Vivo Imaging System (PerkinElmer) bioluminescent imaging. Mice were dissected and IVIS imaged at the time of sacrifice for peritoneal wall and ovary tumor burden. Mice were sacrificed according to 25% or greater increase in circumference, or due to cachexia criteria of body condition score BC1 or BC2. For one experiment, mice were all sacrificed at 8 weeks. For this 8-week experiment, Set #2 of ID8 IP2 luc lines was used (9 Control, 10 Notch3IC). All remaining mice were injected with cells from the lentiviral infection for Set #1. The Columbia University Institutional Animal Care and Use Committee approved all animal experiments. Graphs and statistics were generated with GraphPad Prism 7 software.

RNA sequencing

RNA was extracted using the RNeasy Mini Kit (QIAGEN, 74104) and the RNase-Free DNase Set (QIAGEN, 79254). RNA samples from 4 separate lentiviral infected ID8 IP2 luciferase line pairs (Sets #1 - #4, Control and Notch3IC) were assessed. RNA-Seq data was generated by the JP Sulzberger Columbia Genome Center. Poly-A pull down was used to enrich for mRNA. An Illumina TruSeq RNA Prep Kit was used to prepare libraries. Briefly, library preparation for RNA-Seq entails fragmenting the RNA, strand synthesis with random primers, end repair and addition of adapter sequences that interact with the sequencing platform, and lastly purification and amplification of products. 25 to 30 million 100 base pair single end raw passing filters reads were then sequenced on an Illumina HiSeq 2000 or 2500 instrument. Sequence generated by Illumina software was format converted using bcl2fastq software. TopHat software was used to match generated sequence reads to the murine genome. Cufflinks software was used to determine the number of sequence read counts for each gene. DESeq analysis of gene counts to evaluate differential gene expression was performed followed by selection of genes with adjusted p-value < 0.1 and a 1 Log_2 fold change in expression. The narrowed list of genes was subjected to pathway analysis using The Database for Annotation, Visualization and Integrated Discovery (DAVID) Bioinformatics Resources 6.7 analysis wizard (NIAID, NIH). Pathway analysis was also assessed using the Broad Institute's Gene Set Enrichment Analysis (GSEA) after mouse genes were converted to human orthologs using HomoloGene build 68 (NCBI, NIH). DESeq assessment confirmation and all pathway analysis was completed by Dr. Elham Azizi in the laboratory of Dr. Dana Pe'er (Columbia University/ Memorial Sloan Kettering Cancer Center).

Flow cytometry of Itga1

Flow cytometry was completed on 3 separate lentivirally infected line sets over 2 experiments. ID8 IP2 luc lentiviral Sets #3, #4, and #5 were used. $5x10^6$ were stained in 100µL of flow cytometry buffer consisting of 1X phosphate buffered saline with 0.1%NaN_3 and 0.5% bovine serum albumin. Cells were stained with 0.2µg of either hamster anti-rat/mouse CD49a or isotype control conjugated to Alexa Flour 647 (BD Pharmingen™ 562113, and 562112). All washes were completed in 500µL of flow cytometry buffer described above. After staining, cells were fixed in flow cytometry buffer with 1% paraformaldehyde, and filtered through a cell strainer cap with 35µm nylon mesh. A **Gallios™ flow cytometer (**Beckman Coulter) instrument was used to evaluate samples, and analysis was completed with FlowJo version 10.2 software.

Graphs were generated of all the data points for the two experiments, and for the average of each line set for the 2 experiments (log_{10} transformed data). Graphs and statistics were generated in GraphPad Prism 7.

Flow cytometry of Itga11

Flow cytometry was completed on 3 separate lentivirally infected line sets over 2 experiments. Sets #3, #4, and #5 were used. $5x10^6$ were stained in 100µL (for primary) or 200µL (for secondary) of flow cytometry buffer consisting of 1X phosphate buffered saline with 0.1%NaN_3 and 0.5% bovine serum albumin. Cells were stained with 1.0µg of either rabbit anti-human/mouse/rat ITGA11 (Biorbyt, orb184286) or rabbit IgG isotype control (ThermoFisher Scientific 02-6102) primary antibody. Cells were subsequently washed and then stained with 0.4µg of secondary donkey anti-rabbit IgG Alexa Flour 647 (ThermoFisher Scientific A-31573). All washes were completed in 500µL of flow cytometry buffer described above. After staining, cells were fixed in flow cytometry buffer with 1% paraformaldehyde, and filtered through a cell strainer cap with 35µm nylon mesh. A **Gallios™ flow cytometer (**Beckman Coulter) instrument was used to evaluate samples, and analysis was completed with FlowJo version 10.2.

Adhesion to extracellular matrix (ECM)

24 well plates were coated with extracellular matrix and then blocked with 1% bovine serum albumin. Cells were seeded and incubated at 37°C in 5% CO_2 for 30 to 90 minutes. Medium was removed and non-adherent cells were washed away with phosphate-buffered saline. Adherent cells were fixed with methanol and stained with 0.1% crystal violet. Cell counts for each well were generated with a Celígo instrument and software (Nexcelom Bioscience). The Celígo is an image cytometer which has the ability to scan plates and take brightfield or fluorescent cell images. Brightfield images were taken of the entire well and assessed by direct cell counting. The following extracellular matrices were assessed: collagen I (Corning™ 354236), collagen IV (Corning™ 354233), fibronectin (Corning™ 354008), laminin (Corning™ 354232), and vitronectin (R&D Systems 2349VN100). Three separate lentivirally infected sets of ID8 IP2 luc Notch3IC and Control matched lines were assessed in triplicate on 3 separate occasions (Sets #3 - #5). Means were calculated and the Notch3IC mean was compared to Control for each line. Graphs and corresponding statistics were generated in GraphPad Prism 7.

Adhesion to Collagens with Antibody Blocking of Itga1

96 well plates were coated with rat tail collagen I (Corning™ 354236) or mouse collagen IV (Corning™ 354233) and then blocked with 1% bovine serum albumin. Cells were incubated with 10µg/mL of either Itga1 inhibitory antibody (BD Biosciences, 555000) or isotype control (BD Biosciences, 553961) rotating (ThermoFisher Scientific HulaMixer®) at 37°C in 5% CO_2 for 30min. Bovine serum albumin was removed from wells, and cells were then seeded on collagens. Cells were allowed to adhere at 37°C in 5% CO_2 for 120 minutes. Medium was removed and non-adherent cells were washed away with phosphate-buffered saline. Adherent cells were fixed with methanol and stained with 0.1% crystal violet. Cell counts for each well were generated with a Celígo cytometer instrument and software (Nexcelom Bioscience). Brightfield images were obtained and cells were assessed by direct cell counting. Three separate lentivirally infected sets of ID8 IP2 luc Notch3IC and Control matched line biological replicates were assessed in triplicate (Sets #3 - #5). Means were calculated and the Notch3IC mean was compared to Control for each line. Graphs and corresponding statistics were generated in GraphPad Prism 7.

Migration without extracellular matrix

The migration scratch/wounding assay was performed by scraping a confluent monolayer of cells in a 12-well plate with a p200 tip and allowing the cells to close the gap over the course of 12 hours. Experiments were repeated in triplicate 3 times for 3 separate ID8 IP2 luciferase lentiviral infected line sets (Sets #1, #2, #4). Photos were taken every 3 hours for 12 hours at 10x. Images were adjusted to crop areas outside the microscope camera field, and images were processed with “find edges” and “sharpen” tools to increase contrast between the scratch and cellular areas in ImageJ (NIH) (Schneider et al., 2012). Images were quantified with TScratch (Tobias Gebäck and Martin Schulz, ETH Zürich). Graphs and statistical analysis were generated in GraphPad Prism 7.

Migration over extracellular matrix

Migration experiments were completed in Oris™ cell migration assay collagen I or fibronectin coated 96 well plates (Platypus Technologies, CMACC1.101 or CMAFN1.101). This assay comes as a 96 well plate pre-coated with extracellular matrix and prepared with a stopper/plug in the center of each well. Cells were seeded in the plate around the stopper and incubated at 37°C and 5%CO_2 overnight to create a confluent monolayer around the plug. Once plugs were removed, cells were imaged at 0, 6, 12, and 24 hours. Cells were evaluated and analyzed with a Celígo cytometer instrument and software (Nexcelom

Biosciences). Brightfield images were obtained and confluence was assessed for the cellular area. 3 matched sets of lentivirally infected ID8 IP2 luciferase lines were assessed in quadruplicate twice (Sets #3 - #5). Graphs display the average of the 2 experiments for each line set. Graphs and statistics were generated with GraphPad Prism 7.

Invasion through Matrigel GFR

Invasion assays were performed in triplicate in BioCoat™ 24 well transwell inserts with 8μm pores pre-coated with Growth Factor Reduced Matrigel (Corning, 354483). A total of 3 experiments were performed with one ID8 IP2 luciferase line set (Set #1). After serum starving cells for a minimum of 16 hours, $1x10^4$ cells were seeded in serum free media (1% penicillin/streptomycin) in the Matrigel coated inserts. Media with 10% FBS and 1% insulin, transferrin, sodium selenite was plated below the insert. Cells were incubated for 24 hours at 37°C in 5% CO_2, and were then fixed with methanol and stained with 0.1% crystal violet. 4 20x photos per insert were taken and quantified by counting individual cells in ImageJ (NIH) (Schneider et al., 2012). Data for each 20x field was plotted in GraphPad Prism 7. Data for non-coated transwell inserts without ECM were also collected and analyzed in conjunction with each BioCoat experiment.

Invasion through collagen I

Invasion experiments through collagen I were completed using the CytoSelect™ 24-Well Cell Invasion Assay Collagen I, Colorimetric Format (Cell Biolabs, Inc., CBA-110-COL). 3 separate sets of ID8 IP2 luciferase lines were assed in triplicate (Sets #3 - #5). After serum starvation for a minimum of 16 hours, $2.5x10^5$ cells were seeded per insert in serum free medium, and media with 10% FBS and 1% insulin, transferrin, sodium selenite was added in the well below the insert. Cells were allowed to invade for 72 hours. Cells were stained, and the stain was extracted according to manufacturer protocol. Samples were assessed at 560nm. Graphs and statistics were generated with GraphPad Prism 7.

CHAPTER 3

MOUSE MODELING OF OVARIAN CANCER TO BEST REPLICATE PERITONEAL METASTASIS IN HUMAN DISEASE

INTRODUCTION

In order to study the role of Notch3 signaling in ovarian cancer, we chose an appropriate animal model that would closely resemble patient disease for high grade serous ovarian cancer (HGSC), the most common and deadly histologic subtype of ovarian cancers (Chapter 1). Our goal was to identify a model that would appropriately replicate the peritoneal metastasis characteristic of HGSC as well as display similarity to the histology and environment of HGSC. HGSC presents with metastatic ovarian cancer lesions that seed on the human peritoneal wall and organs as shown in Figure 3.1, and we endeavored to replicate this disease state. In addition to determining if a model was appropriate to replicate HGSC, we sought to determine appropriate methods to characterize and measure disease burden in order to quantify disease progression.

There exist a large number of mouse and other animal models for ovarian cancer which each have advantages and drawbacks. In addition, the tissue of origin of ovarian cancer is currently being debated, and new models posit that ovarian cancer may derive from a variety of tissue sources (Chapter 1). Ovarian cancer may originate either from the ovary or the oviduct/ fallopian tube, and there is evidence to support both origins (see Chapter 1) (Crum et al., 2007, Dubeau, 2008). The model we chose was selected in part to enable study of metastatic spread of ovarian cancer in addition to the clinical features of the disease. We chose not limit ourselves to mouse models originated specifically from either the ovary or oviduct, even though some may argue cells from the “true” origin may be a better or more valid model.

While there are longstanding examples of a variety of animal models for ovarian cancer, such as aged egg laying hens and *in vitro* methods that mimic ovarian cancer interaction with the peritoneum, we elected to use a murine model (Lengyel et al., 2014). Genetically engineered models with mice have been developed to investigate ovarian cancers. These models allow for an intact microenvironment in mice, and the ability to investigate precursor lesions and earlier stages of disease. Some models have employed the use of viral genes like SV40 TAg to drive tumor development. Many models use genetic alterations

identified in human ovarian cancers to replicate disease of particular histologic types (Cho and Shih Ie, 2009, Lengyel et al., 2014). For example, a combination of *Tp53*, Brca, and Pten deletions have been used to model HGSC (Cho and Shih Ie, 2009, Perets et al., 2013). Examples of drivers used to target genetic alterations to the ovary or oviduct include *Keratin-5, MisIIr,* and *Pax8* among others, which are expressed in ovarian or oviductal epithelial cells (Cho and Shih Ie, 2009, Perets et al., 2013, Garson et al., 2012). It should be noted that drivers for the ovary and oviduct have issues with specificity, and often target other parts of the reproductive tract (Garson et al., 2012, Lengyel et al., 2014). An alternate approach used for model development specific to the ovary is extraction of ovarian surface epithelium to induce genetic alterations *in vitro* followed by implantation of cells under the ovarian bursa or IP *in vivo*. (Cho and Shih Ie, 2009, Orsulic et al., 2002, Xing and Orsulic, 2006). Another commonly used method is injection of Cre recombinase adenovirus in the ovarian bursa of mice containing floxed alleles of oncogenes or tumor suppressor genes. This is thought to more precisely drive expression specifically at the site of the ovary than can be accomplished by promoter-driven expression of Cre in transgenics (Cho and Shih Ie, 2009, Lengyel et al., 2014, Garson et al., 2012). Both methods allow for temporal control over induction of mutations. Genetic models however, are subject to wait times for tumor development, and many of them require bursal injections which involves surgery.

Xenograft and allograft models employing injection of tumorigenic cell lines in mice are a well-established method of modeling ovarian cancers (Cho and Shih Ie, 2009, Lengyel et al., 2014). Many established human ovarian cancer cell lines have been shown to generate disseminated peritoneal disease in xenograft models. For xenograft, cell lines derived specifically from a patient with serous cancer can be selected (Lengyel et al., 2014). Syngeneic allograft models derived from mice have also been developed. Human or syngeneic lines have been introduced into mice via subcutaneous, intraperitoneal, or orthotropic bursal injection. It is of note that subcutaneous tumors grow as an individual solid tumor and do not resemble disseminated disease in patients. Bursal injection requires surgery to achieve. There are additional types of xenografts designed to capture the earlier stages of metastasis involving dissociation away from a primary tumor source other than bursal injection. These include the use of human or mouse tumor tissue, rather than cell lines, for IP injection or implantation near the ovary or under the renal capsule (Lengyel et al., 2014).

Recently, available ovarian cancer cell lines have been analyzed to determine if they are representative of the type of ovarian cancer being studied. This has been done through genetic profiling, evaluation of tumor dissemination patterns *in vivo,* and histological evaluation of tumors that arise from implantation of these human cell lines (Beaufort et al., 2014, Anglesio et al., 2013, Domcke et al., 2013, Mitra et al., 2015). Many of the lines were found to have a signature inconsistent with the originally designated type of ovarian cancer. Thus, lines may not represent the type of cancer desired or reported to be investigated. There has also been investigation specifically into misidentification and contamination of lines leading to loss of cell line integrity (Korch et al., 2012).

A key feature of ovarian cancer models is the ability of these models to replicate metastatic spread in the peritoneal cavity. A variety of approaches have been used to quantify spread and the resultant tumor burden. Assessment of tumor burden is complicated by the fact that disease is spread throughout the peritoneal cavity on different organs and as numerous individual lesions on the peritoneal wall. Approaches to quantify tumor burden include measurement of total tumor mass, mouse mass, circumference of the abdomen, ascites volume, counting the number of metastases found on the peritoneal wall and organs, and imaging *in vivo* (Mitra et al., 2015, McAuliffe et al., 2012, Byrne et al., 2003, Hu et al., 2002, Sawada et al., 2007).

At the outset of my thesis research we decided to study the role of *Notch3* signaling in ovarian cancer using both *in vivo* and *in vitro* methods to investigate disease progression and interrogate molecular mechanisms. Our hope was to utilize a model that replicates HGSC and its pattern of disseminated disease (Lengyel et al., 2014). With these points in mind, we decided to utilize ovarian cancer cell lines that would grow in the peritoneal cavity and on organs of the peritoneum after intraperitoneal (IP) injection, focusing on the stages of disease dissemination. As noted, HGSC is typically detected after metastatic spread has already occurred, and treatment of ovarian cancer is typically done on patients who already have multiple lesions in the peritoneum.

Finally, our preference of models was influenced by a desire to use a syngeneic model so that we might be able to benefit from an intact microenvironment of immune competent mice. However, we initially compared and contrasted both murine syngeneic and human derived ovarian cancer cell lines, since the human lines are derived from cancer bearing patients. We chose IP injection as a method of tumor cell

introduction since IP introduction is less intrusive, not requiring surgery, and consistently generates disseminated disease. Here we describe the experiments that aimed to identify a cell line-based ovarian cancer mouse model that best replicated HGSC cancer, while being practical for the generation and assessment of disease burden. We also describe methods we chose to effectively measure disease burden.

Figure 3.1

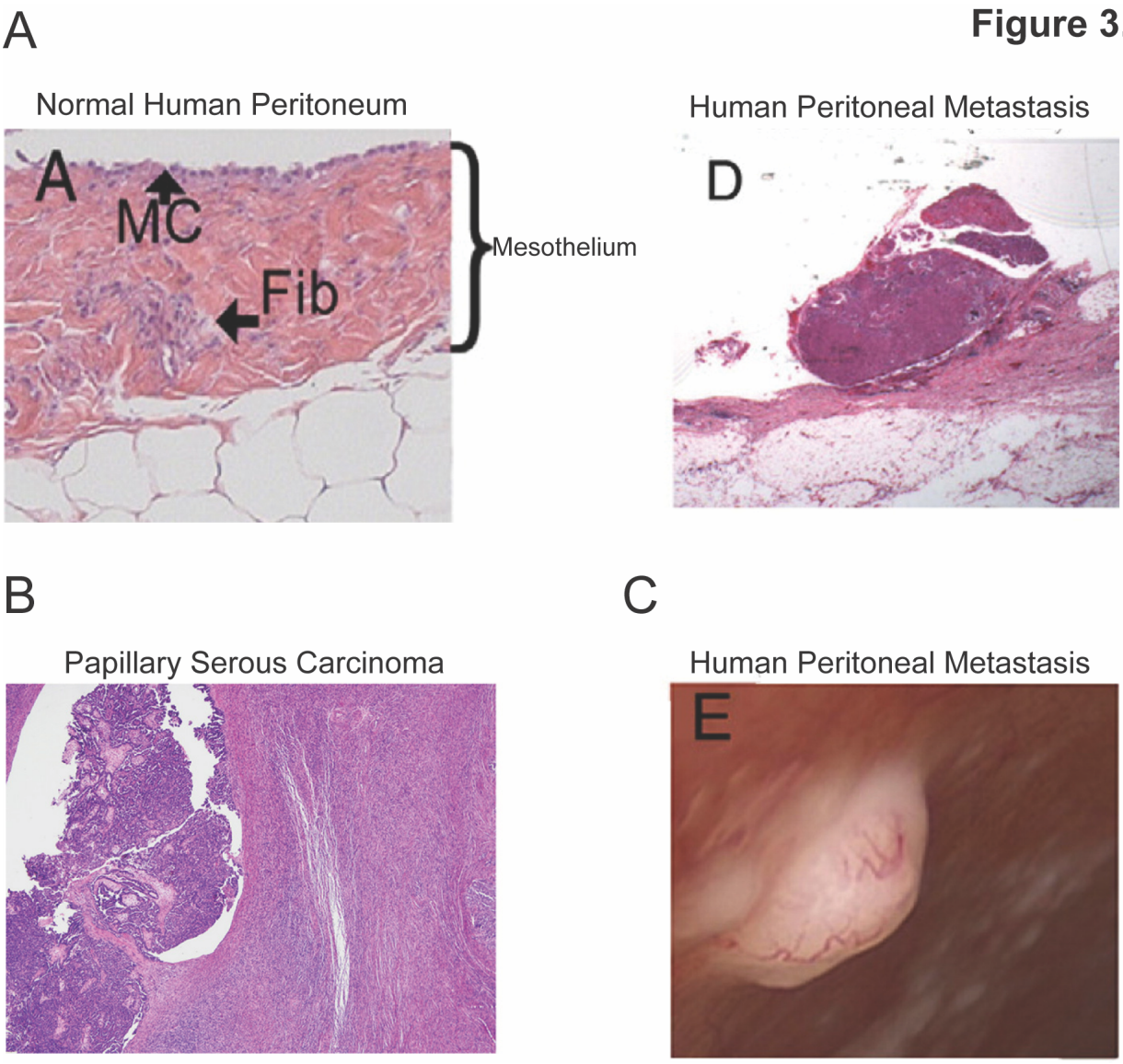

Figure 3.1 Human high grade serous ovarian cancer histology and gross tumor appearance. Images are copied from the published review article "Ovarian Cancer Development and Metastasis" by Ernst Lengyel (Lengyel, 2010) from "Figure 2. Serous ovarian carcinoma metastasis", and the published article "The Origin of Epithelial Neoplasms of the Ovary: An Alternative View" by Elvio G. Silva (Silva, 2016) from "Figure 2. Four different types of serous carcinoma". This figure shows the histology and gross view of tumors in human serous cancer which we want to replicate to the best of our ability in our *in vivo* model. (A) The left panel shows a normal human peritoneal section and is described in the paper as quote, "H&E staining. MC (mesothelial cells), Fib (fibroblasts)". The right panel shows the histology of a peritoneal tumor seed and is described as an, "Implant… in a patient with disseminated ovarian carcinoma on a background of normal peritoneum". (Lengyel, 2010) (B) This image is a H&E stain of papillary serous carcinoma. (Silva, 2016) (C) This image is described as, "Peritoneal implant with neoangiogenesis. Other smaller implants in the background (laparoscopy)". (Lengyel, 2010)

RESULTS

To identify appropriate models for evaluating ovarian metastatic disease, as outlined in the introduction, we assessed two human derived ovarian cancer lines, as well as variants of a syngeneic mouse model line. Our goal was to select a model for the study of the contribution of Notch3 to ovarian cancer disease progression and metastasis.

The PEO1 human derived cell line did not generate IP tumors

We attempted to model peritoneal disease with the human-derived ovarian cancer cell line, PEO1. The PEO1 line was developed from the ascites of a patient with poorly differentiated adenocarcinoma before chemotherapy resistance developed (Langdon et al., 1988, Wolf et al., 1987). Our goal was to determine if the PEO1 line would develop tumors from intraperitoneal injection *in vivo*. We lentivirally infected the line with a FUW plasmid containing the luciferase gene to allow for visualization with an IVIS® Spectrum bioluminescent and fluorescent imager (IVIS) to track tumor signal during the course of possible tumor development. 5 NCR nu/nu mice were injected with $10x10^6$ PEO1 luciferase cells. We measured mouse circumference to assess ascites accumulation and conducted IVIS imaging weekly. The flux measurement (photons per second) from the IVIS bioluminescent signal dropped after initial tumor injection by week 1, and was never able to recover to a flux of $1x10^9$ p/s, which we considered the minimum for tumor burden by 7 weeks. Mice also showed no sign of ascites by circumference increase by 7 weeks. While mice were no longer measured weekly, all 5 mice were kept for a total of 19 weeks without showing any signs of tumor burden or ascites accumulation before they were sacrificed (data not shown). It was determined the PEO1 model would not be a very effective or efficient model for intraperitoneal *in vivo* studies.

The OVCAR5 human line generated small IP tumors, but little ascites

OVCAR5 is a line derived from patient adenocarcinoma ascites (Langdon, 2004).This model was of interest for *in vivo* studies since it is known to show high NOTCH3 expression and the line reportedly generated metastatic peritoneal tumors *in vivo* similar to HGSC (Mitra et al., 2015, McAuliffe et al., 2012). We thought the OVCAR5 line may be useful for investigating the role of NOTCH3 in future ovarian cancer studies.

To assess *in vivo* growth of this line, we injected 5 NCR nu/nu mice with $2.5x10^6$ cells IP in each

mouse. We measured circumference and IVIS imaged once weekly. All 5 mice displayed a bioluminescent signal above $1x10^9$ by 5 weeks showing tumor take for all 5 mice. By 6 weeks all mice had to be sacrificed due to signs of cachexia, or were found dead (see appendix A4.3 panel A for cachexia criteria (Burkholder et al., 2012)). One of the mice did however, display signs of fluid ascites accumulation in the peritoneum despite also showing signs of cachexia, like prominent skeletal features through the skin. Circumference measurements did not display a particular pattern in relation to time or tumor burden, indicating that mice did not consistently accumulate ascites (data not shown). This is consistent with a previous study that reported unreliable ascites formation, despite tumor formation, with the OVCAR5 model (Mitra et al., 2015). Mouse mass stayed fairly constant throughout the weeks until dropping for most mice in the 5^{th} to 6^{th} week due to cachexia (data not shown). This model produced small tumor seeds in the peritoneum (Figure 3.2). We did not select this model for further study.

Figure 3.2

A

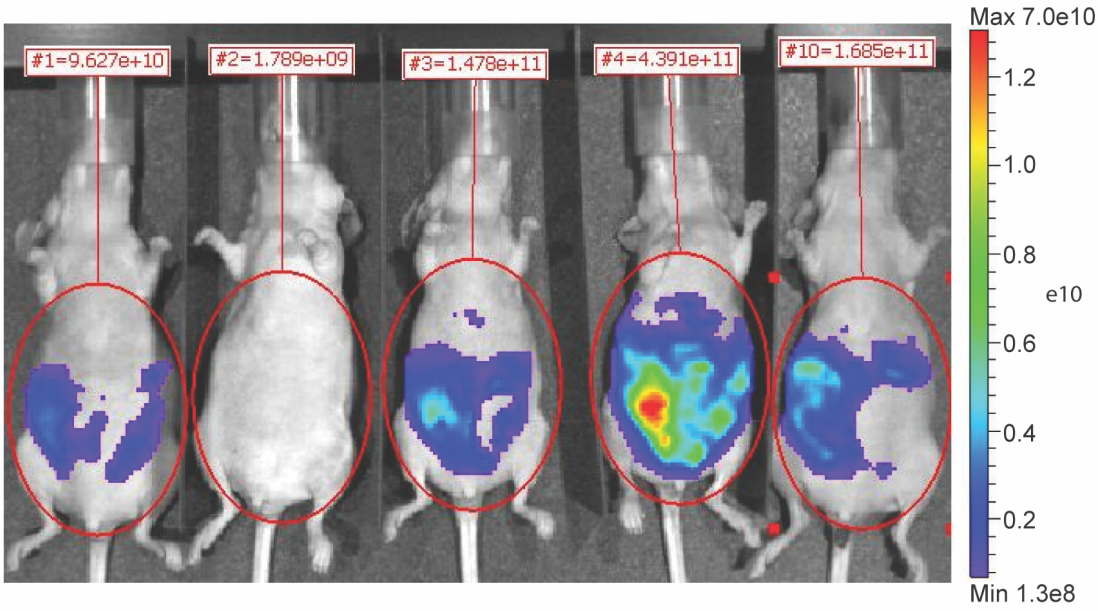

B

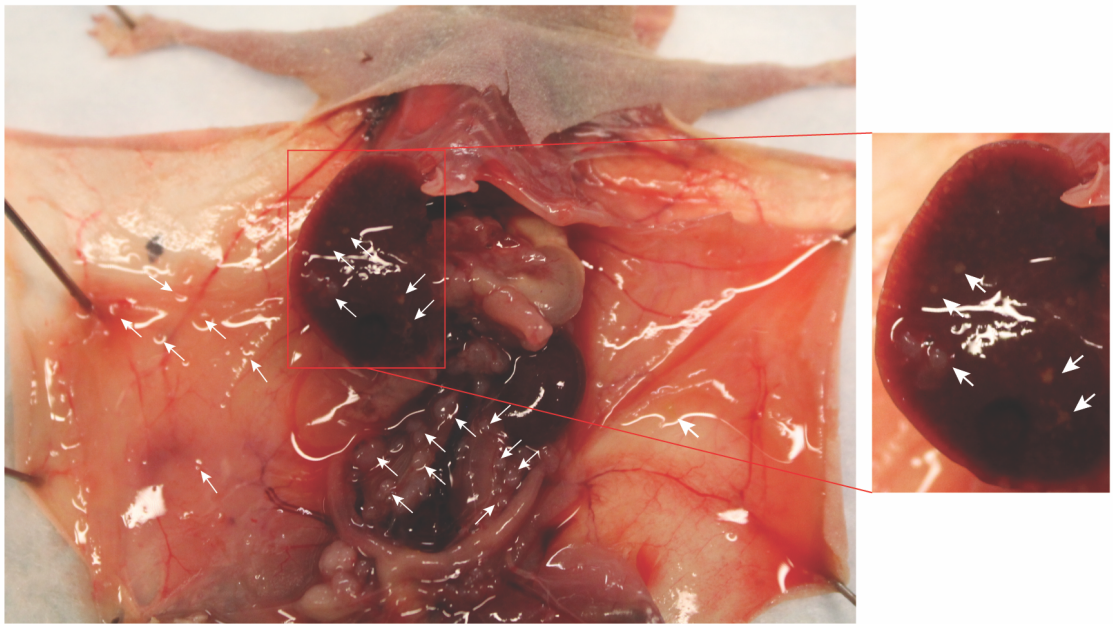

Figure 3.2 OVCAR5 luciferase intraperitoneally injected mice display peritoneal tumor burden. **(A)** Live bioluminescent imaging of mice with OVCAR5 tumors at 5 weeks post injection. Images were taken 10 minutes after injection of each mouse with luciferin. Mouse number is shown with total flux value (p/s). Red circles denote area measured for flux. The signal displayed on the mice, and the color scale show bioluminescence measured in radiance (p/sec/cm^2/sr). **(B)** This figure shows a partially dissected mouse injected with OVCAR5 (mouse #1 in panel A) sacrificed in the 6th week (44 days) post tumor injection. The peritoneal wall has been dissected open and pinned down. White arrows point out examples of tumor seeds on the peritoneal wall and on organs that have not yet been dissected. The red box demonstrates a close up of liver tumor seeds.

Syngeneic tumorigenic ID8 mouse ovarian line generates IP tumors

We explored the use of a syngeneic line that would allow for an intact microenvironment and therefore better replicate patient disease. Implanting human-derived cell lines requires immunodeficient (nude) hosts, but a syngeneic model would allow us to use immune-competent mice while modeling stage III metastasis observed in human ovarian cancers. A syngeneic model would also have the benefit of allowing us to implant tumors into mouse models bred with defined genetic alterations. We could therefore decide to delete or alter genes in the *Notch* pathway in the mouse to investigate their role in the environment of ovarian cancer, or their interaction with ovarian cancer tumor cells. We were also interested in a model that would demonstrate HGSC disease with ascites and larger peritoneal seeds *in vivo*.

The ID8 cell line is a syngeneic tumorigenic murine line that can be used to model intraperitoneal disease and ascites accumulation. ID8 and ID8 luciferase-containing cell lines were acquired from Dr. Katherine Roby at the University of Kansas Medical Center, who developed the line (Roby et al., 2000). ID8 is a mouse ovarian surface epithelial line that was established by removing C57BL/6 ovaries and collecting the normal ovarian surface epithelium. Isolated cells were passaged over 20 times *in vitro*. *In vivo* tumor formation was verified with passaged cells, and original passaged cells were subsequently cloned by limiting dilution from single cells to generate multiple different lines. One of the lines developed was ID8, which was then shown to be tumorigenic in both C57BL/6 and nude mice when injected IP. C57BL/6 mice developed tumors at approximately 114 days (~16 weeks); tumors were widespread throughout the peritoneum, and mice accumulated ascites fluid similar to late stage clinical cases of HGSC (Roby et al., 2000). ID8 has been shown to model human late stage and serous ovarian cancers by peritoneal seeding. Based upon the number of publications using ID8, it is likely the most common syngeneic line used to model ovarian cancer and has been used in several studies to investigate ovarian cancer, as well as ovarian cancer interaction with the microenvironment (Leinster et al., 2012, Cho et al., 2013, Lengyel et al., 2014, Greenaway et al., 2008).

We performed initial evaluation of the ID8 cell line to determine the tumor take rate in our hands. We tested subcutaneous and intraperitoneal tumor take in NCR nu/nu mice as a first step prior to attempting ID8 implantation of immunocompetent mice. We injected 4 mice each with $5x10^6$ ovarian ID8 cells either IP, or under the skin on both the left and right ventral side near the forelimbs. Mice were followed with IVIS

imaging for both types of injection weekly for 8 weeks. Intraperitoneal injected mice were also measured weekly, and caliper measurements were taken for subcutaneous tumors weekly.

We observed strong tumor take in 3 of 4 intraperitoneal injected mice (Figure 3.3). All mice were sacrificed at day 60 to evaluate tumor development. Intraperitoneal tumor cells generated small seeds across the peritoneal wall. The change in mass, however, did not seem to accurately reflect the development of disease burden at the 60-day time point. The mass of all mice appeared to rise steadily over time, but accumulated varying amounts of observable ascites and *in vivo* bioluminescent signal. For example, at 8 weeks (Day 56) mouse #1 and mouse #3 had both increased mass by about 10% (9.9% and 10.6% respectively), but mouse #1 showed no tumor burden by bioluminescent imaging, while mouse #3 appeared positive for tumors (Figure 3.3). We also attempted assessment of peritoneal seeds in intraperitoneally injected mice via hematoxylin and eosin (H&E) stain, and immunofluorescent staining of vasculature with antibodies to CD31 (Figure 3.3). We wanted to determine whether it was possible to evaluate tumor seeds histologically, and if we could observe the pattern of tumor vasculature and quantify tumor vessels. We also wanted to determine whether our histology and gross tumors resembled HGSC.

Tumor take occurred in all 4 subcutaneously injected mice, and mice were sacrificed at 60 days post injection. Subcutaneous tumors developed were small, and were deemed not sufficient for future assessment of tumors (Figure 3.4).

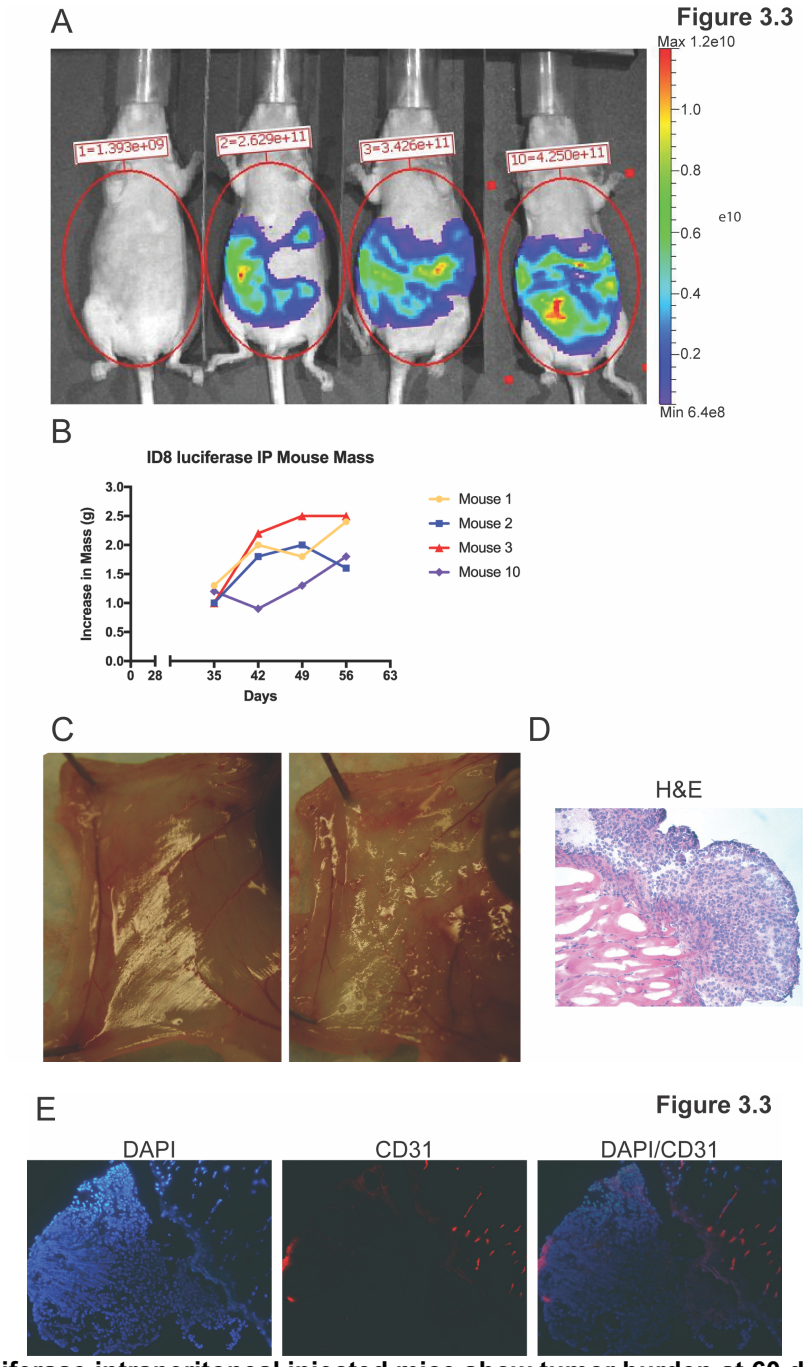

Figure 3.3 ID8 luciferase intraperitoneal injected mice show tumor burden at 60 days. **(A)** IVIS luminescent image displaying all ID8 luciferase intraperitoneal injected mice at day 60. The color shading on mice and the luminescent scale is in radiance (p/sec/cm^2/sr). Values with mouse identification number reflect total flux (p/s) within the designated red circles. **(B)** Graph displaying increase in mass in grams of each intraperitoneally injected mouse measured weekly compared to the first 4 weeks' average. Increase in mass does not appear to correlate with bioluminescent signal for amount of tumor burden in mice. **(C)** Left panel shows the dissected right peritoneal wall of mouse #1 with little to no visible tumor seeds. Right panel shows the dissected right peritoneal wall of mouse #2 with several visible tumor seeds. **(D)** Hematoxylin and eosin stain of a section of peritoneal wall from mouse #3 at 20x displaying the histology of a tumor seed attached to the peritoneal wall. **(E)** Immunofluorescent staining of peritoneal wall section of mouse #2 at 20x. Blue signal shows DAPI staining of DNA in the cell nuclei and red staining shows CD31 positive blood vessels.

Figure 3.4

A

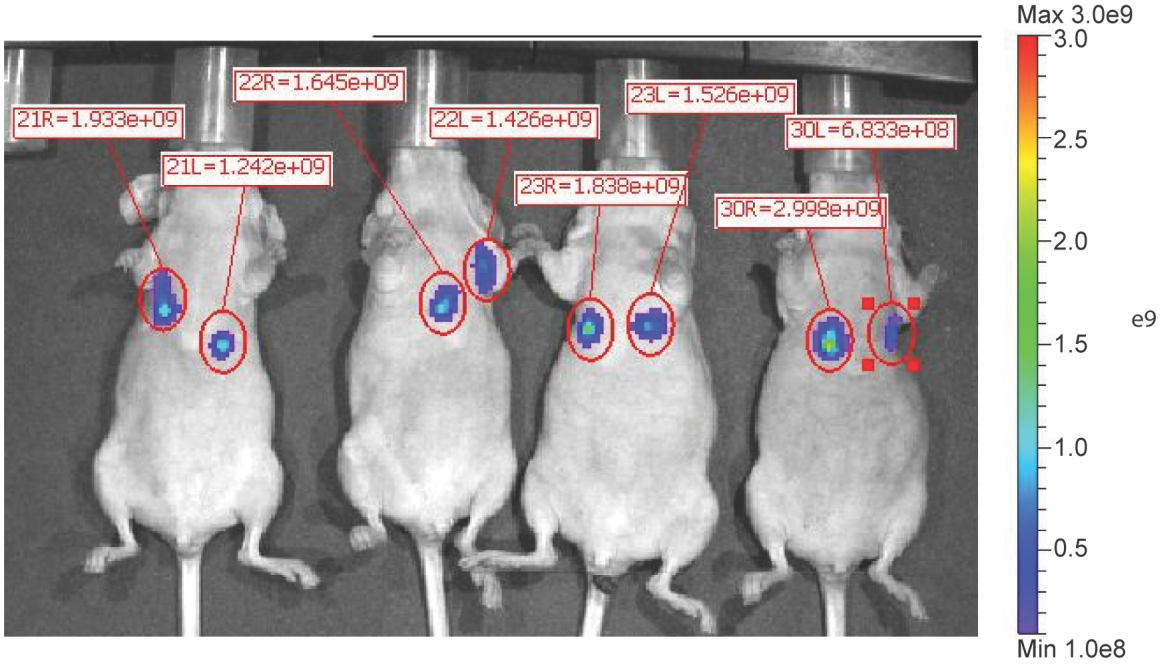

B

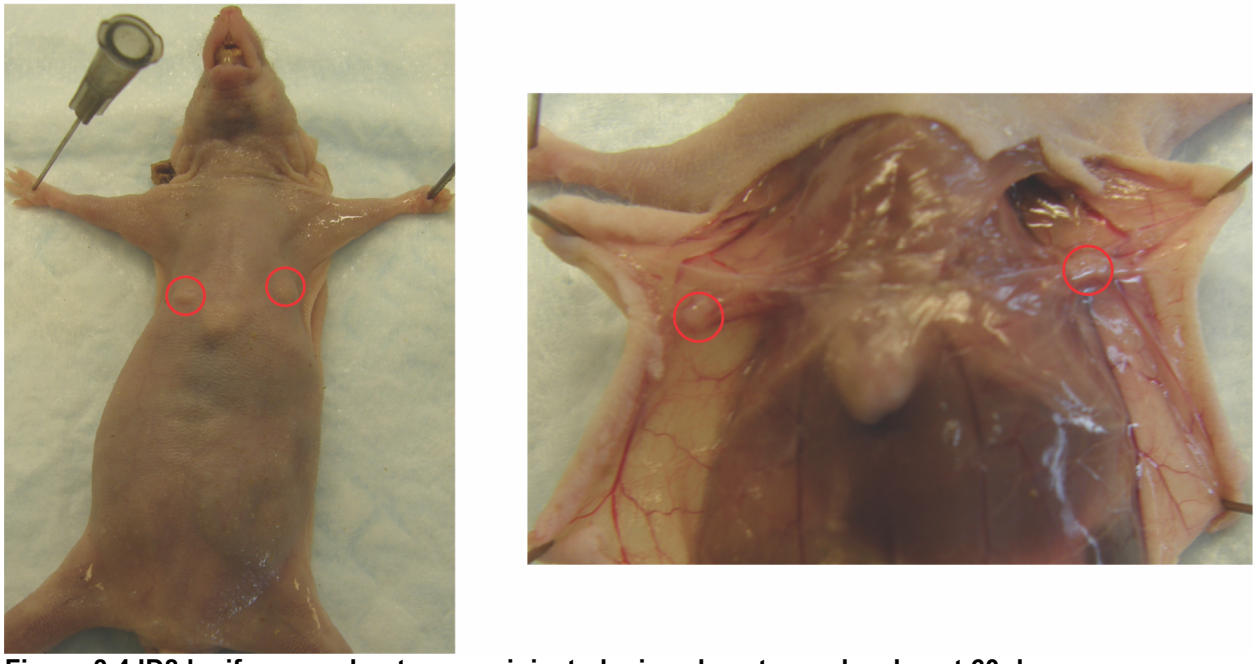

Figure 3.4 ID8 luciferase subcutaneous injected mice show tumor burden at 60 days.
(A) IVIS luminescent image of subcutaneous tumors at 56 days post injection. Image color and scale displays luminescence measured in radiance (p/sec/cm^2/sr). Red circles show area measured for total flux (p/s). Flux vales are listed in boxes with mouse number. **(B)** Image of mouse #30 subcutaneous tumors at time of sacrifice at 60 days. Left panel shows the ventral side of the mouse pre-dissection. Right panel shows a close up of the dissected skin of the mouse. Red circles indicate tumors.

To further examine intraperitoneal take and determine take in syngeneic C57BL/6 mice we carried out an experiment with 4 mice each of NCR nu/nu and C57BL/6 mice injecting $4x10^6$ ID8 cells IP into each mouse. Tumor signal was lost in C57BL/6 mice after 2 weeks in all mice injected. Mice were sacrificed on day 43 showing no visible tumor burden by IVIS (data not shown). NCR nu/nu mice were allowed to develop tumors for longer than in the previous experiment to determine if higher tumor burden and ascites would form, and to let tumors develop closer to the timeline originally reported with ID8 development. Mice were sacrificed between days 106 and 120. We monitored tumor burden via bioluminescent imaging weekly. We observed that tumor burden appeared to rise progressively through the experiment, but then started to reduce once the mice accumulated larger amounts of ascites at time points around 12 to 13 weeks. Mice developed larger peritoneal tumor seeds than in the shorter experiment, and developed more visible seeds on other peritoneal organs (Figure 3.5). One drawback to this model was that it took up to 120 days to generate tumor burden that was easily assessed.

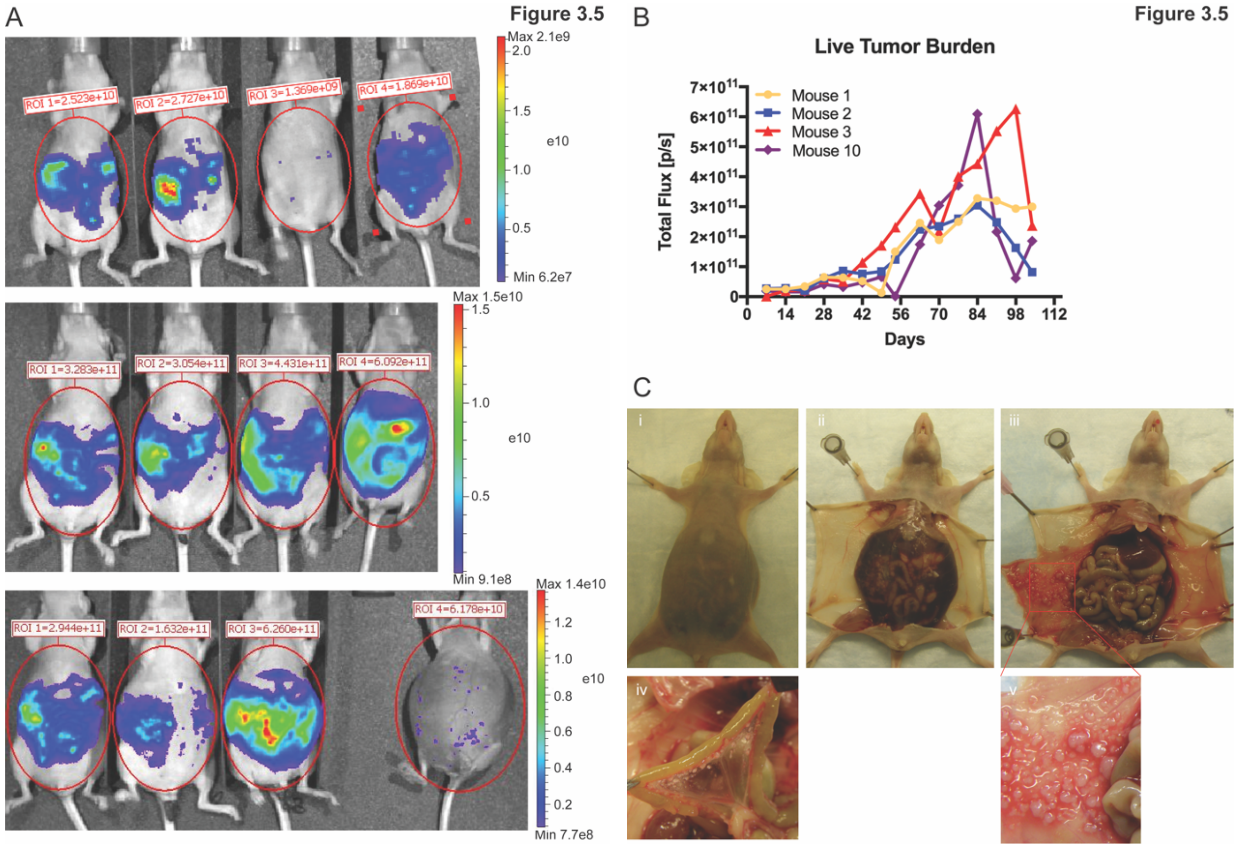

Figure 3.5 Time course analysis of tumor burden in ID8 luciferase intraperitoneally injected mice. **(A)** Live images of IVIS tumor burden at weeks 1, 12, and 14 in NCR nu/nu IP injected mice. Peak signal occurs around week 12 and then decreases with increasing ascites. **(B)** Weekly tumor burden displayed by total flux measurement of luminescence plotted for all 4 intraperitoneally injected NCR nu/nu mice. **(C)** Photographs from dissection of NCR nu/nu IP injected mouse #2. (i) Ventral mouse before dissection. (ii) Skin is dissected back, but peritoneal wall left intact. Bloody ascites is visible through the peritoneal wall. (iii) Peritoneal wall is dissected back and ascites fluid has been removed. Tumors can be seen on the peritoneal wall and organs. (iv) Close up photograph of ID8 tumor seeds on the intestinal mesentery. (v) Close up photograph of ID8 tumor seeds on the peritoneal wall.

ID8 IP2, an ID8 subline, generates similar tumor burden to ID8 at earlier time points

We completed *in vivo* examination of the ID8 IP2 line, a subline of ID8 acquired from Dr. Jill Slack-Davis at the University of Virginia School of Medicine. This subline was created by developing intraperitoneal tumors *in vivo* with the original ID8 line in C57BL/6 mice, and subsequently collecting and culturing the tumor cells *in vitro*. ID8 IP2 were passed through mice followed by culturing twice, thus the name "IP2" (Nakayama et al., 2015). ID8 IP2 had accelerated development of disease burden compared to the original ID8 line, with endpoint disease for ID8 IP2 at approximately 8-10 weeks, as opposed to approximately 20 weeks for ID8. This reduces tumor and ascites development time by half, while still resulting in a similar pattern of disease.

We modified the ID8 IP2 line to express luciferase by lentiviral infection with a FUW plasmid containing luciferase, mCherry, and puromycin resistance genes. Presence of luciferase was confirmed *in vitro* using Promega Dual-Luciferase® Reporter Assay System reagents, and visualization of mCherry expression was confirmed with fluorescence microscopy after lentiviral infection (data not shown).

We attempted *in vivo* tumor growth studies in both NCR nu/nu and C57BL/6 mice, to establish whether IP injection of ID8 IP2 luciferase (ID8 IP2 luc) cells generate metastatic peritoneal disease and ascites accumulation as expected. We intraperitoneally injected 4 NCR nu/nu and 4 C57BL/6 mice with $2x10^6$ ID8 IP2 luc cells in sterile phosphate buffered saline. Mice were followed with weekly IVIS and mass measurements. Some mice developed cachexia; among these some of the cachexic mice developed ascites and some did not. This pattern also occurs in human patient disease, where not every ovarian cancer patient develops ascites (Puls et al., 1996). At the time of sacrifice, the signal for the peritoneal wall tumor burden was assessed by IVIS. Since completing this investigation, other similar methods to track tumor burden at time of sacrifice via tumor reporter in dissected tissue of mice with ovarian cancer have begun to be used confirming our technique (Lewellen et al., 2016). Tumor sections from NCR nu/nu mice were stained for histology by H&E, as well as with endomucin by immune-fluorescence to detect vasculature.

3 of the 4 NCR nu/nu injected mice developed tumor burden and showed bioluminescent signal on weekly imaging and at endpoint. Mice with burden developed ascites, and displayed tumors on the

peritoneal wall and organs. Peritoneal wall luminescence exemplifying tumor burden at end point appeared to correspond to areas of tumor burden observed visually (Figure 3.6).

C57BL/6 ID8 IP2 luc injected mice showed poor bioluminescent signal via IVIS imaging, but 3 of the 4 mice developed ascites. One expects bioluminescent signal to decrease after large amounts of ascites accumulation develop, as seen in the ID8 luc experiments. When ID8 IP2 luc was implanted in C57BL/6 mice the IVIS signal drops below that of the initial tumor take, as expected, but then the signal remains low for the duration of the experiment until endpoint without ever recovering to initial levels. In the nude mice, as with the ID8 luc, once the tumor burden begins to rise it continues until ascites accumulation occurs (Figure 3.5, data not shown). For the ID8 IP2 luc experiments in C57BL/6, upon imaging the peritoneal wall at sacrifice, it was seen that only a subset of tumors visualized on the peritoneal wall were bioluminescent (Figure 3.7).

A second experiment where an additional 4 C57BL/6 mice were injected with $2x10^6$ ID8 IP2 luc cells displayed similar results where the bioluminescent signal did not correspond to all of the tumor seeds for each mouse at endpoint (Figure 3.8). In this second experiment, we measured circumference of each mouse weekly to measure ascites accumulation throughout the experiment. We calculated the percent increase in circumference at endpoint to represent the amount of ascites accumulation over the course of tumor development (Figure 3.8). The percent increase was determined by the circumference measurement around the widest part of the mouse abdomen at a given time point compared to the average circumference over the first 4 weeks before ascites accumulation occurs. We were able to remove ascites with a syringe through the peritoneal wall and measure the volume. Increase in ascites both visually and by volume appears to correlate with circumference, and may be useful to measure in this model.

The ID8 IP2 luc model looked promising as a model to evaluate ovarian cancer by following tumor burden with IVIS, but only in NCR nu/nu nude mice. These mice were able to generate tumors and ascites similar to the ID8 model, but in a shorter time frame. The histology of tumor seeds from both ID8 luc and ID8 IP2 luc appear similar indicating that ID8 IP2 luc are similar to HGSC since it has already been shown ID8 are similar to HGSC (Cho et al., 2013, Greenaway et al., 2008). In addition, in nude mice we were able to follow live tumor burden by bioluminescent imaging. We concluded that circumference measurement may

be a good way to measure ascites accumulation that is representative of disease burden and that tumors can be evaluated histologically if desired.

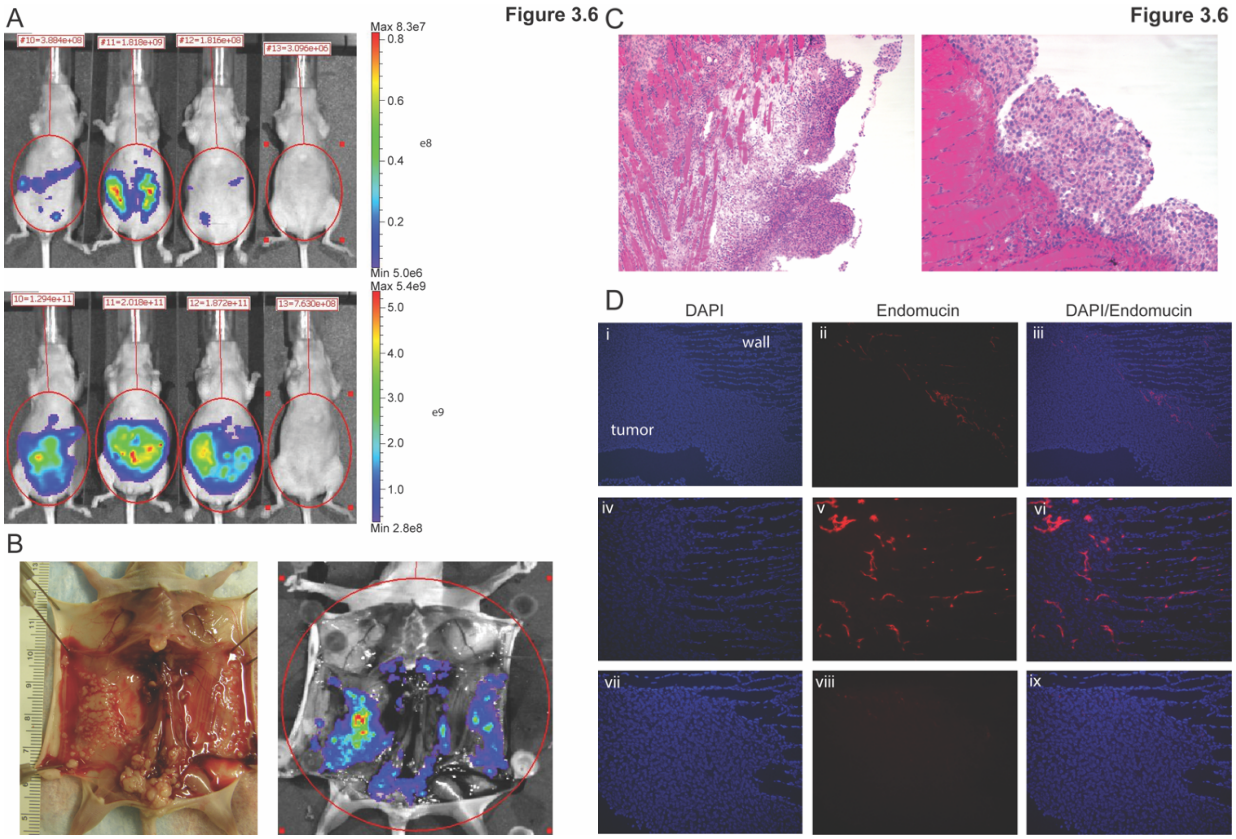

Figure 3.6 The ID8 IP2 luciferase line produces tumors when injected intraperitoneally in less time than the ID8. (A) IVIS imaging displaying tumor burden at 1 week (top panel) and 6 weeks (bottom panel). **(B)** Dissected peritoneal wall of mouse number 12 at endpoint on day 46. Left panel displays photograph of tumors in dissected mouse. Right panel shows IVIS imaging directly after sacrifice. Colored tumor burden signal on IVIS (radiance) at endpoint appears to match with tumors seen in the photograph of peritoneal wall. **(C)** Mouse number 11 peritoneal wall ID8 IP2 luc tumors stained with hematoxylin and eosin. Left panel shows a 10x photograph demonstrating tumor seeds infiltrating the peritoneal wall. Right panel shows a 20x photograph of a separate region of peritoneal wall and tumors attached to the surface. ID8 IP2 luc generate tumors that are consistent with the formation of ID8 tumors and with similar histology to ID8 tumors (Figure 3.3). **(D)** Mouse number 11 peritoneal wall sections with endomucin immunofluorescent staining for blood vessels. An example of the architecture of the tumor vs. the peritoneal wall in these immunofluorescent images is designated in (i). (i-iii) 10x section of peritoneal wall shows blood vessels by endomucin stain at the edge of the tumor seed on the wall. (iv-vi) 20x photo of area where peritoneal wall and tumor seed meet. This area appears rich in vasculature compared to the tumor seed and the rest of the visible wall. (vii-ix) a peritoneal wall tumor seeding section negative control for endomucin staining.

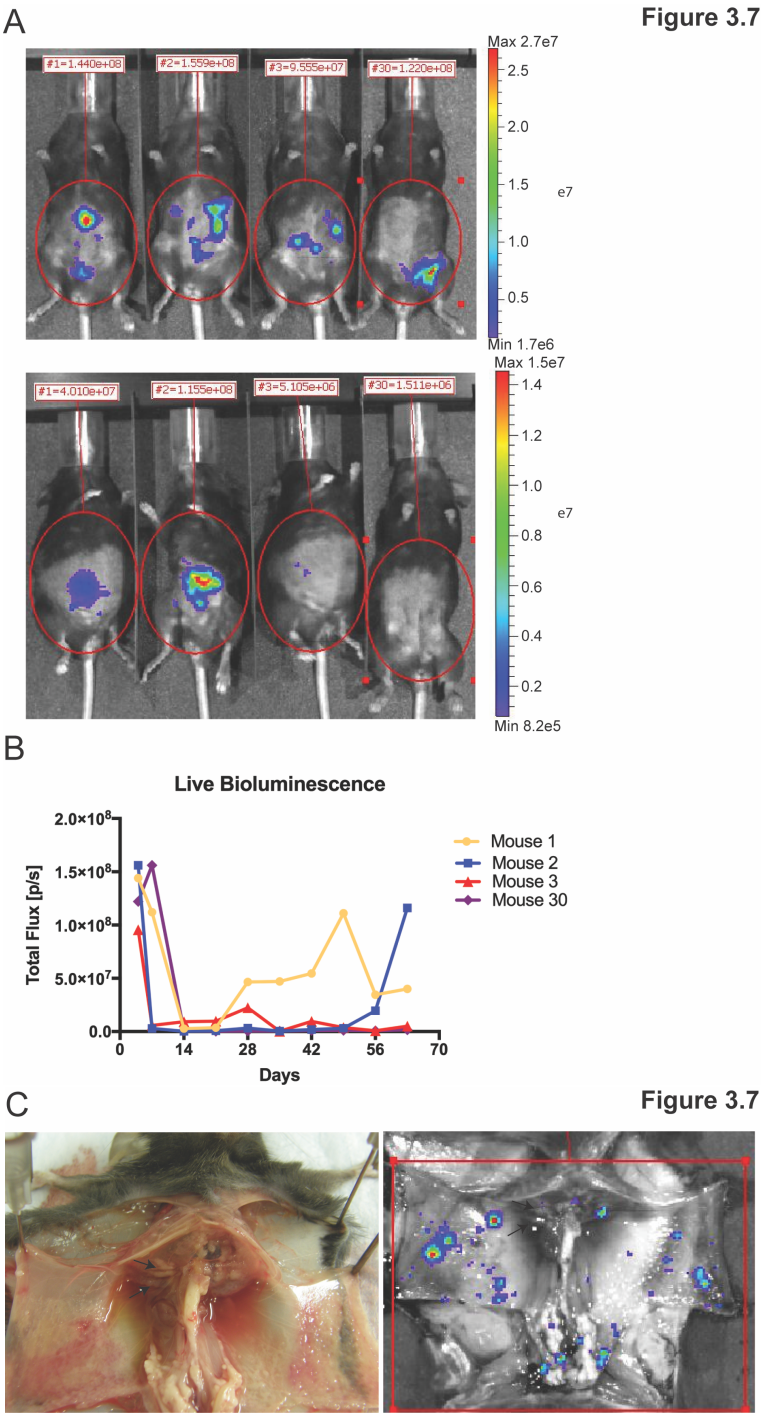

Figure 3.7 ID8 IP2 luc tumors may lose their bioluminescence when implanted intraperitoneally in vivo in immunocompetent mice. (A) Top panel shows mice 4 days after tumor injection and initial tumor take. Bottom panel shows mice at 9 weeks. Bioluminescent signal is reduced from initial tumor take despite ascites accumulation indicating disease development. **(B)** Graph displaying the measurable weekly tumor burden by bioluminescence for each mouse. Measured bioluminescence does not show a consistent pattern of growth. **(C)** Left panel shows dissected mouse #3 peritoneal wall. Right panel shows the same mouse imaged by IVIS for tumor burden. Not all tumors visualized show bioluminescent signal. This is most apparent on the diaphragm and the mouse's left peritoneal wall. Arrows denote some examples of these areas on the diaphragm.

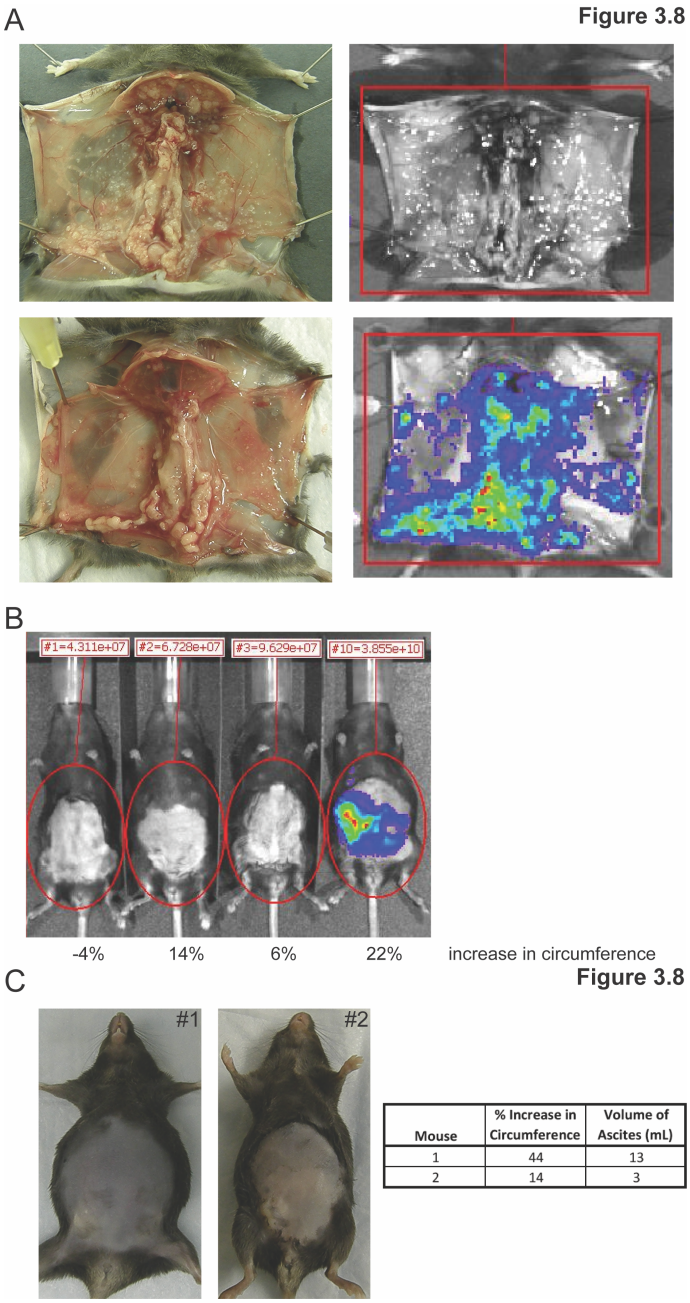

Mouse	% Increase in Circumference	Volume of Ascites (mL)
1	44	13
2	14	3

Figure 3.8 Bioluminescent evaluation of ID8 IP2 luciferase tumors implanted in C57BL/6 does not correlate with tumor burden but abdominal circumference measurement relates to ascites accumulation. (A) The top 2 panels show mouse #1 dissected at time of sacrifice. Despite the development of many tumors (left panel photo), there is no bioluminescent signal visualized on IVIS (right panel IVIS image). Bottom two panels show mouse #10 at the time of sacrifice. Tumors seen in photograph (left panel), appears to correlate with bioluminescent signal (colored radiance in the right panel). **(B)** All 4 mice at 9 weeks post tumor injection side by side for size comparison. Boxes show the total flux measured for bioluminescence per area in the circle (p/s). The percent increase in circumference at 9 weeks is displayed below each mouse. Increase in circumference does not appear to correlate with presence or absence of bioluminescent signal. **(C)** Photographs at time of sacrifice for mice #1 and #2. Note that mice were sacrificed at different time points (days 105 and 70 for mouse #1 and mouse #2 respectively) showing increase in ascites over time after injection. The percent increase in circumference at the time of sacrifice and the approximate volume of ascites collected from each mouse is displayed in the chart. The percent increase in circumference appears to correlate with amount of ascites.

Generation of an ID8 IP3 subline did not affect tumor development or bioluminescent tracking in syngeneic mice

To determine if there was a way to optimize the ability to track ID8 IP2 luc tumor seeds *in vivo* in immunocompetent C57BL/6 mice, we attempted another passage of the cells through mice by collecting tumor cells from a tumor bearing C57BL/6 mouse with high bioluminescent signal. We collected tumor cells from ascites, as well as from tumor seeds on the peritoneal wall. We subsequently sorted isolated tumor cells using flow cytometry by the mCherry in the original infected plasmid with the luciferase. Sorted cells were then cultured *in vitro*. We assessed the ability of these cells to develop tumors, and bioluminescent signal related to those tumors in mice. We identified these newly sorted cells as ID8 "IP3" luc cells. We injected 4 mice with ID8 IP3 luc ascites generated cells, and 4 additional mice with ID8 IP3 luc peritoneal wall tumor derived cells. All mice were injected with $2x10^6$ cells. We observed, however, that if tumors formed, there was a loss of bioluminescent signal with both types of tumors developed from cells derived from ascites and peritoneal seeds (Figure 3.9). There appeared to be no correlation between the live IVIS bioluminescent signal and the resultant amount of tumor burden observed at endpoint. All mice showed little to no signal on IVIS imaging even though they displayed varying amounts of tumor seeds upon dissection. These ID8 IP3 luc lines also generated fewer mice with tumor burden at similar time points to the previous assessment of ID8 IP2 luc in C57BL/6.

Figure 3.9

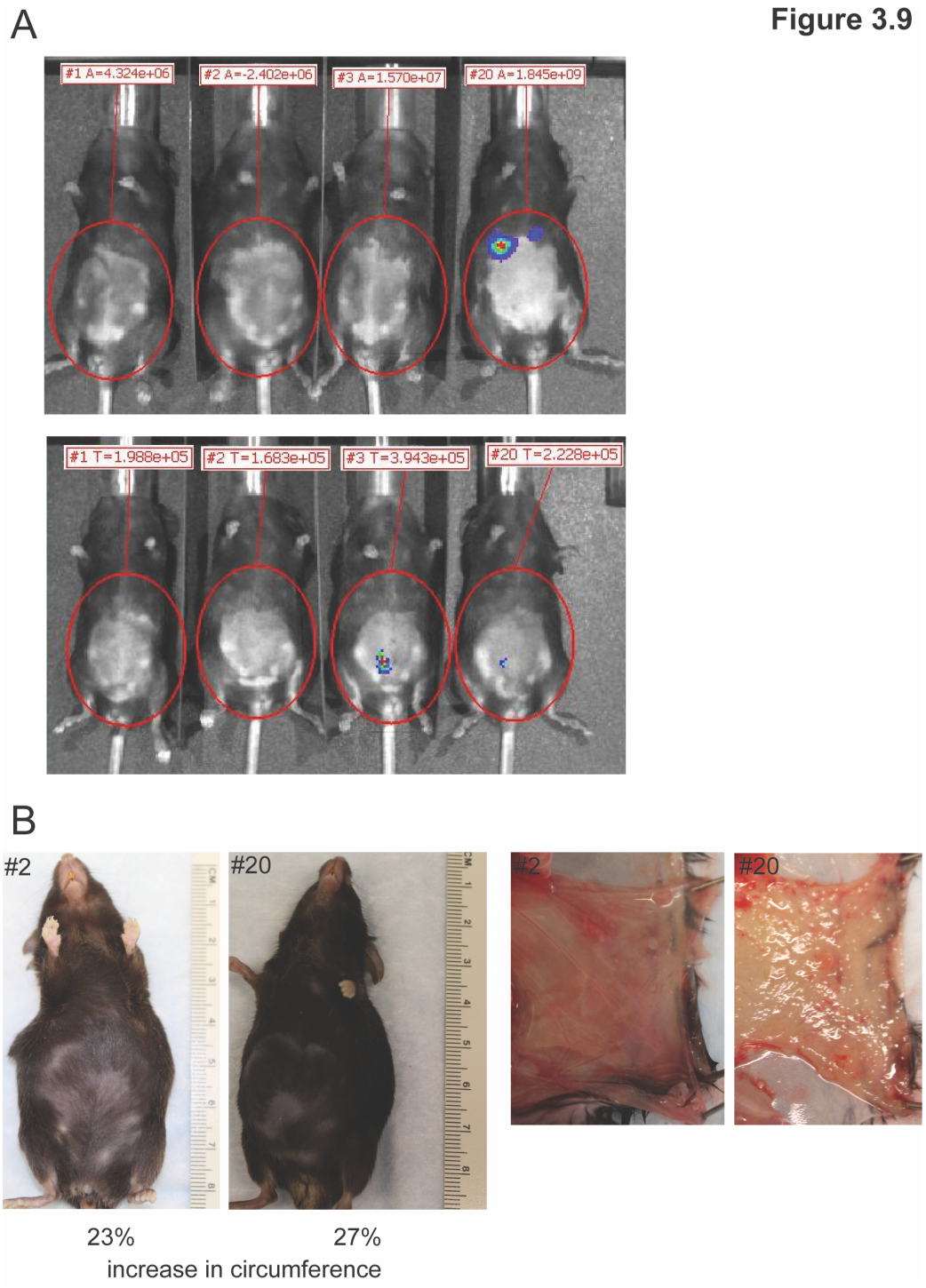

Figure 3.9 ID8 IP3 luciferase lines do not generate peritoneal tumors that display consistent bioluminescence with whole mouse live imaging. (A) Top panel shows mice intraperitoneally injected with ID8 IP3 luciferase ascites derived cells. The lower panel shows the mice injected with ID8 IP3 luciferase peritoneal tumor seed derived line. At 6 weeks, little bioluminescent signal by radiance is displayed. **(B)** Ascites derived ID8 IP3 luciferase tumor bearing mice. The left 2 panels show mouse #2 and mouse #20 at the time of sacrifice, and the percent increase in circumference at that time. The right two panels show the dissected left peritoneal wall of mouse #2 and mouse 20. There is a wide variation in the amount of visible tumor burden generated in injected mice on the peritoneal wall showing less consistent results in tumor generation for ID8 IP3 injected mice that generate ascites.

DISCUSSION

The experiments we conducted using the ID8 IP2 luc model generated tumors *in vivo* more quickly than other tested cell lines, such as ID8, while also generating intraperitoneal tumor seeds and ascites accumulation. Unfortunately, we found that the ability to track ID8 and subline tumors in C57BL/6 mice via bioluminescence was unreliable. One possible explanation for this loss of signal in tumors could be due to the interaction of these cells with host cells of the mice silencing the signal by one or several mechanisms. Previous analysis in one study has demonstrated similar loss of a fluorescent signal in a colon cancer model in immune competent rats (Garcia-Olmo et al., 2008). They observed a population of non-fluorescent cells within tumors, and a greater reduction in the proportion of fluorescent-positive tumor cells over progressive weeks of tumor development *in vivo.* Furthermore, they identified non-fluorescent tumors that demonstrated evidence of the GFP gene upon PCR analysis. In addition, none of the metastases identified in lymph nodes or the lungs in their study showed observable fluorescence (Garcia-Olmo et al., 2008). Eventually over time the tumor cells even lost the GFP gene, but still contained mutations from the original tumor not in the host cells. The authors speculate that recruitment of host cells to the tumor may be involved in generating tumor cells with no fluorescence (Garcia-Olmo et al., 2008). Perhaps host cells are generating additional tumor cells, or the immune system of these rats is silencing the expression of the reporter. Another study showed an increase in tumor cells and metastases observed by GFP fluorescence in a murine colon tumor model in SCID mice compared to C57BL/6 and nude mice at later time points suggesting a role of the immune system in silencing GFP positive tumor cells (Steinbauer et al., 2003). One study also demonstrated that three different syngeneic cancer lines lentivirally infected with a luciferase-GFP reporter lost bioluminescence in metastases in wild type albino C57BL/6 or FVB/N mice (Day et al., 2014). Furthermore, tumors generated *in vivo* from re-implantation of cells from bioluminescent metastases did not retain the same ability to bioluminesce. This seems similar to our unsuccessful attempt to increase bioluminescence with generation of the ID8 IP3 luciferase lines. Since the fluorescence used in these studies and the bioluminescence we use are introduced and act in similar ways as reporters in tumor cells described in the literature, we hypothesize similar mechanisms may be affecting signal from ID8 IP2 tumor cells grown in C57BL/6 mice. Perhaps the reliance of the ovarian model on metastatic tumor formation without a primary

solid tumor increases our loss of bioluminescent signal, as these studies indicate a particular loss of reporter activity related to metastases.

Based on our results demonstrating this lack of reliable bioluminescent signal to track tumor burden in C57BL/6 mice, we decided to conduct future experiments in NCR nu/nu mice. Despite the lack of a complete tumor microenvironment in nude mice, we wanted to be able to follow bioluminescent signal throughout disease development, and to assess tumor burden at endpoint in the peritoneal wall and other organs.

We also chose an ovarian derived mouse model (ID8) over a fallopian derived model based on the lack availability of fallopian derived mouse cell lines suitable for IP injection available at the time of experiments. We have more recently acquired murine fallopian derived tumorigenic cells lines from Dr. Joana Burdette at the University of Illinois at Chicago, which could be tested in the future as a model (Endsley et al., 2015). In addition, the human derived lines we tested failed to generate tumors as quickly and efficiently as our ID8 IP2 luc model, and ID8 have been shown to have characteristics such as morphology of tumors, ascites accumulation, and histological features similar to HGSC (Cho et al., 2013, Greenaway et al., 2008).

Thus, the ID8 IP2 luc in NCR nu/nu mice model was chosen to investigate *Notch3* signaling in ovarian cancer based on the ability to replicate HGSC and generate tumors and ascites in a much faster time period, with injection of fewer tumorigenic cells. Using the ID8 IP2 line, we observed large tumor seeds and more robust ascites development at similar time points than that of other tumor models we tested. Importantly, studies of ID8 IP2 luc in NCR nu/nu allowed us to follow tumors by IVIS throughout the development of tumors and at end point.

CHAPTER 4

NOTCH3 INTRACELLULAR DOMAIN AFFECTS ASCITES ACCUMULATION AND REDUCES SURVIVAL IN TUMOR BEARING MICE

INTRODUCTION

NOTCH3 expression has been found to associate with the severity of ovarian cancer. Elevated NOTCH3 expression in ovarian cancer patients has been linked to shorter overall survival and more advanced tumor stage, grade, and ascites accumulation (Hu et al., 2014, Jung et al., 2010, Liu et al., 2016, Park et al., 2010, Park et al., 2006b). NOTCH3 expression is correlated with chemotherapy resistance and recurrent tumors in patients (Park et al., 2010, Rahman et al., 2012).

NOTCH3 is thought to promote viability of ovarian cancer cells. Cell lines with high *Notch3* expression have been shown to display reduced viability and increased apoptosis when NOTCH3 is inhibited by either GSI or siRNA knockdown (Hu et al., 2014, Park et al., 2006b). In particular, NOTCH3 has specifically been linked to viability of ovarian tumor cells being treated with chemotherapeutic agents and tumor cells that have demonstrable resistance to chemotherapy. Ovarian cancer cells grown *in vitro* high in NOTCH3 treated with platinum or already chemotherapy resistant have reduced viability, increased apoptosis, and display a reduced IC_{50} of cancer cells in the presence of a Notch inhibitor (Park et al., 2010, Rahman et al., 2012). Under treatment with chemotherapy, ectopic overexpression of NOTCH3 intracellular domain (ICD) in ovarian cancer cells exhibit increased viability, reduction in apoptosis, increase in IC_{50}, as well as increased expression of proteins involved in epithelial to mesenchymal transition (Gupta et al., 2013, McAuliffe et al., 2012, Park et al., 2010). NOTCH3 expressing ovarian cancer lines implanted in mice respond to combined chemotherapy and Notch inhibition, as exhibited by a reduction of tumor burden and tumor microvasculature density on staining (Groeneweg et al., 2014a, Hu et al., 2014, McAuliffe et al., 2012, Shah et al., 2013).

Our goal is to discover the mechanism by which NOTCH3 expression in ovarian cancer cells contributes to increased tumor development, viability of cancer cells, poor survival, and chemotherapy resistance. This understanding will lead to better treatment strategies and shed light on major hurdles in treatment which arise from late stage of detection, poor response to chemotherapy, and high rate of

recurrence of ovarian cancers. We will confirm the previous aforementioned results which used human ovarian cancer cells with high NOTCH3 by using a ID8 IP2 mouse ovarian cancer cell lines. ID8 IP2 have the ability to seed intraperitoneal tumors in mice that display similarities to HGSC. This line has been programmed to express luciferase (ID8 IP2 luc), thus optimizing our ability to follow tumor development (see Chapter 3). ID8 IP2 develop tumors faster than the rates of tumor growth described for other lines (see Chapter 3). We hypothesize that introduction of ectopic NOTCH3 ICD into the mouse ovarian surface epithelial cell line ID8 IP2 luc will induce growth, increased viability, and chemotherapy resistance of these tumorigenic cells. Furthermore, we hypothesize that these *Notch3*-activated ovarian cancer cells will become faster-growing tumors *in vivo* and lead to a reduction of survival in tumor-implanted mice.

RESULTS

ID8 IP2 cells have low expression of *Notch3*

We were seeking to the confirm the published effects of NOTCH3 in human ovarian cancer cells so we could subsequently investigate the mechanism of the influence of *Notch3* upregulation in ovarian cancer in mice. We explored the use of the ID8 IP2 line to address this goal since we had previously determined its efficacy in producing intraperitoneal tumors *in vivo.* We evaluated the level of Notch protein, Notch pathway component genes, and Notch ligand genes present in the ID8 IP2 line. Ovarian cancer cell lines with known expression of Notch pathway components were used as controls (Figure 4.1). Semi-quantitative RT-PCR indicated no observable Notch3 was present in ID8 IP2 cells upon visualizing agarose gel electrophoresis with PCR products. However, Notch receptors *Notch1*, *Notch2*, and *Notch4* were present in ID8 IP2 cells. Ligands present include *Jag1* and *Dll1*, however *Dll4* was not observed. These results indicate expression of Notch pathways genes in the ID8 IP2 lines at the RNA level (primers Appendix Table A4.1). The lack of NOTCH3 protein expression in the ID8 IP2 line was confirmed by western blot analysis using known NOTCH3 expressing human ovarian cancer lines as a positive comparison (Figure 4.1) (McAuliffe et al., 2012, Park et al., 2006b, Hu et al., 2014). The parental ID8 line also appears to have low levels of NOTCH3 observed on western blot (Figure 4.1), but expresses fewer other Notch receptors, which may confound our results. However, using the ID8 IP2 line is preferable to the original ID8 line, since it develops tumor seeds more efficiently and faster; an advantage for future *in vivo* studies (Chapter 3). ID8 IP2 lacked detectable expression of NOTCH3. As noted, NOTCH3 is specifically linked to high grade serous ovarian cancer. We therefore concluded that ID8 IP2 was an appropriate model for investigating NOTCH3 effects on ovarian cancer cells by experimentally promoting Notch3 signal activation.

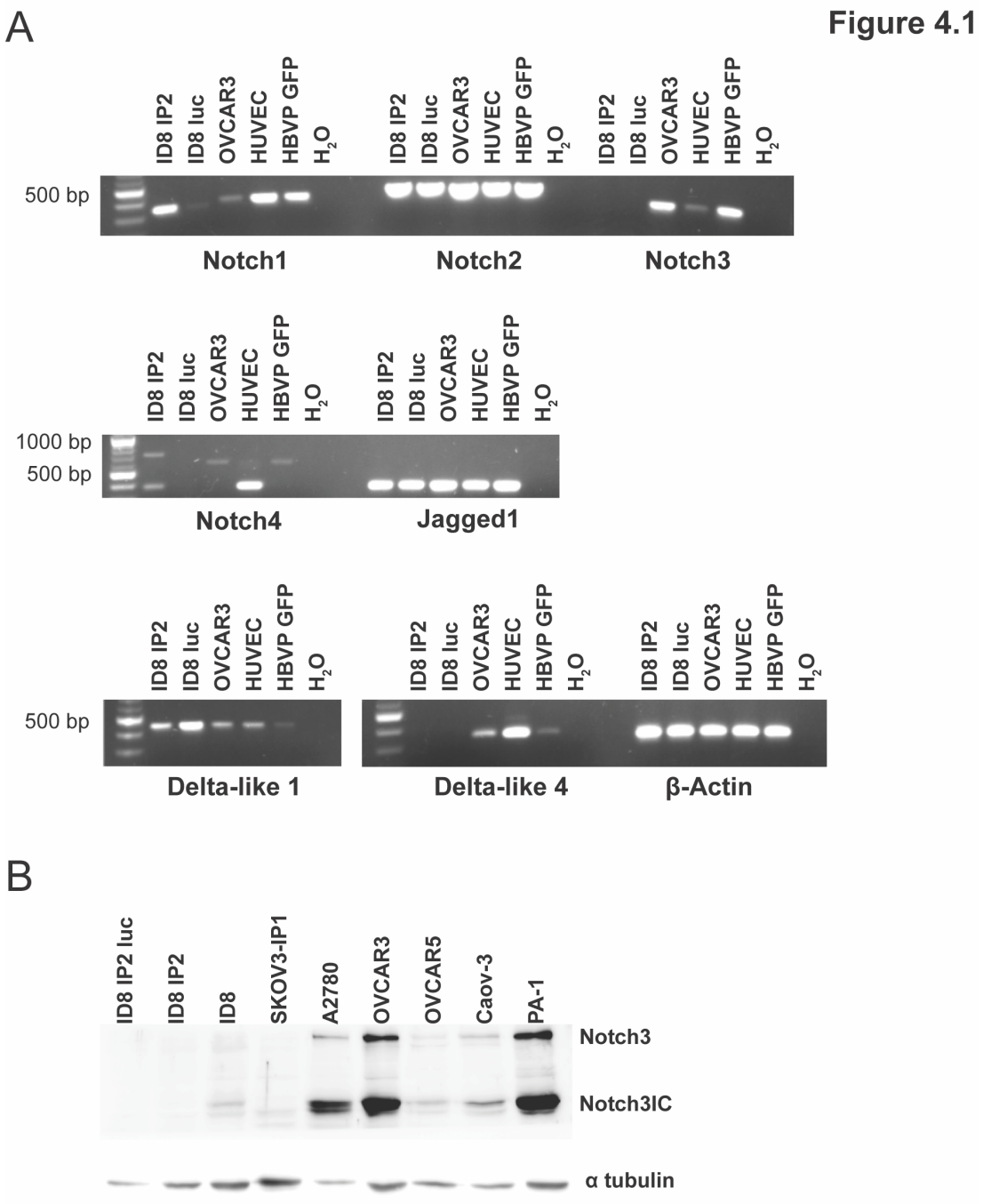

Figure 4.1 NOTCH3 is not notably expressed in ID8 IP2 ovarian tumorigenic cells.
ID8 IP2, its parental line ID8, and other cells lines with known Notch receptor and ligand status were evaluated. HUVEC are human endothelial cells known to express *Notch1*, and *4*, but not *Notch3* (Kofler et al., 2015). HBVP are human pericytes known to express high levels of *Notch3* (Kofler et al., 2015). Lanes marked H_2O are negative for cDNA and molecular grade water was added instead of cDNA sample. Primers are listed in Appendix Table A4.1. **(A)** Semiquantitative RT-PCR demonstrating cDNA for *Notch1*, *Notch2*, and *Notch4* receptors, but no observable *Notch3* cDNA in ID8 IP2 cells. ID8 IP2 cells also show *Jagged1* and *Delta-like 1* ligand expression. **(B)** Western blot demonstrating lack of NOTCH3 protein expression in ID8 IP2 and ID8 IP2 luc ovarian cancer lines. SKOV3 are known to be NOTCH3 negative. All other non-ID8 lines have previously been shown to express NOTCH3 (Park et al., 2006b, McAuliffe et al., 2012, Hu et al., 2014).

Generation and characterization of NOTCH3 expressing ID8 IP2 cells

Human high grade serous ovarian cancers display increased expression of full length *Notch3* or increased copy number of the *Notch3* gene. We introduced the *Notch3* intracellular domain into ID8 IP2 cells, as the intracellular domain ensures robust ligand-independent signaling. Using the intracellular domain removes the requirement for ligand interaction and the S1-S3 cleavage events needed for Notch3IC to activate signaling in the nucleus (Kopan and Ilagan, 2009, Radtke et al., 2005). Robust and constitutive Notch3 signaling can therefore occur without direct contact with ligand presented by other ID8 IP2 cells or other potential ligand-presenting cells in the environment. In preliminary experiments, we have introduced full length *Notch3* into ID8 IP2 cells, and while protein expression was confirmed by western blot, active signaling induced by ligand from tumor or other cell types was never confirmed (Appendix Figure A4.1).

We engineered the ID8 IP2 luciferase (ID8 IP2 luc) line to drive the expression of the *Notch3* intracellular domain. Cells were lentivirally infected with pCCL plasmids containing human phosphoglycerate kinase promoter upstream of either the mouse *Notch3* intracellular domain (Notch3IC) or empty vector (Control) (Dull et al., 1998). The Notch3IC construct was modeled after published *Notch3* ICD (Beatus et al., 1999) and contains a C-terminal HA tag fused to the *Notch3* intracellular domain centered around the Ankyrin repeats (codons 1664-2318 (Lardelli et al., 1996)) followed by an Internal Ribosome Entry Site (IRES) GFP (Kofler et al., 2015). The control vector used was the unmodified pCCL plasmid with only the multiple cloning site downstream of the promoter. A total of five independently generated cell lines were used as Notch3IC and Control biological replicates.

We confirmed the presence of Notch3 mRNA and protein in lentivirally infected cells to ensure effective expression was achieved. Western blot analysis using antibodies against the NOTCH3 ICD demonstrated expression of NOTCH3 ICD in Notch3IC cells (Figure 4.2). Quantitative RT-PCR confirmed the presence of *Notch3* mRNA in these lines (Figure 4.2, Table 4.1). We confirmed activation of *Notch3* signaling across all five sets of lines by demonstrating increased expression of *Notch3* downstream targets relative to Control lines via RT-qPCR (primers Appendix Table A4.2). A significant increase in downstream *Notch3* targets *Hey1* and *HeyL* was seen compared to Control (Figure 4.2). We observed very little change in *Hes1*, which is a known target of other *Notch* receptors but does not typically respond well to *Notch3* signaling, indicating that our *Notch* activation was specific to *Notch3* (Beatus et al., 1999, Shimizu et al.,

2002, Ong et al., 2006). We were therefore confident that *Notch3* specific signaling was active in these ID8 IP2 luc Notch3IC cell lines. Since *Notch3* signaling was successfully induced in ID8 IP2 luc, the matched Notch3IC and Control lines were used to evaluate the growth, tumorigenic, and metastatic properties influenced by *Notch3* in ovarian cancer.

Figure 4.2

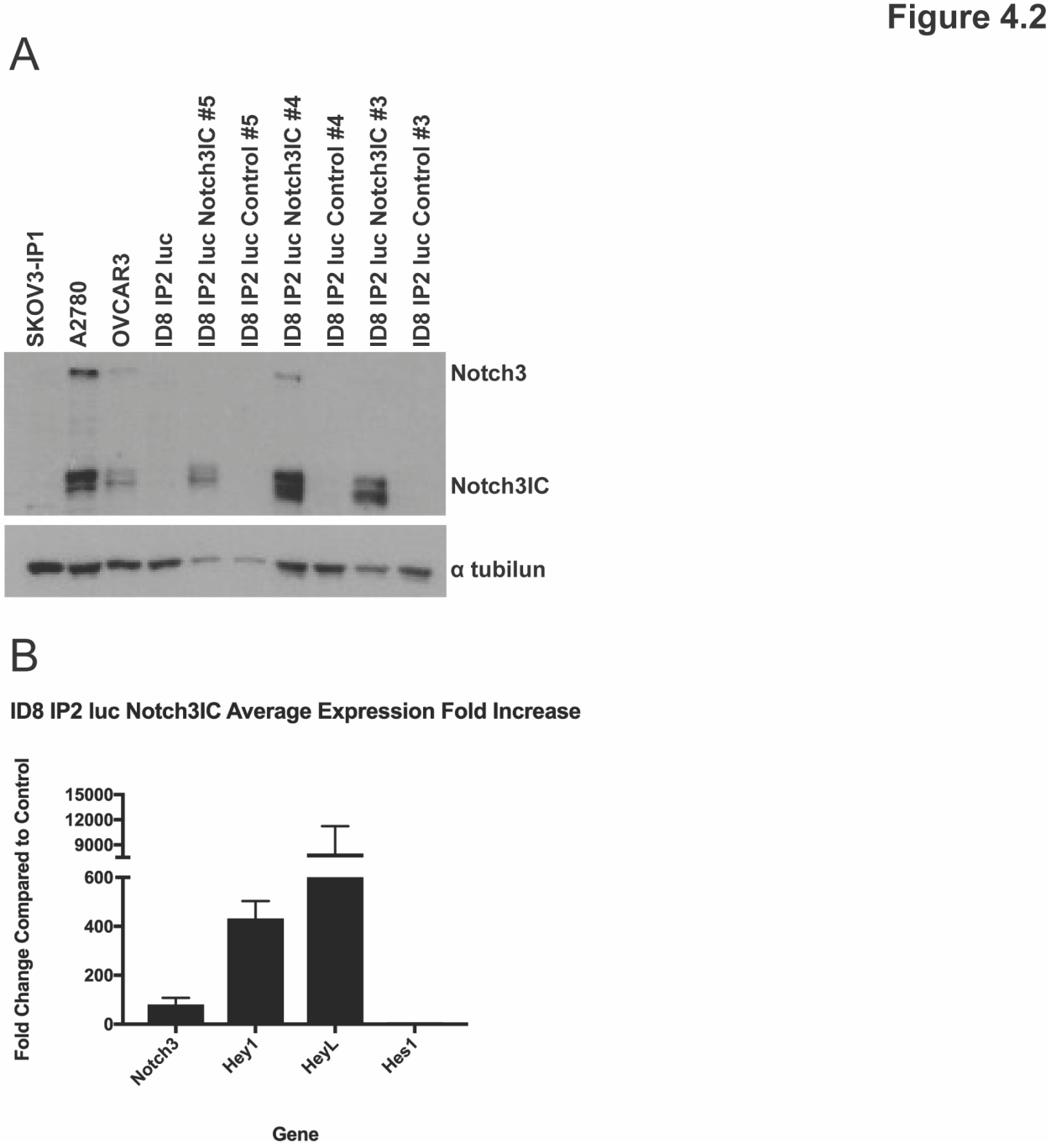

Figure 4.2 Notch3 expression and signal activation is present in lentivirally infected ID8 IP2 luc cells. **(A)** Western blot demonstrating increased NOTCH3 ICD in Notch3IC infected ID8 IP2 luc compared to Control infected cells. OVCAR3, A2780 and SKOV3-IP1 are used as positive and negative controls as described above. **(B)** RT-qPCR demonstrating *Notch3* and downstream *Hey* targets increase in gene transcripts for Notch3IC compared to Control. No induction of *Hes1* was observed. Graph displays the average of the 5 sets of infected lines. *Notch3* primers are targeted to sequence in the intracellular domain, and therefore should recognize both endogenous and exogenous *Notch3*. Primer sequences are in Appendix Table A4.2.

ID8 IP2 Luc	*Notch3*	*HeyL*	*Hey1*	*Hes1*
Set 1	67.52	4219.01	579.49	2.43
Set 2	13.23	3636.05	198.33	1.35
Set 3	118.64	13771.97	476.06	1.15
Set 4	164.50	17569.83	560.19	0.93
Set 5	38.70	667.23	346.19	1.44

Table 4.1 Notch3 and downstream target activation for each lentiviral infected line set shows consistent activation of the Notch pathway. The difference between Control and Notch3IC expression of *Notch3* and downstream target genes in each set of lentiviral infections, as measured by RT-qPCR. *Notch3, HeyL,* and *Hey1* all increase in fold change compared to Control, while Hes1 shows little fold change for all 5 sets.

NOTCH3 ICD expression did not promote significant changes in ID8 IP2 growth properties

We first sought to confirm an increase in growth of ovarian cancer cells based on the evidence in the literature for a role of Notch3 in the growth and viability of different ovarian cancer cell lines. ID8 IP2 luc Notch3IC and Control lines were evaluated for viability/proliferation by seeding $2.5x10^3$ cells per well and staining after 48 hours with WST-8, a tetrazolium salt, which indicates viable cells (Berridge et al., 2005). We also evaluated anchorage independent growth by quantitating colony formation on soft agar. Based upon previous studies, we expected that expression of NOTCH3 ICD would increase the viability and colony forming ability of ID8 IP2 ovarian cancer cells. The results, however, indicated no significant difference in the viability or anchorage independent growth of Notch3IC activated ovarian cells ($p = 0.9397$, $p = 0.9927$ Welch's t-test, Figure 4.3).

After determining that there was no apparent increase in viability for NOTCH3 ICD expressing cell lines, we considered this may be due to a heterogeneous population of Notch3IC infected and non-infected cells. We therefore sought to purify a set of cells that uniformly expressed Notch3IC at high levels. Using a freshly infected matched set of Notch3IC and Control ID8 IP2 lines, we sorted the Notch3IC line for GFP, which has an IRES-GFP and therefore co-expressed with NOTCH3 ICD (Appendix Figure A4.2). The Control cell line did not express GFP and thus were sorted for mCherry (expressed from a previously infected construct) to ensure similar treatment of Notch3IC and Control ovarian cancer cell lines. The GFP-high expressing population therefore should have higher NOTCH3 ICD expression, since these are cells that incorporated the pCCL plasmid. We then compared the FACS-sorted Notch3IC to Control by a WST-8 assay to determine if uniformly positive NOTCH3 cells would now display an increase in viability. However, Notch3IC activated cells displayed significantly reduced cell count determined by 450nm absorbance of WST-8 indicating a loss of living cells compared to Control ($p = 0.0022$, Welch's t-test) (appendix Figure A4.2). FACS-sorted lines were analyzed in additional assays as well that demonstrated further results differing from data collected on the heterogeneous population of infected cells (appendix Figure A4.2). We interpreted these results as evidence that very high levels of NOTCH3 ICD may be deleterious to cell viability.

We sought to confirm the effect of NOTCH3 expression on chemotherapy resistance previously described in the literature using our ID8 IP2 luciferase lines. We expected Notch3IC would display higher

amounts of cell survival/growth of cells compared to Control in the presence of chemotherapy. We therefore evaluated the effects of cisplatinum treatment on the growth of ID8 IP2 luc Notch3IC and Control ovarian cancer cells *in vitro*. Both lines were treated with cisplatinum at the following doses: 0μM, 2μM, 4μM, 8μM, and 16μM. The number of remaining live cells after cisplatinum treatment was assessed with a DIMSCAN instrument. The DIMSCAN cytotoxicity assay is a semiautomatic fluorescence digital imaging system, which quantifies viable cells using a fluorescein diacetate dye read by the instrument (Frgala et al., 2007, Keshelava et al., 2005). No significant difference was observed between ID8 IP2 luc Notch3IC and Control lines when evaluating the number of living cells after culture in the presence of cisplatinum. The $LogIC_{50}$, a measure of the inhibitory concentration at which 50% of cells are inhibited/ non-viable, was not significantly different between Notch3IC and Control cell line dose curves where $LogIC_{50}$ for Notch3IC and Control was 0.385 and 0.3796 respectively (Figure 4.3).

Figure 4.3

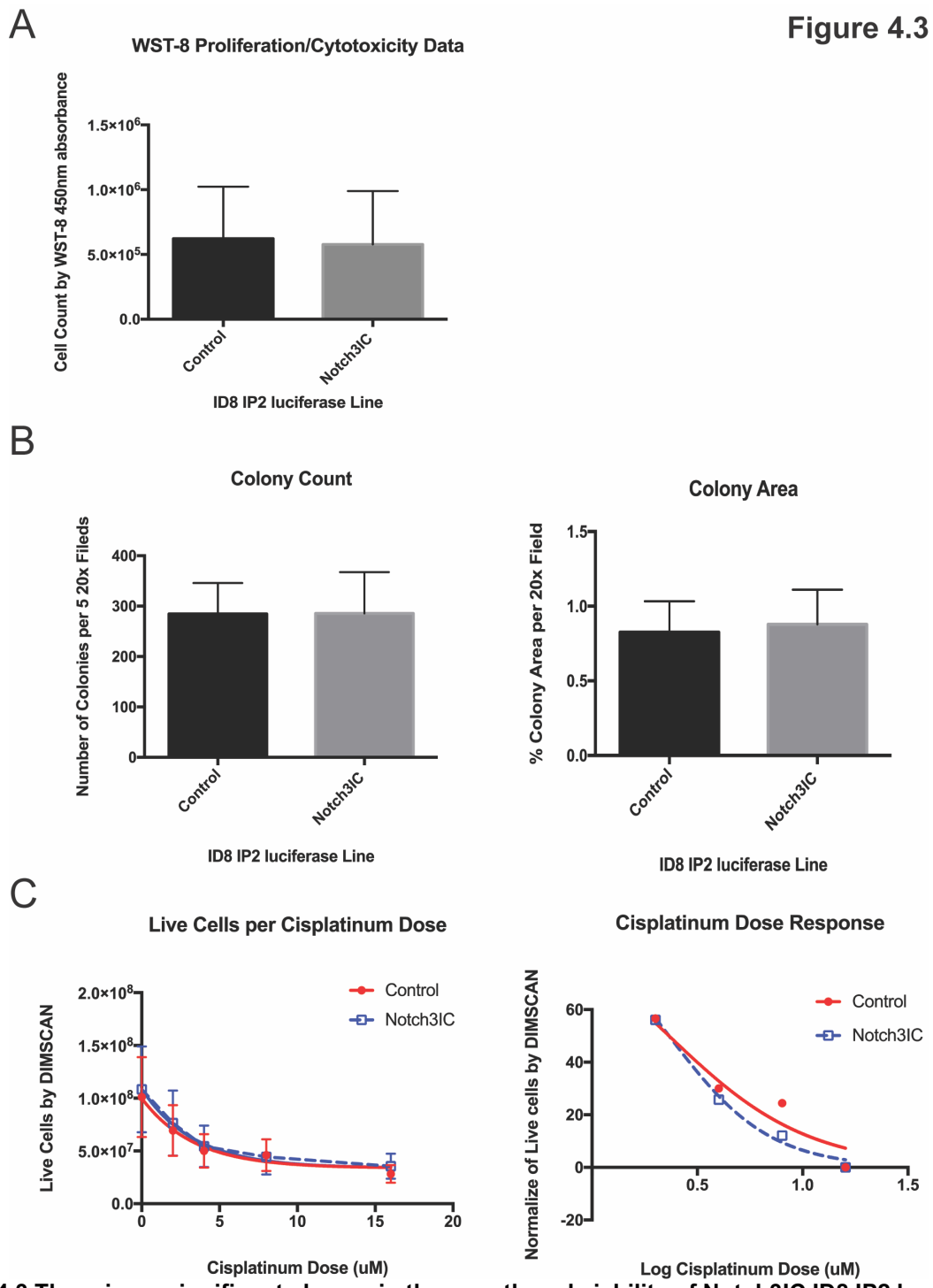

Figure 4.3 There is no significant change in the growth and viability of Notch3IC ID8 IP2 luc ovarian cancer cells *in vitro*. (A) A WST-8 assessment of growing Notch3IC and control cells showed no difference in the absorbance of WST-8 and therefore the number of viable cells after 48 hours of growth (p = 0.9397, Welch's t-test). **(B)** Colony formation in soft agar stained with MTT showed no significant change in the number of colonies or total colony area per well for Notch3IC compared to Control (p = 0.9927, p = 0.8744 Welch's t-test). **(C)** There is no significant difference in the response to cisplatinum chemotherapy treatment of Notch3IC and control cells for a direct count of surviving cells or for the $\log_{10}$ transformed and normalized data (p = 0.9466 nonlinear regression comparison of fit Y=100/(1+10^((X-LogIC50)))).

NOTCH3 ICD promotes ascites accumulation and reduces survival in mice bearing ID8 IP2 luc cells

Based on previous data demonstrating a correlation between NOTCH3 expression and poor patient survival we sought to assess the effects of Notch3 activation on tumor development and metastasis in mice. Despite the lack of effect *in vitro,* we hypothesized that Notch3 signal activation may influence ovarian cancer cell growth and metastatic spread when implanted in mice.

While ID8 cells are derived from C57Bl/6 mice and can be implanted into syngeneic immunocompetent mice, we decided to use nude mice to better track tumor burden via luciferase visualization throughout the experiment and at endpoint by IVIS Spectrum bioluminescent imaging (see Chapter 3). This choice was made as a result of apparent "quenching" of luciferase signal when ID8 IP2 luc cells were implanted in C57BL/6 mice (Chapter 3).

NCR nu/nu mice were intraperitoneally injected with $2x10^6$ ID8 IP2 luc Notch3IC or Control ovarian cancer cells. Successful formation of disseminated tumors from injected cells (i.e. "tumor take") was determined by weekly luciferin injection and imaging via IVIS spectrum. In addition to IVIS tumor burden assessment, ascites accumulation was determined using a circumference measurement around the abdomen of mice. Circumference measurements were done weekly and compared to the average of the circumference measured during the first 4 weeks post tumor injection in the same mouse, before high tumor take or ascites accumulation is normally observed. Mice were sacrificed when they reached a 25% or more increase in abdominal circumference. A small number of mice from both groups were also sacrificed based on cachexia criteria, but all tumor bearing mice were included in assessment. Cachexia was qualitatively determined by body condition score below 3 (Ullman-Cullere and Foltz, 1999) (Appendix Figure A4.3).

Notch3IC tumor bearing mice displayed reduced survival compared to Control using a Gehan-Breslow-Wilcoxon test ($p = 0.0183$, Figure 4.4). No significant difference was observed when analyzed with a Log-rank/Mantel-Cox assessment ($p = 0.0592$, Log-rank for the same experimental data). The Gehan-Breslow-Wilcoxon test does not assume a consistent hazard ratio across the experiment and weights early time points more, so a significant result with this test suggests that there is a greater difference in early deaths between groups (Martinez and Naranjo, 2010, Tarone and Ware, 1977). A total of 52 tumor-bearing mice were assessed (27 control and 25 Notch3IC). The median survival of Notch3IC mice was 4 days shorter than Control mice (65 vs. 69 days). In addition to the Kaplan Meier analysis, the mean survival of

Control mice was 72 days, while the mean Notch3IC mice survival time was 65 days ($p = 0.0356$, t-test) indicating the mice with Notch3IC active tumors succumb to disease a week sooner.

We compared the amount of ascites accumulation, an indirect measure of tumor burden, between Notch3IC and Control mice at 8 weeks after tumor injection. This time point was chosen as this is the time when we first started sacrificing mice due to an increase in circumference greater than or equal to 25% in the survival study (Figure 4.4). Circumference of each mouse was assessed to determine ascites accumulation for 69 total mice (35 Control, 34 Notch3IC). Notch3IC mice displayed significantly increased circumference by 5% over control, where the average increase in circumference for Notch3IC mice was 14.3% compared to the Control mice mean of 8.9% ($p = 0.0423$, t-test on direct data, $p = 0.0017$ on Log_{10} transformed data. Figure 4.4). The increase in absolute circumference was significantly increased for Notch3IC tumor bearing mice compared to Control; Notch3IC tumor bearing mice displayed an average increase of 1.08cm, whereas Control mice which showed an average increase of 0.69cm in circumference ($p = 0.0386$, Welch's t-test, Figure 4.4).

In one of the independent trials, with a cohort of 17 tumor bearing mice (8 Control and 9 Notch3IC), we assessed the peritoneal wall and ovary tumor burden at endpoint by measuring bioluminescent signal of these organs with the IVIS. We compared the total luminescent signal between Notch3IC and Control mice that were all sacrificed and measured at 8 weeks. There appeared to be a potential trend indicating more bioluminescent signal from tumors in Notch3IC tumor bearing mice, however, there was no significant difference between the tumor burden on the peritoneal wall or right ovary and uterine horn in Notch3IC mice compared to Control in this smaller set of assessed mice ($p = 0.1686$, $p = 0.2015$ respectively, Appendix Figure A4.4).

Taken together, this data show that Notch3IC activation in ID8 IP2 ovarian tumors reduces survival of the tumor bearing mice and leads to an increase in ascites accumulation. We interpreted these results as demonstration that NOTCH3 ICD expression my promote metastatic spread or influence the process of tumor-driven ascites accumulation.

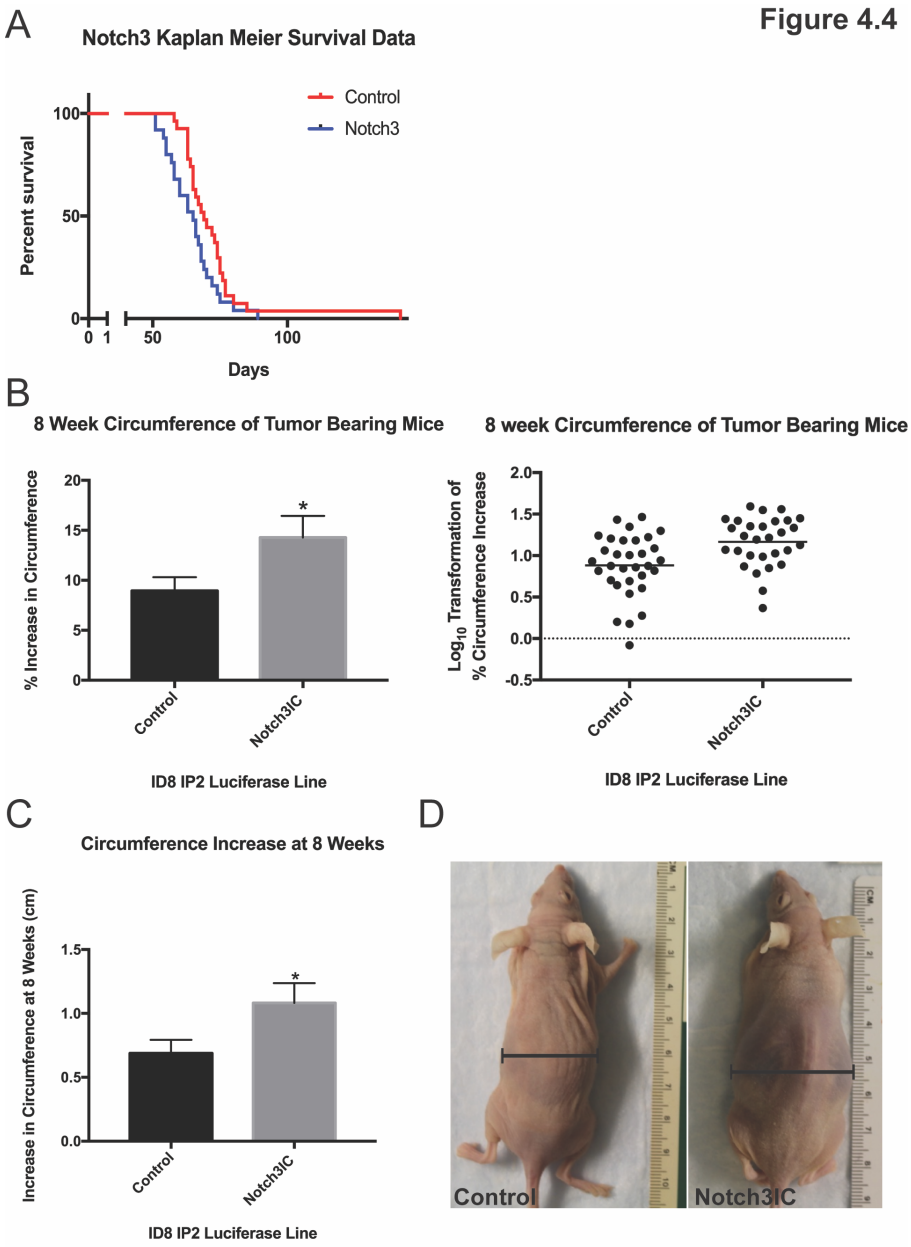

Figure 4.4 Notch3IC causes a reduction in mouse survival and an increase in disease burden *in vivo.* **(A)** Kaplan Meier survival curve demonstrating a significant decrease in survival for Notch3IC mice ($p = 0.0183$, Gehan-Breslow-Wilcoxon). **(B)** A significant increase in circumference and therefore ascites accumulation is observed in Notch3IC tumor bearing mice compared to Control at the 8-week time point ($p = 0.0423$, Welch's t-test on direct data, $p = 0.0017$ Welch's t-test on $\log_{10}$ transformed data). The log transformed data displays the distribution tumor bearing mouse population for Notch3IC and Control. **(C)** There is a significant difference in the absolute increase in circumference compared to pre-tumor burden circumference between Notch3IC and Control at 8 weeks. The increase in circumference is significantly higher in the Notch3IC tumor bearing mice ($p = 0.0386$, Welch's t-test). **(D)** Representative images of ID8 IP2 luc Control and Notch3IC tumor bearing mice sacrificed at 8 weeks. The Control mouse on the left has a 7.5% increase (0.5cm) increase in circumference, while the Notch3IC mouse on the left has a 11.6% increase (0.9cm) increase in circumference. These mice demonstrate an approximation of the visual increase in disease burden displayed in B and C. The Notch3IC tumor bearing mouse also displays increased signs of underconditioning (prominent spine) despite ascites accumulation increasing mouse mass and circumference.

DISCUSSION

We demonstrated that the ID8 IP2 ovarian cancer line has little to no expression of NOTCH3 and were able to robustly induce Notch3 signaling in these cells. Ectopic expression of NOTCH3 ICD in ID8 IP2 cells did not significantly alter the *in vitro* growth properties or survival of these mouse ovarian surface epithelial cells. This was contrary to previous results with other ovarian cancer cell lines, which respond to ectopic NOTCH3 ICD expression with increased growth and viability *in vitro* (Gupta et al., 2013, McAuliffe et al., 2012, Park et al., 2010). These experiments using other cell lines, however, were conducted under conditions of chemotherapeutic treatment, differing from the experiments we conducted with ID8 IP2 cells. The majority of previous studies linking Notch3 activity to increased growth or reduction of apoptosis were conducted in ovarian cancer cell lines expressing high levels of NOTCH3, and used reduced expression or inhibition to study the role of NOTCH3 (Hu et al., 2014, Park et al., 2006b). In contrast, we focused on ectopic expression to analyze an ovarian cancer cell with low Notch3 signaling. Both approaches have their merits. In ID8 IP2 cells, Notch3 signaling did not influence cisplatinum resistance (Figure 4.3). This is also contrary to *in vitro* and *in vivo* studies previously performed with different cell lines, which suggest Notch3 signaling promotes resistance to platinum therapy (Groeneweg et al., 2014a, Gupta et al., 2013, McAuliffe et al., 2012, Park et al., 2010, Rahman et al., 2012, Shah et al., 2013). One can speculate that the ID8 IP2 cell line represents an early stage ovarian cancer cell which has not acquired other alterations that may be necessary, and Notch3 may not be sufficient to cause these changes. Alternately, the ID8 IP2 cells may resemble another subtype of ovarian cancer.

The ID8 IP2 cell represented an excellent model for the study of metastatic spread of ovarian cancer. The analysis of Notch3 oncogenic function in ID8 IP2 cells uncovered a novel role for Notch as an oncogene by potential promotion of early metastasis. This early metastasis was defined by an accelerated disease burden/ascites; that is ascites accumulation was more significant at 8 weeks in ID8 IP2 Notch3IC bearing mice as compared to Control.

One must consider that the lack of an observable effect of Notch3IC on ID8 IP2 growth *in vitro* may stem from excessively high levels of NOTCH3 ICD being potentially toxic to the cells. Since we are using a constitutively active form of the NOTCH3 receptor that likely induces super-physiologic levels of Notch signaling, the NOTCH3 ICD may be toxic. The observation that cells subjected to FACS for a purer high

NOTCH3 ICD expressing population did show a reduction in viability of the Notch3IC cells compared to control indicates a possibility of toxicity to this line. It is difficult to know how our ectopic expression of NOTCH3 ICD compares to ovarian cancer cells with amplification of NOTCH3, and further examination of upregulation of full length NOTCH3 may be warranted.

We discovered that NOTCH3 signaling in ID8 IP2 cells leads to a significant increase in mortality, defined as endpoint triggered by measured ascites accumulation. The significant survival data indicated a role for earlier phase tumorigenesis or metastasis. The Gehan-Breslow-Wilcoxon assessment signifies that the risk of death for the Notch3IC mice is higher early on. The data suggest that Notch3 signaling may contribute to early steps in disease progression, such as adhesion and invasion of cells into the peritoneum, rather than later subsequent growth of established metastatic lesions. We therefore wanted to further investigate the mechanism of the differences between the Notch3IC compared to Control to determine what leads to the reduced survival and increased disease burden we observe in mice.

CHAPTER 5

NOTCH3 ACTIVATION IN ID8 IP2 OVARIAN CANCER CELLS AFFECTS EXPRESSION OF CELL ADHESION GENES

INTRODUCTION

After an increase in expression of the Notch3 signaling pathway components was found in ovarian cancer by TCGA analysis and other studies, there have only been a few attempts to investigate the downstream affected gene signature of NOTCH3 expressing ovarian tumors (Cancer Genome Atlas Research, 2011, Lu et al., 2004, Nakayama et al., 2007, Park et al., 2006b). Among a handful of genes correlated with *NOTCH3* high expressing ovarian cancer lines, Pbx1 has been shown to regulate survival of ovarian cancer cells in high NOTCH3 expressing lines (Park et al., 2008). It was also shown Col4a2 is upregulated in high NOTCH3 ovarian cancer lines and is associated with anoikis resistance through subsequent kinase activation (Brown et al., 2015). Another study found an association with expression of cell cycle checkpoint and nucleotide synthesis pathways to a high NOTCH3 expressing human cell line (Chen et al., 2012).

We wanted to comprehensively determine the downstream targets and pathways affected by Notch3 signal activation in the ID8 IP2 luc model to help elucidate the mechanism of NOTCH3 effect on ovarian cancer cells. In the previous chapter, we documented an effect on survival of tumor bearing mice and wanted to further determine what induced pathways could be the cause of this effect. The effect we observed on survival is consistent with studies showing a correlation in humans between poor prognosis and reduced survival with increased *NOTCH3* expression (Hu et al., 2014, Jung et al., 2010, Liu et al., 2016, Park et al., 2010). Since NOTCH3 is a transcriptional regulator, we used RNA-Seq analysis of our Notch3IC and Control ID8 IP2 luc lines to determine what pathways may be influenced by Notch3 signaling. This may give insight into what makes Notch3 active ovarian cancers more aggressive.

RESULTS

RNA-Seq analysis confirms that NOTCH3 ICD expression activates Notch targets

We determined that NOTCH3 signaling activation in ID8 IP2 luc cells reduced tumor-bearing mouse survival *in vivo*, and increased the disease burden of mice at similar time points. In addition, there was minimal effect of NOTCH3 on the growth of ovarian cancer cells *in vitro*. We, therefore, wanted to determine what pathways may be responsible for the effect we observed in our ID8 IP2 mouse model.

We evaluated the gene profile of the ID8 IP2 luc Notch3IC cells compared to Control by RNA sequencing (RNA-Seq) and interrogated the data to determine which pathways were influenced by NOTCH3 signaling. We hypothesized that pathways related to metastasis and peritoneal growth may be affected because our statistical analysis of the survival data indicating an early tumor phase effect, as well as the evidence that the effect was unlikely directly related to proliferation or survival of the cancer cells.

We evaluated 4 separate sets of ID8 IP2 luc Notch3IC and matched Control lines by RNA-Seq (Sets #1 - #4, previously described in Chapter 4). Briefly, these lines were generated by lentiviral infection of the tumorigenic mouse line ID8 IP2 luc with pCCL (Control), or pCCL containing the *Notch3* intracellular domain (Notch3IC). RNA was isolated from each line, and 30 million sequence reads for each line were obtained. Data collected from RNA-Seq was processed in Cufflinks software to generate counts, the number of reads for each gene determining expression level. The data was then assessed by DEseq software to determine the differential expression between Notch3IC and Control for the average counts per gene for repeated samples.

The generated counts were evaluated for Notch pathway genes in order to confirm that NOTCH3 ICD expression led to regulation of canonical Notch target genes. We found that the RNA-Seq data confirmed the data that we previously observed with RT-qPCR (See Chapter 4, Figure 5.1) for several Notch target genes. First, the gene *Notch3* was significantly enriched in Notch3IC lines. Several canonical Notch downstream targets such as *HeyL, Nrarp, Hey1,* and *Hey2* (adj p = 1.93E-04, adj p = 5.39E-06, adj p = 1.24E-05, adj p = 1.84E-04, adj p = 1.29E-04 respectively) were upregulated. The pattern of Notch target gene response was similar to the previously generated RT-qPCR data, with upregulation of *Hey* genes but not *Hes* genes, consistent with NOTCH3 signaling. This data adds to the confidence that NOTCH3 signaling is properly induced in the ID8 IP2 luc Notch3IC, and that the RNA-Seq data is accurate.

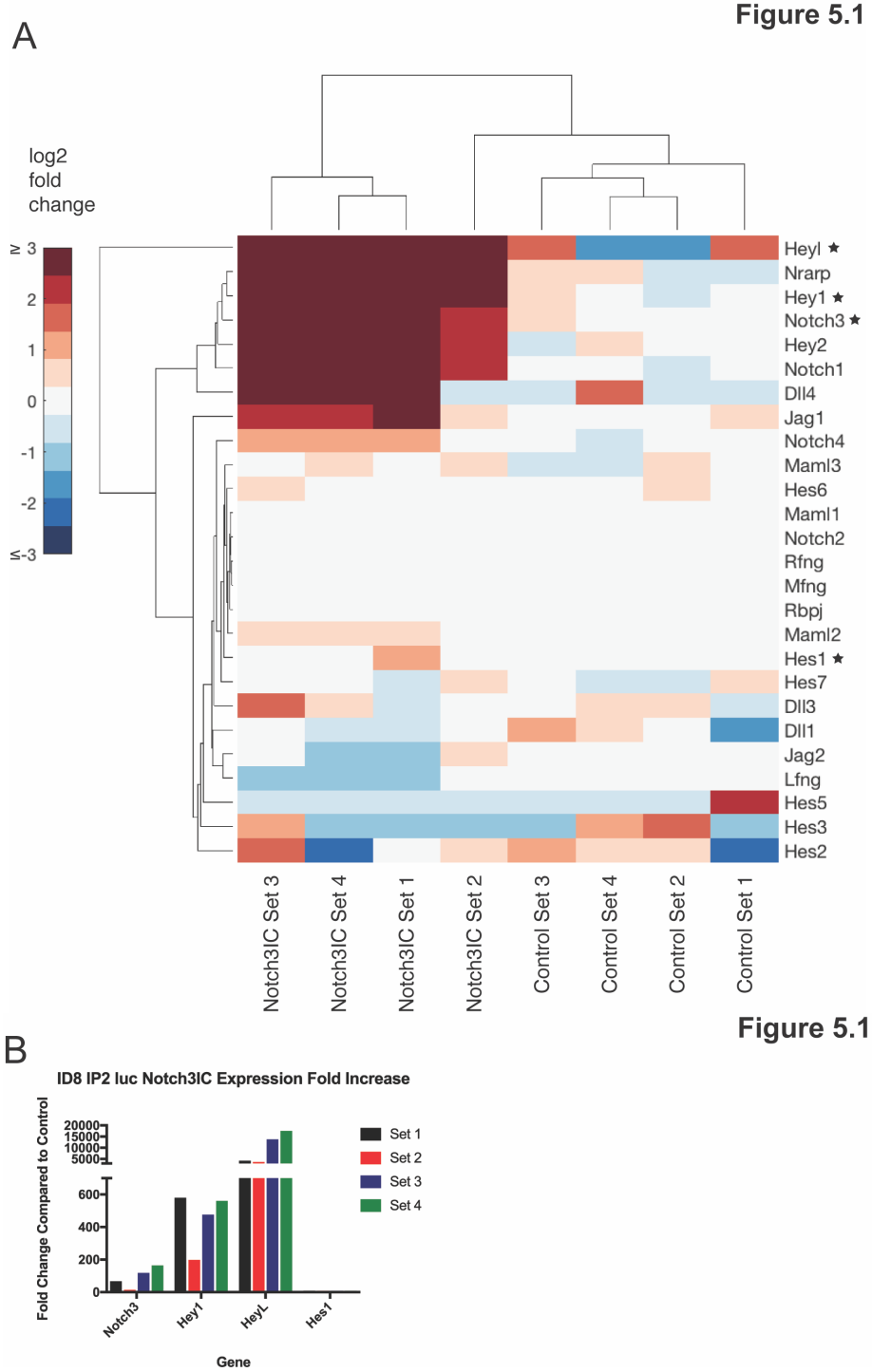

Figure 5.1

Figure 5.1 A Notch3 signaling signature is enriched in the RNA-Seq analysis of ID8 IP2 luc Notch3IC compared to Control. (A) Heat map showing $\log_2$ fold change of each ID8 IP2 luc line compared to the $\log_2$ fold change for the mean of the Controls. Genes represented are *Notch3* pathway and known Notch target genes. There is significant upregulation for *Notch3* and known downstream targets, demonstrating active *Notch3* signaling. Stars denote genes also assessed by RT-qPCR shown in B. **(B)** RT-qPCR data described in Chapter 4 for lentiviral infected Sets #1 - #4 of ID8 IP2 luc. Graph displays fold change for Notch3IC compared to Control for each line set. Data show a similar pattern, but greater magnitude, to changes observed in RNA-Seq data. See starred genes in A for comparison.

Analysis of RNA-Seq data uncovers pathways regulated by NOTCH3 ICD in ID8 IP2

In order to determine which pathways were altered in the NOTCH3 activated ovarian cancer cells, we examined our RNA-Seq data for up- or downregulated genes in Notch3IC lines compared to the Control. We chose genes to evaluate further by selecting genes with an adjusted p value < 0.1 and average $\log_2$ fold change ≥ 1 or ≤ -1(Appendix Figures A5.1 and A5.2). This created a list of 478 upregulated genes, and a list of 163 downregulated genes. We then subjected each list of genes to pathway analysis to determine which cellular pathways were most affected by the expression of the *Notch3* intracellular domain.

We completed pathway analysis in the Database for Annotation, Visualization and Integrated Discovery (DAVID) developed by the National Institute of Allergy and Infectious Diseases at the National Institutes of Health. Many pathways were affected, but we chose to focus on the most significantly upregulated pathways (Tables 5.1 and 5.2) from the 355 pathways identified as significantly upregulated across 4 databases.

We chose not to focus on enriched pathways determined from the genes significantly downregulated with adjusted p < 0.1 and $\log_2$ fold change ≤ -1 (appendix Figure A5.2). DAVID pathway analysis of downregulated genes produced fewer pathways to assess (76 pathways versus 355 pathways for upregulated genes). In addition, fewer genes were identified per pathway where all pathways found to be significantly enriched (p<0.5) all contained 10 or fewer of our selected downregulated genes, whereas our significantly upregulated pathways showed up to 56 of our selected upregulated genes identified within a pathway (data not shown). This is likely because fewer genes were significantly downregulated. This may be because the NOTCH3 receptor and its nuclear complex is a transcriptional activator. Of note, we did see some downregulation of cell adhesion pathways, described in further detail below, in this set (appendix Table A5.2). The remaining pathways may warrant further analysis in the future (appendix Table A5.1).

Pathway Database	Pathway Name	Gene Count	p Value	Fold Enrichment
KEGG	mmu04510:Focal adhesion	21	1.65E-08	4.66
KEGG	mmu04512:ECM-receptor interaction	14	4.18E-08	7.31
KEGG	mmu04151:PI3K-Akt signaling pathway	25	4.51E-07	3.27
KEGG	mmu05410:Hypertrophic cardiomyopathy (HCM)	10	4.70E-05	5.82
KEGG	mmu05412:Arrhythmogenic right ventricular cardiomyopathy (ARVC)	9	1.35E-04	5.82
BIOCARTA	m_slrp2Pathway:Function of SLRP in Bone: An Integrated View	3	6.84E-03	21.02
BIOCARTA	m_tob1Pathway:Role of Tob in T-cell activation	4	2.99E-02	5.60
BIOCARTA	m_nktPathway:Selective expression of chemokine receptors during T-cell polarization	4	7.71E-02	3.87
BIOCARTA	m_erythPathway:Erythrocyte Differentiation Pathway	3	9.38E-02	5.60
GO TERM	GO:0007155~cell adhesion	43	5.07E-14	3.97
GO TERM	GO:0007275~multicellular organism development	56	1.75E-09	2.42
GO TERM	GO:0014031~mesenchymal cell development	6	1.09E-07	38.37
GO TERM	GO:0001525~angiogenesis	22	1.14E-07	4.09
GO TERM	GO:0001568~blood vessel development	12	4.53E-07	7.57
REACTOME	Integrin cell surface interactions	12	4.00E-06	5.98
REACTOME	ECM proteoglycans	9	5.44E-06	8.85
REACTOME	Collagen biosynthesis and modifying enzymes	9	1.60E-04	5.66
REACTOME	cGMP effects	5	2.61E-04	14.76
REACTOME	Syndecan interactions	5	4.78E-04	12.79

Table 5.1 Most significant pathways by p value for each database sampled by DAVID show many pathways related to adhesion and ECM are regulated by active Notch3. This table demonstrates the pathways most significantly enriched from analysis of our selected upregulated genes with adjusted $p < 0.1$ and $\log_2$ fold change of 1 or greater. Pathways related to adhesion or the extracellular matrix are listed in red.

The pathways with the most significantly enriched genes appearing in our list of upregulated genes included pathways related to cell adhesion and the extracellular matrix for 3 of the 4 databases probed by DAVID. We were intrigued by this since cell adhesion and migration have obvious implications for tumor metastasis. We, therefore, looked at all the pathways significantly enriched for Notch3IC upregulated genes that were related to cell adhesion and adhesion to the extracellular matrix (Table 5.2, see appendix Figure A5.3 for genes).

Pathway Database	Pathway name	Gene Count	p Value	Fold Enrichment
GO TERM	GO:0007155~cell adhesion	43	5.07E-14	3.97
KEGG	mmu04510:Focal adhesion	21	1.65E-08	4.66
KEGG	mmu04512:ECM-receptor interaction	14	4.18E-08	7.31
REACTOME	Integrin cell surface interactions	12	4.00E-06	5.98
REACTOME	ECM proteoglycans	9	5.44E-06	8.85
GO TERM	GO:0030199~collagen fibril organization	8	2.15E-05	9.18
REACTOME	Collagen biosynthesis and modifying enzymes	9	1.60E-04	5.66
GO TERM	GO:0033630~positive regulation of cell adhesion mediated by integrin	5	2.73E-04	14.92
REACTOME	Syndecan interactions	5	4.78E-04	12.79
GO TERM	GO:0030198~extracellular matrix organization	10	1.02E-03	3.93
REACTOME	Molecules associated with elastic fibres	6	1.68E-03	6.77
GO TERM	GO:0007160~cell-matrix adhesion	8	1.89E-03	4.53
REACTOME	A tetrasaccharide linker sequence is required for GAG synthesis	5	3.10E-03	7.99
GO TERM	GO:0006024~glycosaminoglycan biosynthetic process	5	3.26E-03	7.99
GO TERM	GO:0033627~cell adhesion mediated by integrin	4	4.10E-03	11.94
REACTOME	Collagen degradation	7	8.11E-03	3.95
REACTOME	Assembly of collagen fibrils and other multimeric structures	6	1.08E-02	4.43
GO TERM	GO:0030155~regulation of cell adhesion	5	1.40E-02	5.33
GO TERM	GO:0007229~integrin-mediated signaling pathway	7	1.77E-02	3.37
REACTOME	Laminin interactions	4	3.49E-02	5.48
REACTOME	NCAM1 interactions	4	3.49E-02	5.48
REACTOME	Non-integrin membrane-ECM interactions	4	4.53E-02	4.95

Table 5.2 Notch3 intracellular domain significantly upregulates many significant adhesion and extracellular matrix pathways identified by DAVID analysis. The table shows all the significantly enriched pathways for upregulated genes that are related to adhesion and the extracellular matrix, arranged by significance.

We wanted to more closely examine the gene signature in these adhesion and ECM pathways to identify candidates that could affect metastasis. We decided to focus on collagen and integrin genes because these gene are critical in attachment of ovarian tumor cells to the peritoneum and the signaling involved in subsequent formation of metastatic lesions (Shen et al., 2012, Lengyel, 2010). Collagens and integrins were also upregulated genes from our RNA-Seq data that were frequent components of the pathways identified as significantly enriched (appendix Figure A5.3). Several collagen genes, *Col3a1, Col5a3, Col6a2, Col8a1, Col14a1, Col15a1,* and *Col18a1* were significantly upregulated (adj p = 1.51E-02, 9.85E-03, 3.76E-02, 2.30E-02, 3.16E-09, and 4.12E-04 respectively) (Figure 5.2). Significantly upregulated integrin genes include Itga1, Itga7, Itga9, Itga11, Itgb3, and Itgb5 (adj p = 7.70E-03, 2.30E-02, 5.80E-06, 1.32E-06, 6.51E-03, and 6.17E-03 respectively) (Figure 5.3).

Figure 5.2

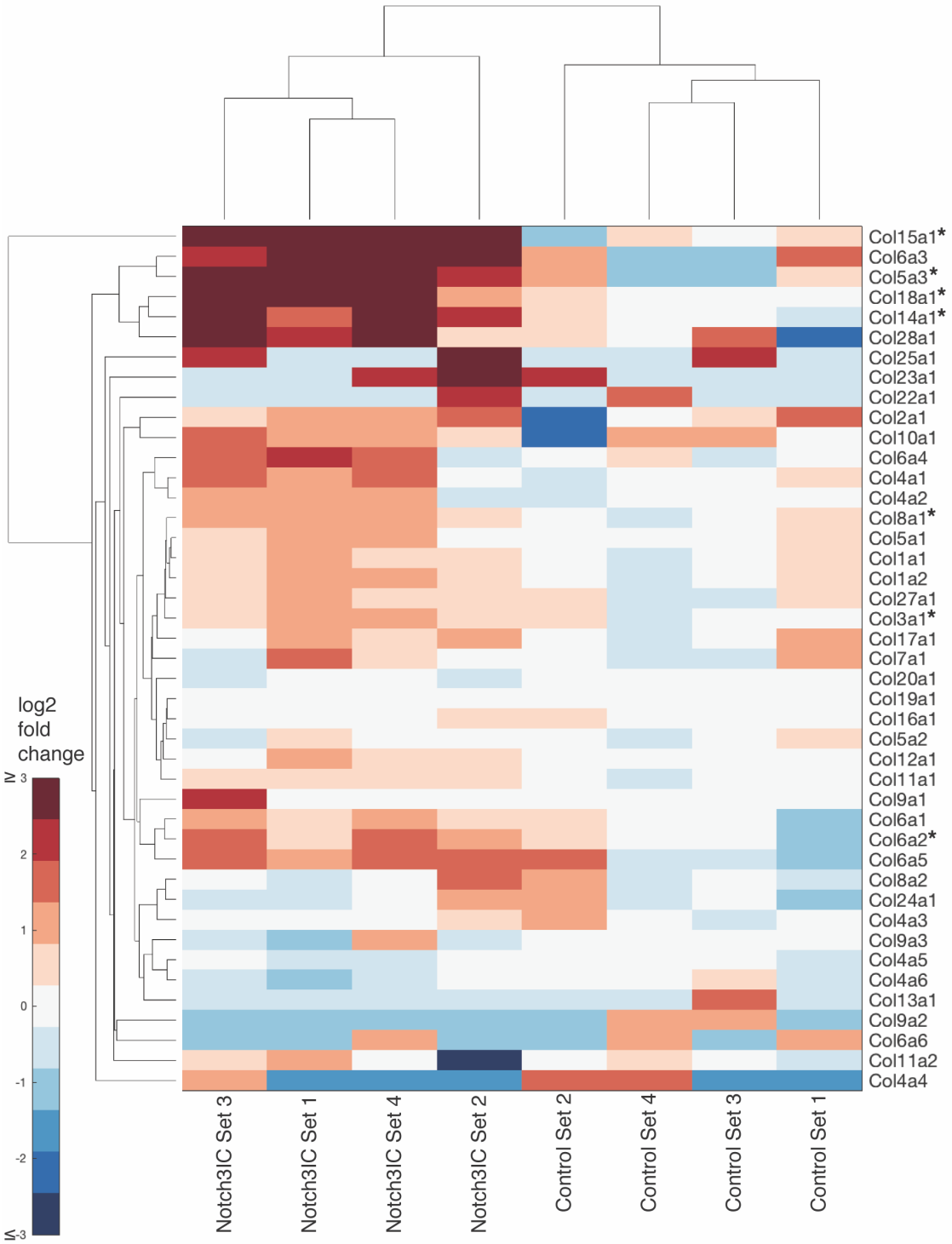

Figure 5.2 Expression of collagen genes for all samples subjected to RNA-Seq show a subset of enriched collagen genes induced by Notch3 intracellular domain. The heat map displays the $\log_2$ fold change in ID8 IP2 luc Notch3IC and Control lines for each collagen gene compared to the mean $\log_2$ fold expression of the Controls for each gene. Genes with an asterisk have adjusted p value less than 0.1 and average log2 fold change greater than 1 for the average Notch3IC fold change compared to Control.

Figure 5.3

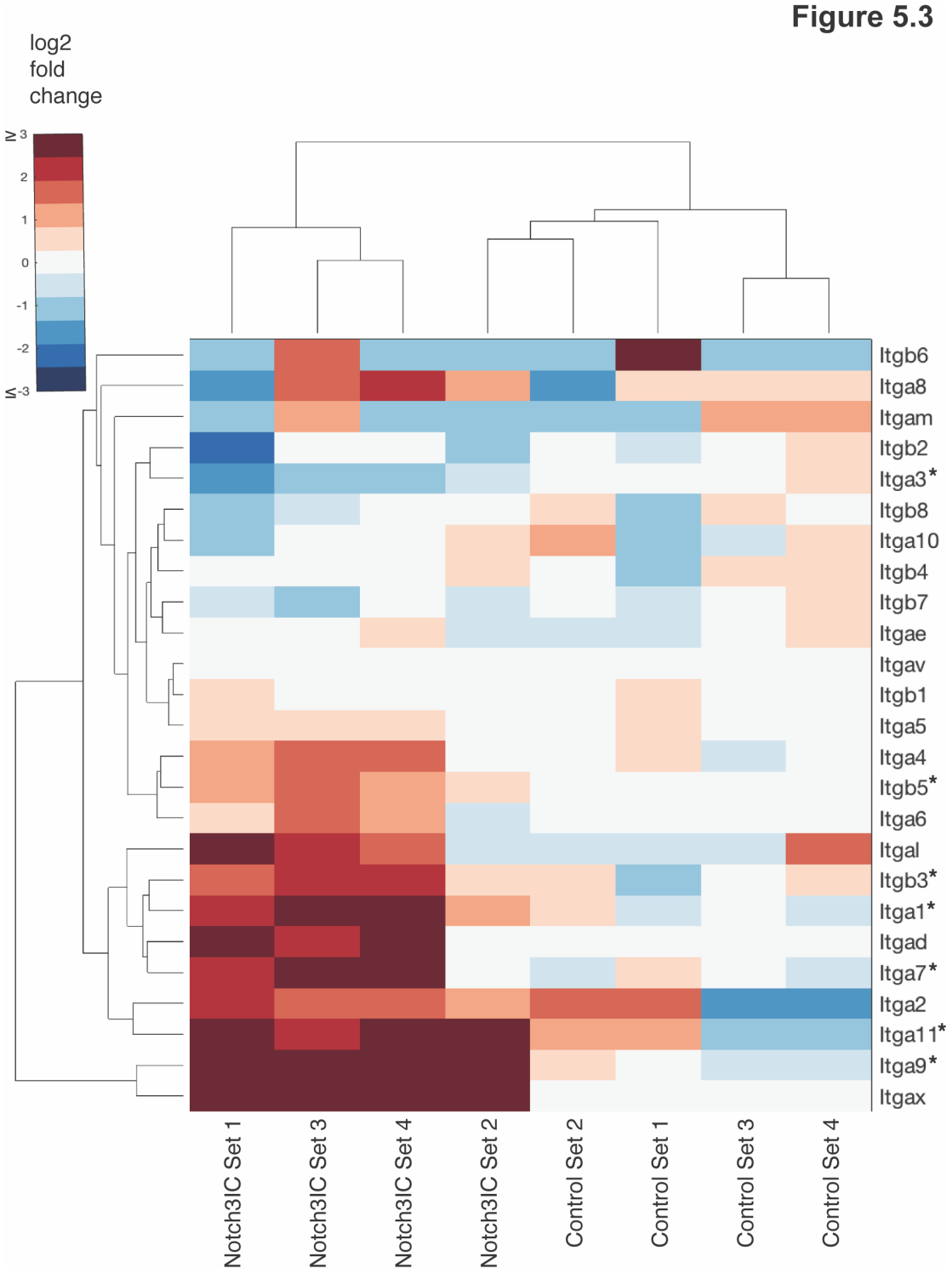

Figure 5.3 Integrin receptor genes expression for all samples assessed by RNA-Seq show a set of enriched integrin genes induced by Notch3 intracellular domain activity. This heat map displays the log_2 fold change in ID8 IP2 luc Notch3IC and Control lines for each collagen gene compared to the mean log_2 fold expression of the Controls for each gene. Genes with an asterisk have adjusted p value less than 0.1 and average log2 fold change greater than 1, or less than -1 for the average Notch3IC fold change compared to Control.

We sought to confirm pathway results generated in DAVID by completing a separate pathway analysis on our RNA-Seq results. We converted the selected genes to human orthologues and assessed the data with the Gene Set Enrichment Analysis (GSEA) database developed by the Broad Institute. This analysis was completed on the $\log_2$ fold change of all genes assessed by RNA-Seq and processed through DEseq. Unlike the DAVID analysis, which simply assesses whether there is a connection between genes entered into the analysis, GSEA takes into account the magnitude of each $\log_2$ fold change value and the weight each individual gene has in a given pathway comparison. In addition to other pathways, we did see significant enrichment for adhesion and extracellular matrix pathways concurrent with DAVID results (Table 5.3). Again, we saw multiple pathways related specifically to collagen and integrin genes (Table 5.3, Table 5.4) Other significantly enriched pathways can be viewed in appendix Table A5.4. We also saw significant enrichment of downregulated pathways related to adhesion, most of which were related to cell to cell adhesion. This was similar to results for enhanced pathways identified by DAVID analysis (appendix Table 5.5).

Pathway Name	Gene Count	NOM p-val	Normalized Enrichment
NABA_COLLAGENS	29	2.37E-03	1.73
REACTOME_COLLAGEN_FORMATION	30	1.83E-02	1.66
PID_INTEGRIN1_PATHWAY	42	1.73E-02	1.62
ONDER_CDH1_TARGETS_2_UP	69	1.61E-02	1.61
NABA_BASEMENT_MEMBRANES	24	3.14E-02	1.58
PID_INTEGRIN_CS_PATHWAY	16	4.95E-02	1.54
REACTOME_INTEGRIN_CELL_SURFACE_INTERACTIONS	36	7.26E-02	1.47

Table 5.3 Adhesion and extracellular matrix pathways are significantly enriched in Notch3IC cells when analyzed by GSEA pathway analysis. This table displays the pathways that were determined to be upregulated by analysis with GSEA comparison to pathway databases when assessing all gene expression changes in Notch3IC compared to Control RNA-Seq data.

Figure 5.4

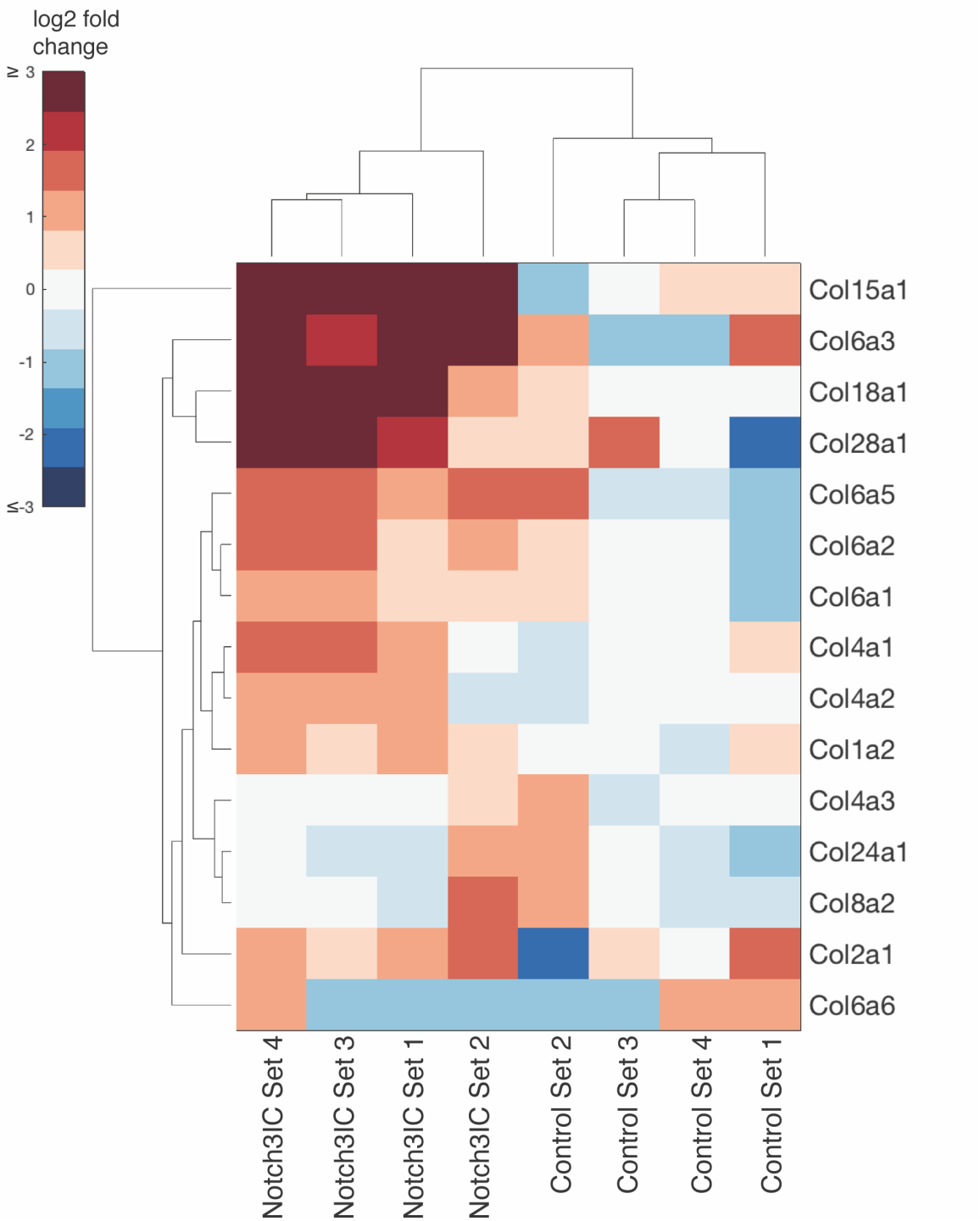

Figure 5.4 GSEA data analysis of Notch3IC compared to Control data shows collagen genes among the top 20 enriched pathways, and as the most significantly enriched of the adhesion and extracellular matrix pathways. This figure displays the core enrichment genes from the NABA_COLLAGENS pathway which was significantly enriched by GSEA analysis (NOM p = 0.002366864). Genes with a standard deviation less than 0.5 with small variance were removed from this list. To view all collagen genes in the pathway, refer to Figure 5.2.

DISCUSSION

We determined Notch3 pathway activation led to a reduction in survival of mice implanted with tumor cells *in vivo*, but saw little evidence *in vitro* for an effect of NOTCH3 on growth properties of cells, and no significantly increased tumor burden at time sacrifice relative to control tumor cells. We therefore chose to further investigate the cause of increased tumor lethality with Notch3IC expression. We evaluated the gene signature of Notch3IC and Control ID8 IP2 luc ovarian cancer lines by RNA-Seq and analysis of the genes and pathways produced. We found through this analysis that adhesion and extracellular matrix pathways were significantly enriched in Notch3IC ID8 IP2 luc compared to Control. Upregulated pathways showed a pattern of collagen and integrin gene involvement.

For enriched pathways containing downregulated genes, only the GO Consortium database returned any pathways connected to adhesion in DAVID analysis. These pathways appear to be mostly involved in cell to cell interactions rather than cell to matrix interactions emphasized in the upregulated data (see Appendix Table A5.2). GSEA analysis returned similar results in relation to enriched pathways identified with downregulated adhesion genes (Appendix A5.5). This upregulation of adhesion of and extracellular matrix pathways, but downregulation of cell to cell adhesions may be consistent with the idea that metastasis of tumor cells need both to be able to detach from each other or the ovary/ fallopian tube, to be mobile, but also attach to the peritoneal ECM to seed metastatic lesions. Downregulated genes related to ECM attachment may also represent fine tuning in the cancer cells to specifically attach to particular peritoneal ECM, which is rich in collagen I. This can be assessed by reviewing which collagens and integrin receptor components show a greater $\log_2$ fold change in the heat maps for each class of gene (Figures 5.2 and 5.3, Figure A5.3). For example, *Itga3*, which generally binds laminin, is significantly downregulated, while *Itga1*, which binds collagen I, is upregulated (Hynes, 2002, Witz et al., 2001).

Based on these consistent results found from both pathway analyses in the enhancement of adhesion and ECM pathways, we hypothesized that Notch3 signaling activation affects the adhesion or migratory properties of ID8 IP2 ovarian cancer cells. In the following chapter, we explored if activation of *Notch3* generates a specific phenotype related to adhesion on extracellular matrix in the ovarian cancer

ID8 IP2 model. Upregulated adhesion and ECM genes may explain reduced survival in the context of enhancing the ability of metastatic tumor seeds to adhere to the peritoneum.

CHAPTER 6

ACTIVE NOTCH3 SIGNALING EFFECTS ADHESION TO COLLAGENS IN OVARIAN CANCER CELLS *IN VITRO*

INTRODUCTION

Our previous data showed an enrichment for gene expression of proteins involved in adhesion and extracellular matrix, as identified by pathway analysis. We also determined that Notch3 signaling in ovarian cancer cells was associated with a reduction in survival and accelerated disease development. We therefore wanted to explore the role of adhesion to the peritoneal extracellular matrix (ECM) as a potential factor in *Notch3*-driven ovarian tumor progression.

In ovarian cancer, adhesion represents an important part of disease development. Adhesion characteristics are critical to the attachment of tumor cells to the ECM of peritoneal organs and wall, which are the sites of metastasis in ovarian cancer. These metastases are what characterize late stage disease, often already present at the time of diagnosis. Adhesion to the peritoneum promotes cell viability by allowing tumor cells to evade anoikis and lymphatic clearance, which can occur while detached in the peritoneum (Sodek et al., 2012).

Adhesion of metastases occurs as tumor cells or spheroids of tumor cells attach to the ECM in a metastatic site via cell surface receptors. The most common sites of peritoneal metastasis, in order of preference for tumor cell attachment, are the contralateral fallopian tube and ovary, followed by the omentum, right diaphragm, and mesentery of the small intestine (Lengyel, 2010). Collagens I and IV, laminin, and fibronectin are the most abundant components in the peritoneal lining and omental ECM, (Lengyel, 2010). The matrix composition of peritoneal ECM is rich in collagen I, which is also the most diffuse and widespread matrix component around the mesothelium, the cells which compose the surface of the peritoneum (Witz et al., 2001). Collagen I is high in preferentially adhered omental locations. It has been shown ovarian cancer cells preferentially bind to collagen I over other ECM components. (Sorensen et al., 2009, Moser et al., 1996). The cellular receptors that bind ECM include integrins, which are essential

to the attachment of ovarian cancer cells to ECM (Lengyel, 2010, Moser et al., 1996, Sodek et al., 2012). Not only is the establishment of metastatic sites through tumor cell binding dependent on collagens, but ovarian tumor cells bound to fibrillar collagen I via integrin receptors engage in cell signal regulation, which better enable migration and invasion, the subsequent steps of metastasis (Shen et al., 2012).

ECM and integrin signaling is important to non-adhered cells and ECM and integrins assist in the formation of spheroids. As ovarian cancer cells must survive in the peritoneal fluid or ascites in order to travel to metastatic sites, there are mechanisms to resist anoikis and other apoptotic signals (Sodek et al., 2012). Collagen-integrin signaling contributes to cancer cell survival after detachment of cancer cells and spheroids from the tumor (Symowicz et al., 2007, Lengyel, 2010). Formation of spheroids assists in cell survival; integrin presence in spheroids contributes to survival signaling in cancer cells that assists in surviving while detached, as well as chemotherapy resistance (Sodek et al., 2012). ECM components collagens, laminin, and fibronectin are present in ascites (Lengyel, 2010), which may help in producing survival signals for cells until they reach a peritoneal metastatic site. Collagen expression in ovarian cancer patient samples has been associated with poor patient survival; a gene signature was identified related to poor overall survival in HGSC patients, including *COL11A1*, *COL5A2*, and *COL6A2* (Cheon et al., 2014). *COL11A1* knockdown in implanted cell lines was also linked to reduced tumor progression in mice (Cheon et al., 2014).

Previous work by Brown and colleagues (2015) has demonstrated a link between *Notch3* and induction of collagen in ovarian cancer cells, and the importance of this induction to ovarian cancer cell survival. Increased *Notch3* levels were connected to significantly increased levels of *Col4α2* in ovarian cancer cells. Furthermore, culture with collagen IV led to an increase in cell viability in *Notch3* siRNA knockdown cells. *Col4α2* was found to be necessary for survival of ovarian cancer cells, as direct knockdown of *Col4α2* led to a reduction in viable cells which is rescued by growth on collagen IV (Brown et al., 2015). The RNA-Seq data we generated showed a significant enrichment in expression of collagen pathway genes and collagen-binding integrin genes (see Chapter 5, Figure 6.1). While *Col4α2* was not significantly upregulated in the RNA-Seq data we generated, there was an increase in *Col4α2* in our data with introduction of *Notch3* intracellular domain (DEseq baseMean Control 6520.7, baseMean Notch3IC 17086.5 with a $\log_2$ fold increase of 1.4 p = 0.009, adj p = 0.148). *Col4α2* was labeled as a core enrichment

gene in GSEA analysis compared to the NABA_COLLAGENS significantly upregulated pathway (Chapter 5). We thus hypothesized that *Notch3* may influence the ability of ID8 IP2 luc cells to survive during metastasis during growth in the peritoneum. This state may be promoted by interaction with collagen in the extracellular matrix of metastatic sites.

In summary, the RNA-Seq data comparing ID8 IP2 luc Notch3IC and Control suggested a role for adhesion and ECM interactions in connection with high *Notch3* expression, which indicates that adhesion may be a mechanism for increased tumor aggressiveness linked to *Notch3*. Based on the known roles of adhesion and extracellular matrix in ovarian cancer metastasis and the results of RNA-Seq analysis demonstrating upregulated adhesion and extracellular matrix genes, we wanted to further investigate the adhesive properties of ovarian cancer cells with Notch3 signal activation. We hypothesized that an increase in adhesive ability to extracellular matrix in NOTCH3 intracellular domain overexpressing ovarian cancer cells could explain the quicker progression to ascites accumulation and decreased survival of tumor bearing mice.

Figure 6.1

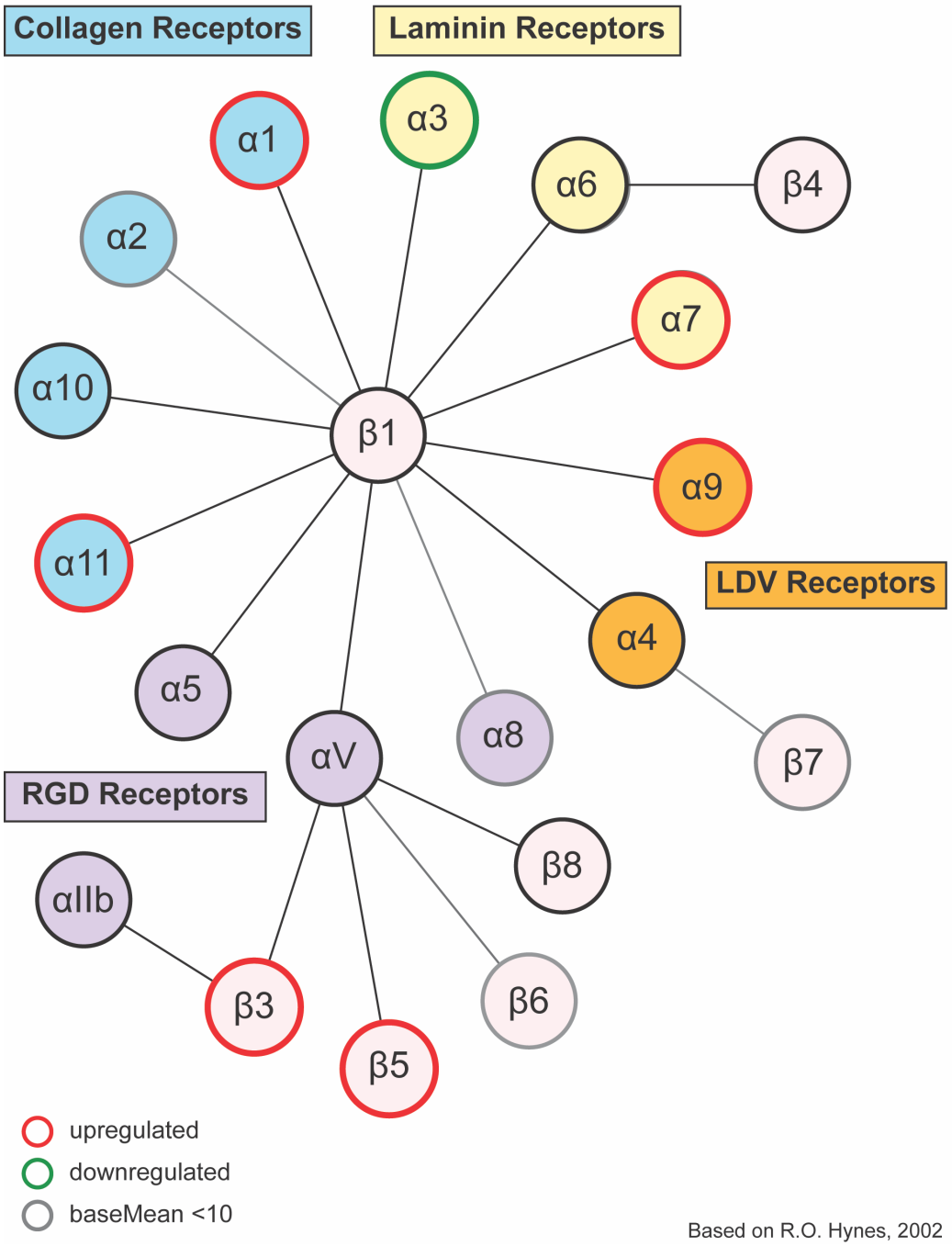

Figure 6.1 Integrin receptor components altered in Notch3IC compared to Control determined by RNA-Seq. This figure displays a subset of mammalian integrin receptor family proteins that create αβ integrin heterodimer receptors. Each α subunit is shown with its corresponding receptor category and has a line connecting to its associated β dimerization partners. Receptor components with red circles are upregulated in our RNA-Seq data, and the green circle represents downregulation. Gray circles represent genes that displayed low expression in both Notch3IC and Control lines. Low expression was defined as a DEseq baseMean below 10 transcripts for the averages of both lines. LDV are leucine-aspartate-valine containing ECM components such as fibronectin, (Hynes, 1992, Humphries et al., 2006). RGD is an arginine-glycine-aspartate motif found in ECM components like fibronectin and vitronectin (Hynes, 2002). This figure does not show all integrin genes. Image is based on a figure from (Hynes, 2002).

RESULTS

ITGA1 cell surface expression is increased with Notch3 signal activation

RNA-Seq data indicated a role for Notch3 signaling in adhesion and extracellular matrix pathways with strongest significance in the pathways involving collagens and integrins (See Chapter 5, Figure 6.1). We wanted to delve deeper into the role of these genes in the ID8 IP2 ovarian cancer model. Based on the adhesion and extracellular matrix pathways identified by RNA-Seq, we sought to confirm whether upregulated mRNAs resulted in increased expression levels of adhesion proteins on the cell surface of Notch3IC activated tumor cells compared to Control.

We specifically chose to examine ITGA1, a collagen receptor component significantly upregulated in the RNA-Seq assessment (log_2 fold change 3.8, adj p = 0.00770), highlighted in Figure 6.1. ITGA1 dimerizes with ITGB1 in order to bind collagens; this dimer pair binds collagens I, IV, VI, and fibrillary collagens (Leitinger and Hohenester, 2007). As previously mentioned, the peritoneal ECM is rich in collagens I and IV, and ovarian cancer cells preferentially bind collagen I (Lengyel, 2010). The level of ITGB1 did not change significantly in Notch3IC cells, but was found at high levels in both Control and Notch3IC (DEseq baseMean Control 17,913.9, baseMean Notch3IC 19,414.9), suggesting abundant availability for dimerization with ITGA1. In order to analyze cell surface expression of ITGA1, we stained 3 sets of Notch3IC and control cell lines with antibodies against ITGA1 and subjected them to flow cytometry in two duplicate experiments. We observed an increase in the percent of ITGA1 positive cells in Notch3IC compared to Control, confirming our RNA-Seq analysis (p = 0.0414, Welch's t-test) (Figure 6.2).

We attempted to determine if there was a similar increase in surface ITGA11, the other collagen receptor gene identified as significantly upregulated in our RNA-Seq data (log_2 fold change 3.4, adj p = 1.32E-06) in Notch3IC compared to Control. However, the only antibody available to recognize mouse ITGA11 did not produce usable flow cytometry data (data not shown).

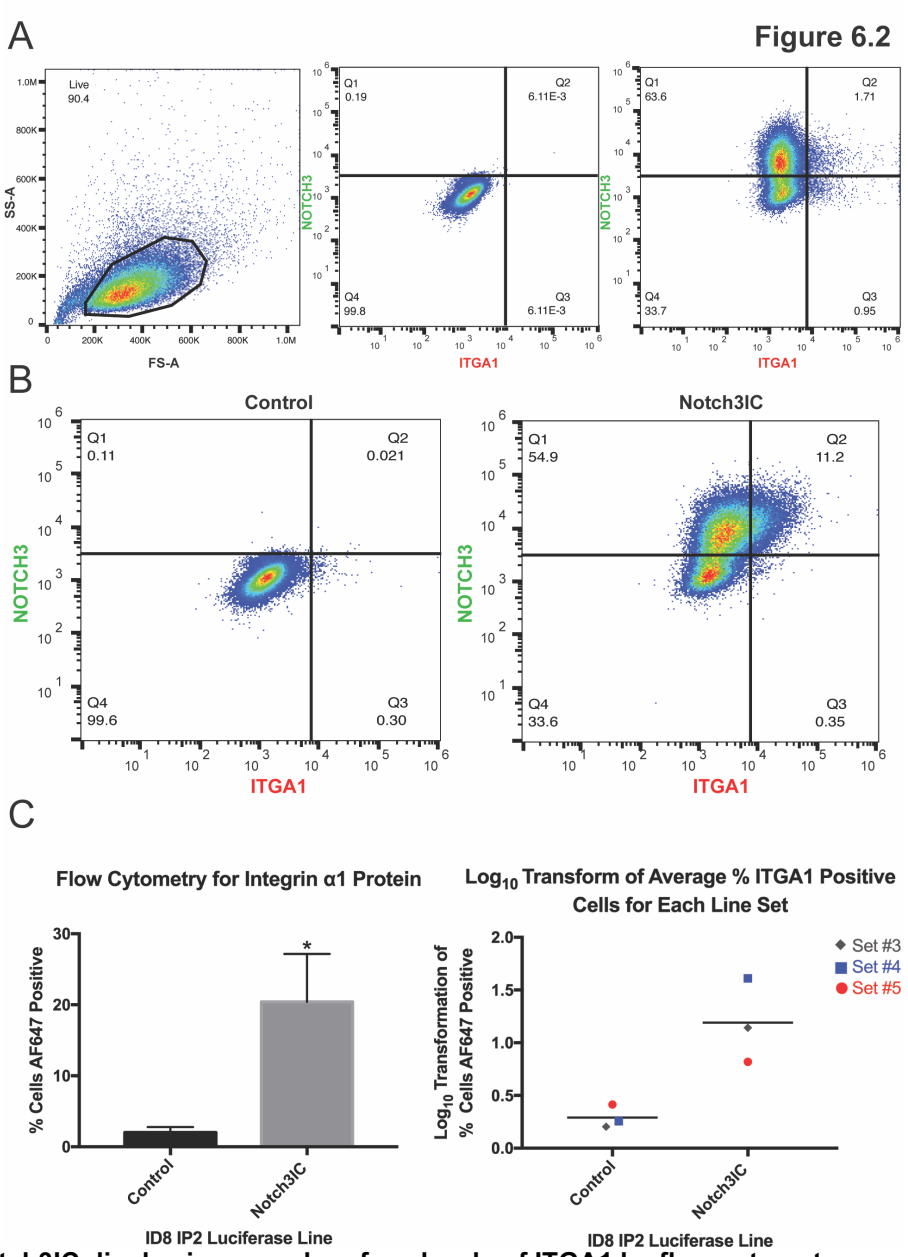

Figure 6.2 Notch3IC display increased surface levels of ITGA1 by flow cytometry.
(A) The left panel shows an example of the gate used to determine live cells for each population. It shows forward and side scatter area for an ID8 IP2 luc only sample. The center panel shows the live cells of ID8 IP2 luc plotted for GFP (an indicator of NOTCH3 expression, as discussed in chapter 4) and AF647-conjugated anti-ITGA1. This demonstrates an unstained Control population that should be negative for both NOTCH3 and ITGA1. The right panel displays isotype control staining of live gated Notch3IC cells that are positive for NOTCH3, and is set to minimize background signal for ITGA1. **(B)** The left panel shows an example of a Control population of cells, while the right panel shows a Notch3IC cell line. NOTCH3-expressing cells were determined by GFP positive signal, and ITGA1 positive cells were determined by AF647 positivity. As is demonstrated in the figure, the NOTCH3 positive cell population contains a shift toward ITGA1 positive cells (Q2). **(C)** The left graph demonstrates the significant increase in the percent of cells with ITGA1 surface expression in Notch3IC compared to Control measured by the percent of AF647 positive cells in each live population ($p = 0.0414$, Welch's t-test). The right graph displays the distribution of Log_{10} of the averages for the two experiments for each line set ($p = 0.0195$, Student's t-test).

Notch3 signaling leads to an increase in adhesion of ID8 IP2 cells to collagens

Based on the RNA-Seq upregulation of extracellular matrix ligand and receptor genes, as well as the confirmed expression of surface integrin α1, we sought to determine if different extracellular matrices known to be in the peritoneum interacted differentially with Control and Notch3IC activated tumor cells. We assessed the ability of Notch3IC and Control cell lines to attach to five different extracellular matrices *in vitro*; we investigated interaction with fibronectin, laminin, vitronectin, collagen I, and collagen IV (Lengyel, 2010, Witz et al., 2001). We added equal numbers of Notch3IC or Control cells to plates coated with an ECM component, allowed the cells to settle and attach for a specified period of time, and determined the number of cells which had successfully attached to the ECM. It was found that all ID8 IP2 cells bound well to vitronectin and fibronectin coated plates, and NOTCH3 ICD expression did not further enhance attachment (Figure 6.3, Figure A6.1). All ID8 IP2 luc cells bound more poorly to collagens and laminin coated dishes than to fibronectin and vitronectin, adhering at lower numbers over the same period of time with equal numbers of cells (Figure A6.1, data not shown). Notch3IC activated tumor cells, however, were able to better adhere to collagens than Control, while binding equally well to the other matrices (Figure 6.3). There was a significant increase in the proportion of Notch3IC cells compared to Control adhering to both collagen I ($p = 0.0118$, Welch's t-test) and collagen IV ($p = 0.0163$, Welch's t-test).

We evaluated whether specifically blocking ITGA1 binding would reverse the observed increase in collagen I or collagen IV binding of Notch3IC cells. We used a putative mouse ITGA1 blocking antibody as outlined in published experiments (Gotwals et al., 1996, Mendrick et al., 1995, Miyake et al., 1994). We expected that blocking ITGA1 may inhibit the increased capacity of Notch3IC cells to adhere to collagens. It was found, however, that the number of Notch3IC cells Compared to control was not significantly different between treatment of cells with ITGA1 antibody compared to isotype control antibody for either collagen I ($p =0.5616$, Welch's t-test) or collagen IV ($p =0.6888$, Welch's t-test) (Appendix Figure A6.2). There may be several reasons why ITGA1 antibody blocking was not observed to reduce the attachment of Notch3IC active cells to collagen extracellular matrix. This result could be due to the increased presence of ITGA11 dimerizing with ITGB1 and attaching to collagens. In addition, the antibody to ITGA1 may not be providing a complete block of activity, since it is not a verified activity specified in the source documents.

Figure 6.3

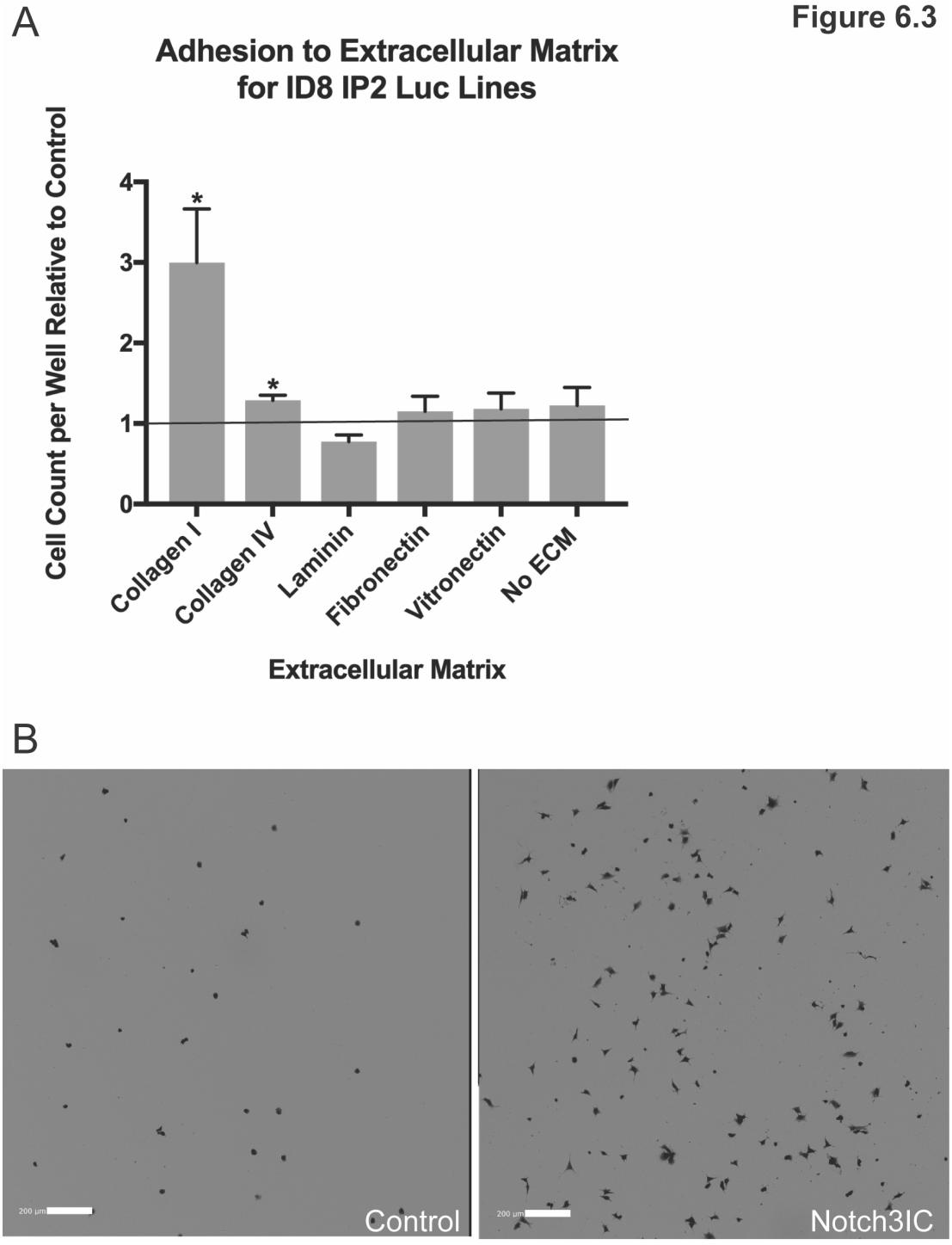

Figure 6.3 ID8 IP2 luc Notch3IC more adherent to collagens than Control. (A) The graph shows the proportion of adhered Notch3IC cells compared to adhered Control cells for each extracellular matrix examined. The line at 1 therefore represents the Control compared to itself for each matrix. Notch3IC display a significant increase in the number of cells adhering to collagen I ($p = 0.0118$) and collagen IV ($p = 0.0136$, Welch's t-test). There is no significant difference in adhesion to laminin, fibronectin, or vitronectin for Notch3IC and Control ($p = 0.0474$, $p = 0.6237$, $p = 0.3075$, Welch's t-test). There is no significant difference in adhesion to tissue culture plates without extracellular matrix coating ($p = 0.4206$, Welch's t-test). **(B)** Representative images of ID8 IP2 luc cells on collagen I fixed, stained, and imaged with a Celígo instrument for adhesion experiments. Scale bar represents 200µm.

Notch3 signaling causes reduced migration of ID8 IP2 on extracellular matrix proteins

The discovery that Notch3IC tumor cells adhere better to collagens suggested that we further explore the interaction of Notch3IC cells with collagen extracellular matrix. As previously mentioned, once adhered to collagen I, ovarian cancer cells can engage in signaling that allows tumor cells to better participate in the next steps of peritoneal metastasis such as migration and invasion (Shen et al., 2012). We endeavored to investigate the effect of Notch3IC signaling levels in ovarian tumor cells on migration over collagen I coated surfaces. We proposed that cells might be able to migrate better along collagen I based on its increased ability to adhere to collagen I.

We investigated migration on collagen by assessing the ability of cells to fill in a cell-free gap (a "wound") on collagen-coated plates. A confluent monolayer was seeded and grown on collagen I-coated plates around a plug; a wound was created by removal of the plug covering part of the plate, and then the percent area of the wound covered by cells was measured over time. We assessed 2 experiments of quadruplicates for 3 ID8 IP2 luc line sets and examined the average for each set. Surprisingly, Notch3IC cells seeded on collagen I displayed a significant reduction in capacity to migrate across collagen I and fill the wound. Notch3IC cells were shown to migrate significantly more slowly across collagen I at both 6 and 12 hours ($p = 0.0432$, $p = 0.0181$, Welch's t-test).

Migration in the absence of extracellular matrix was assessed similarly, with a wound created by scratching a pipette tip across a confluent monolayer on an uncoated tissue culture plate. It was determined there was no significant difference in the ability of cells to close a wound created by a scratch in a confluent monolayer at several time points post formation of the scratch/wound ($p = 0.4142$, $p = 0.5422$, $p = 0.4133$, $p= 0.9637$ for 3, 6, 9, and 12 hours respectively, Welch's t-test).

We wanted to determine if the effect on Notch3IC migration observed on collagen I was unique to collagen, or similar to behavior on another extracellular matrix. We repeated the migration assay performed previously over collagen I with fibronectin, seeding cells around a wound area on fibronectin coated plates. Notch3IC migration on fibronectin also displayed a significant reduction in migration compared to Control at both 6 and 12 hours ($p = 0.0004$, $p = 0.0020$, Welch's t-test). Thus, we posit that changes in migration due to Notch3 signal activation are not matrix specificity but possibly a general feature of the migration machinery of the cancer cells.

Figure 6.4

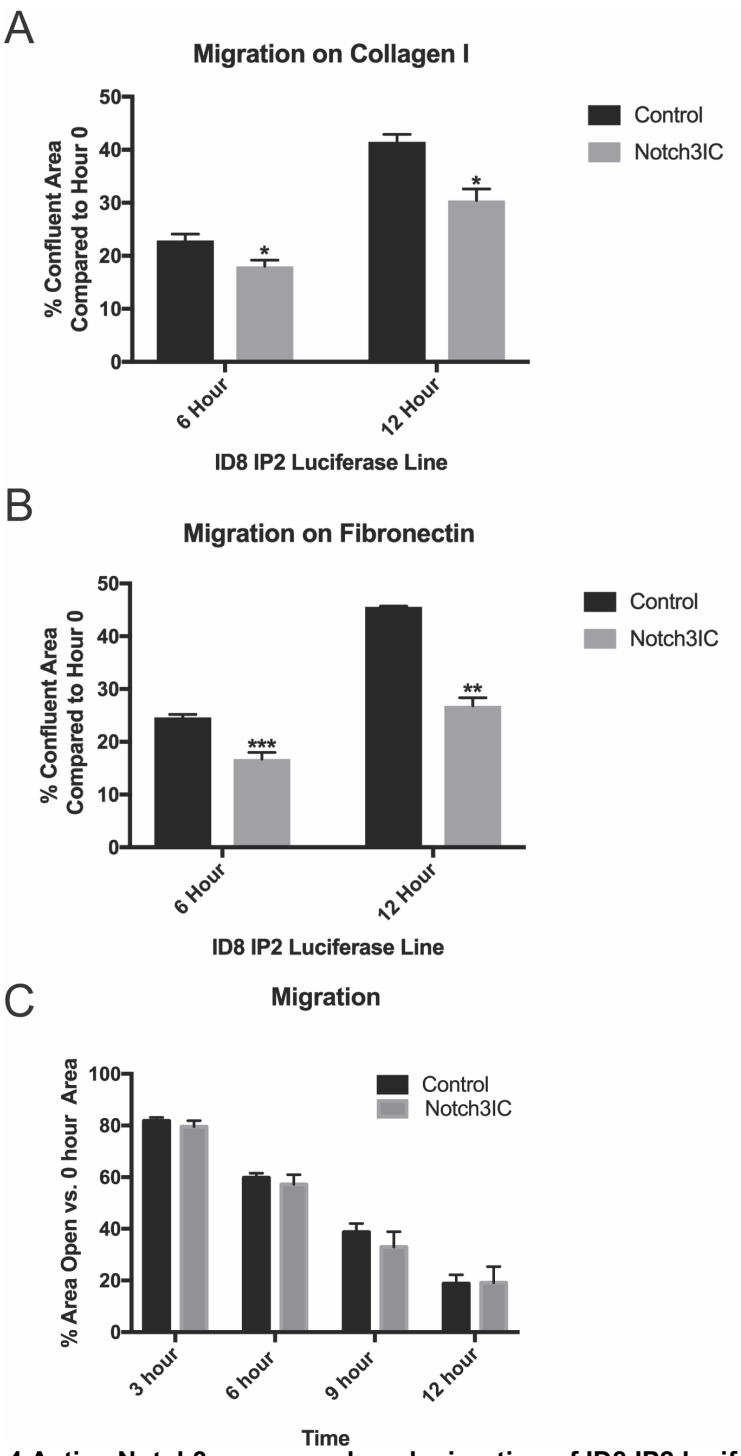

Figure 6.4 Active Notch3 causes reduced migration of ID8 IP2 luciferase on extracellular matrix. **(A)** Migration of ID8 IP2 luc Notch3IC cells is significantly reduced on collagen I at both 6 hours and 12 hours ($p = 0.0432$, $p = 0.0181$, Welch's t-test). The graph displays area of cells migrated into the open area at time 0. **(B)** Migration of ID8 IP2 luc Notch3IC is significantly reduced on fibronectin at both 6 and 12 hours ($p = 0.0004$, $p = 0.0020$ Welch's t-test). The graph displays area of cells migrated into the open area from time 0. **(C)** There is no significant difference in migration without extracellular matrix into a scratch wound ($p = 0.4142$, $p = 0.5422$, $p = 0.4133$, $p= 0.9637$ for 3, 6, 9, and 12 hours respectively, Welch's t-test). The graph shows area remaining open in the scratch (not yet covered in migrated cells) compared to the area open at the time of scratch generation.

Notch3 signal activation does not alter *in vitro* invasion properties of ID8 IP2 cells

In light of the findings demonstrating that adhesion to and migration over extracellular matrix are altered between Notch3IC and Control cells, we explored whether an effect on invasion through extracellular matrix would be observed as well. We investigated the ability of Notch3IC lines to invade through collagen I compared to Control. We measured invasive capacity by the amount of cell migration through a Boyden chamber pre-coated with collagen I. This assay requires that the cells not only migrate through a porous membrane to the other side of a trans-well insert (designed with space between the membrane and bottom of the well), but invade through the extracellular matrix coating to do so (Albini et al., 1987). We quantified the number of cells able to pass through the matrix and to the other side of the membrane. There was no significant difference in invasion observed across the chamber insert ($p = 0.5634$, Welch's t-test). The same was observed for invasion through Matrigel® GFR (growth factor reduced). Matrigel is an amalgam of ECM largely containing laminin, collagen IV, and proteoglycans, along with a number of other components derived from murine tumors (Englebreth-Holm-Swarm tumor) (Hughes et al., 2010, Kleinman and Martin, 2005). The number of cells invading through the Matrigel® GFR ($p = 0.8634$, Welch's t-test), and the percent invasion through Matrigel® GFR compared to migration through the chamber alone ($p = 0.6076$) were both not significantly different between Notch3IC and Control lines. In addition, there was no change in migration through chambers without extracellular matrix between Notch3IC and Control lines either ($p = 0.1205$, Welch's t-test) based on the number of cells on the bottom of the chamber.

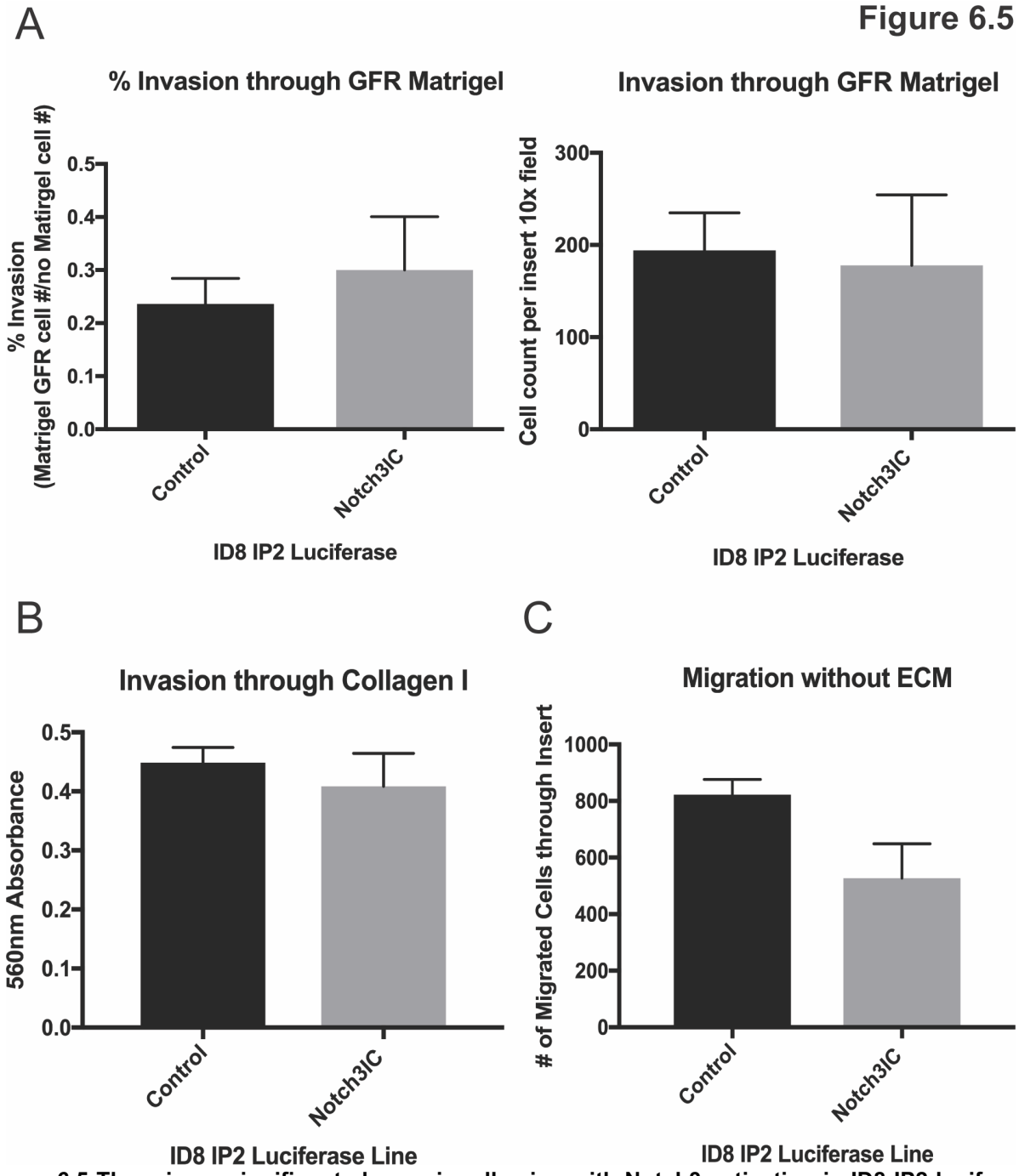

Figure 6.5 There is no significant change in adhesion with Notch3 activation in ID8 IP2 luciferase cells. (A) Invasion through Matrigel GFR coated chamber inserts shows no difference between Control and Notch3IC. The left panel displays the percent invasion through Matrigel GFR compared to migration across the chamber membrane without extracellular matrix ($p = 0.6076$, Welch's t-test). The right panel shows the direct cell count for Control and Notch3IC cells invaded through Matrigel GFR ($p = 0.8634$, Welch's t-test). **(B)** There is no change in invasion through collagen I with *Notch3* signal activation ($p = 0.5634$). Graph displays the 560nm absorbance generated by dye extracted from cells invaded through, and attached to the bottom of chambers coated with collagen I. **(C)** There is no change in migration across the chamber insert membrane without extracellular matrix ($p = 0.1205$, Welch's t-test). Data was collected from non-coated chambers assessed along with Matrigel GFR invasion. Graph displays the number of cells crossing and attaching to the bottom of the chamber.

DISCUSSION

RNA-Seq data indicated an enrichment for adhesion and extracellular matrix genes with induction of Notch signaling induced by the expression of the NOTCH3 intracellular domain. Two classes of ECM related proteins highlighted in our analysis were collagen and integrin genes. We show that Notch3 signaling induces increased collagen binding of ID8 IP2 Notch3IC ovarian cancer cells over Control. Focusing on ITGA1, we found that NOTCH3 induced higher levels of ITGA1 on the surface of ID8 IP2, possibly causing increased binding to collagens. Tumor cells with active NOTCH3, therefore, may have increased ability to interact with collagens in the peritoneum, promoting their attachment and the formation of metastatic seeds. These results suggest that the influence of NOTCH3 is specific to the attachment of cancer cells to extracellular matrix, and not subsequent steps of metastasis formation, since adhesion was increased, but migration was reduced and invasion was unaffected. Since the Notch3IC tumor cells adhere better to collagens, they may not be able to migrate as well along the collagen since they are firmly adhered. This would indicate the role of NOTCH3 may increase adherence to new metastatic sites as opposed to directly assisting the spread across the peritoneum once cells are attached.

We did not, however, asses for the ability of cells to survive prior to attachment to extracellular matrix *in vivo* or in *in vitro* assays that may simulate this earlier stage of metastasis. Based on the other known role for extracellular matrix and adhesion molecules in anoikis resistance previously discussed, there may also be a role for NOTCH3 in maintaining survival of cells in the peritoneum to reach metastatic sites. We have shown there is a potential role for Notch3 signaling in the attachment to metastatic sites by demonstrating an increased ability to attach to collagens, especially collagen I the most abundant extracellular matrix in the surface of the peritoneum. We may, however, want to further investigate in the future if NOTCH3 expression in our model yields similar results to Brown et al in anoikis resistance, or in the maintenance of spheroids which also increase resistance to cell death while travelling in the peritoneum.

CHAPTER 7

GENERAL DISCUSSION

A model for the effect of Notch3 on metastatic adhesion in ovarian cancer

The process of metastasis in ovarian cancer begins with the detachment of ovarian cancer cells and/or spheroids from the primary tumor (Lengyel, 2010, White et al., 2014). Tumor cells are then distributed throughout the peritoneum in the peritoneal fluid or ascites (Kenny et al., 2011, White et al., 2014). Ovarian cancer cells have also been demonstrated to have the ability to spread hematogenously, through the blood circulation (Pradeep et al., 2014). However, ovarian tumor cells are more likely to form metastases when they are spread within the peritoneum, and even hematogenous tumor cells preferentially form metastases in the omentum and infrequently form metastases outside the peritoneum (Pradeep et al., 2014, Gerber et al., 2006, Tarin et al., 1984). Furthermore, patients succumb to peritoneal disease burden, and not distant metastases when they do occur (Tarin et al., 1984). In order to achieve dangerous metastatic spread, tumor cells must survive in the peritoneal fluid long enough to reach a metastatic site in the peritoneal lining, evade anoikis (apoptosis due to loss of anchorage signals) and lymphatic clearance (Sodek et al., 2012). Tumor cells acquire anoikis resistance by forming spheroids and by eventual attachment to the peritoneum. Spheroids of cancer cells have been shown to escape this type of apoptosis by mutual integrin/ECM signaling, cadherin signaling, and VEGF-A/VEGFR2 signaling (Lengyel, 2010, Sher et al., 2009, Sodek et al., 2012). Spheroids also enhance chemotherapy resistance by reduced proliferation, increased integrin signaling, upregulation of chemotherapy resistance genes, and shielding cells inside spheroids from exposure to chemotherapy (Lengyel, 2010, Sodek et al., 2012).

Attachment of tumor cells to the peritoneal surface to form metastases is a critical step that follows release from the primary site and survival in the peritoneum. The peritoneal cavity consists of the pelvic and abdominal spaces including all the organs within. The peritoneal lining covers all the tissues within the peritoneum including the pelvis, cavity wall, and all organs (Sodek et al., 2012). The surface of the peritoneum is comprised of a single confluent layer of mesothelial cells on top of a layer of extracellular matrices with sparse fibroblasts and macrophages beneath (Kenny et al., 2009, Lengyel, 2010). Ovarian

cancer cells preferentially bind to the surface of the contralateral ovary, the omentum, the right diaphragm, and mesentery of the small intestine when seeding metastases (Lengyel, 2010).

The mesothelial cells in the peritoneal lining normally secrete glycosaminoglycans, surfactant, and proteoglycans that prevent fusion or adhesion between the peritoneal organs and may form a poor attachment point for tumor cells (Sodek et al., 2012). However, the composition of the ECM under the mesothelium includes collagens I and IV, fibronectin, laminin, and vitronectin, where collagen I is the most abundant (Kenny et al., 2009, Lengyel, 2010, Witz et al., 2001). It has been shown that ovarian cancer cells preferentially adhere to the extracellular matrix versus mesothelial cells, and that mesothelial cells themselves can be inhibitory to tumor cell attachment (Niedbala et al., 1985, Kenny et al., 2011, Kenny et al., 2007, Ksiazek et al., 2009) (Figure 7.1).

The omentum is seeded by many ovarian tumors due to its unique environment. The omentum is attached to the greater curvature of the stomach and is comprised largely of fat layers and immune aggregates, but contains the same surface lining of mesothelial cells and ECM as the rest of the peritoneum (Gerber et al., 2006). Tumor cells preferentially bind to the areas containing immune aggregates, which provide exposed extracellular matrix, particularly collagen I, and areas that are highly vascularized with both blood and lymph vessels (Gerber et al., 2006, Sodek et al., 2012). The area surrounding immune aggregates has been shown to be high in mesothelial VEGF-A and comprises a natural environment of constitutive angiogenesis that is easily co-opted by tumor cells (Gerber et al., 2006, Sorensen et al., 2009). Omental immune aggregates also contain pro-inflammatory cytokines and chemokines (Gerber et al., 2006).

In the normal peritoneal environment, there are areas of exposed extracellular matrix at mesothelial intercellular junctions and in the omentum at immune aggregates (Sodek et al., 2012). As cancer progresses, further damage to the mesothelium allows for increased exposure of the ECM and therefore provides more chance of attachment for tumor cells (Sodek et al., 2012, Niedbala et al., 1985). Tumor cells preferentially attach to these areas of damage and exposed ECM (Niedbala et al., 1985, Sodek et al., 2012). Mesothelial cells are damaged or signaled to retract after interaction with spheroid integrin and inflammatory signals allowing for enhanced ECM exposure and tumor cell adherence (Iwanicki et al., 2011, Sodek et al., 2012).

Within ECM, ovarian cancer cells show a preference for binding collagen I over other matrices, and spheroids show a preference for collagen I and fibronectin binding (Kenny et al., 2009). Collagen I is particularly exposed between mesothelial cell junctions at lymphatic portal areas that occur frequently in the omental immune aggregates and in the diaphragm, where ovarian cancer cells show preferential binding (Sodek et al., 2012); these areas have larger gaps between mesothelial cells due to pro-inflammatory cytokine signaling which signals the mesothelial cells to contract/retract (Sodek et al., 2012) (Figure 7.1). The tumor cells can then secrete factors that remodel the ECM at attached locations furthering metastasis (Niedbala et al., 1985). The fibroblasts present produce ECM and assist with regulation of the pro-invasive signals in the ECM (Kenny et al., 2009). Once attached to collagen I, additional invasive behavior ensues; tumors are activated to migrate and proliferate, which is enhanced the denser the collagen is from increased deposition during disease (Sodek et al., 2012).

Figure 7.1

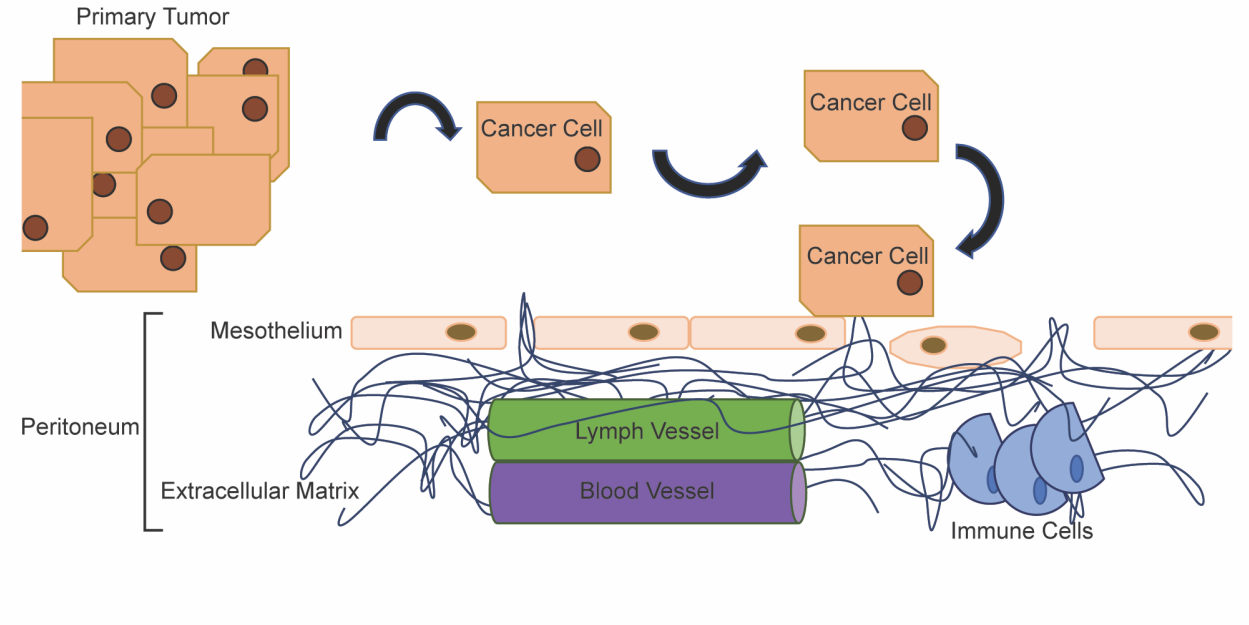

Figure 7.1 Attachment of ovarian cancer cells to the ECM of the peritoneum.
Ovarian cancer cells adhere to the collagen rich ECM underlying the mesothelium of the peritoneal lining of the wall and organs. Extracellular matrix is exposed between gaps in the mesothelium. These gaps occur more frequently at areas of higher lymph vascularization and at immune deposits in normal tissue. As cancer develops, more mesothelial cells are signaled to retract.

Based on the process of adhesion to the peritoneal lining by ovarian cancer metastases, we propose a model explaining the ability of NOTCH3 expressing ovarian cancer cells to better engage in the early steps of metastasis. Our studies have shown an increase in the expression of extracellular matrix and adhesion genes, predominantly integrins and collagens, with the activation of Notch3 signaling in ID8 IP2 cells. We have demonstrated upregulation of integrin α1, which can cooperatively bind collagen I, on the surface of Notch3IC cells. We observed an increased affinity of ID8 IP2 Notch3 activated cells for adhesion to collagens I and IV *in vitro*. Our data indicate that Notch3 signaling in tumor cells is correlated with a reduction in survival *in vivo*. Given our results, we hypothesize that the increased ability to adhere collagens by integrin receptor expression effects the attachment of ovarian cancer cells to the peritoneum during metastasis (Figure 7.2). Peritoneal sites most likely to be chosen for metastasis, as described in the literature, are those with exposed collagen I, consistent with our hypothesis.

Integrin signaling from tumor cells in spheroids has been implicated in the ability to expose additional sites of extracellular matrix between the mesothelium for tumor cell adhesion; this may mean that in addition to increasing adhesion to collagens in the ECM, which we have shown in this study, there may be a further role for upregulated integrin expression in exposing the ECM for attachment. This role of integrins in exposure of the ECM for attachment could be further investigated in the future.

Figure 7.2

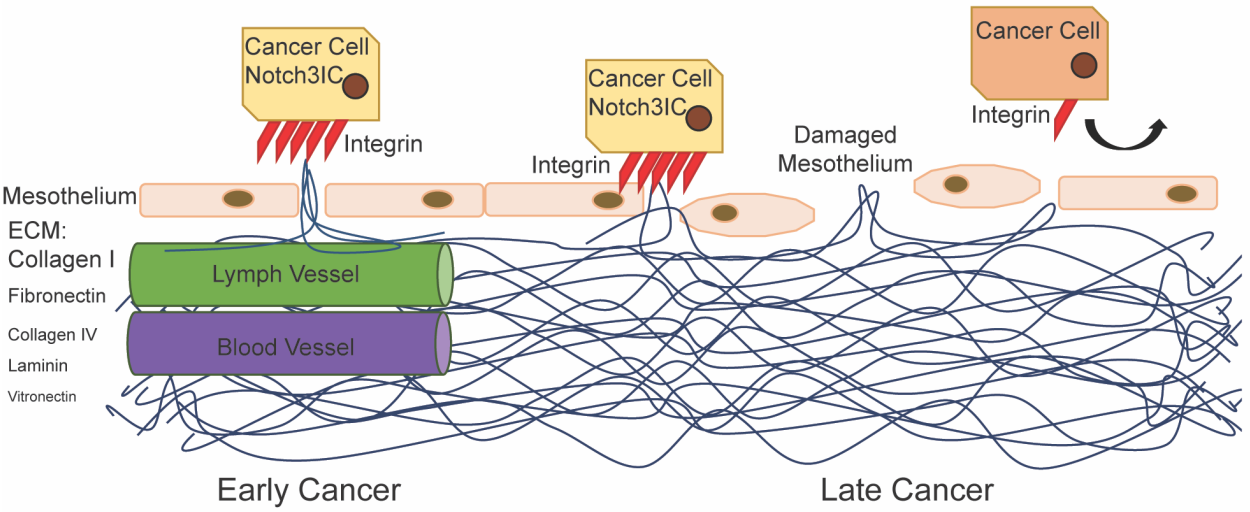

Figure 7.2 Proposed model of the influence of Notch3 on ovarian cancer cell metastatic attachment to the peritoneum. This model examines the process of adhesion to the peritoneum of already detached tumor cells. Tumor cells preferentially adhere to areas where ECM, particularly collagen I, is exposed. As cancer progresses, the area of exposed ECM will increase as mesothelial cells are damaged or retract. The induction of Notch3 signaling in ovarian cancer cells upregulates integrin receptors able to bind collagens in the ECM, and increases the likelihood that tumor cells will be able to attach to these exposed areas of ECM.

Future directions: further investigation of the Notch3 pathway in ovarian cancer metastasis

The investigations described here used the ID8 IP2 model, which is derived from mouse ovarian surface epithelium, but HGSC may derive from ovarian surface epithelium, fallopian epithelium, or ectopic endosalpingiosis (Chapter 1). The results observed in ID8 IP2 may be explored in a fallopian derived line to show that Notch3 affects adhesion and extracellular matrix pathways in ovarian cancer cells of multiple organs of origin. Our lab has acquired mouse oviduct surface epithelial derived lines from the Dr. Joanna Burdette lab at the University of Illinois at Chicago (Endsley et al., 2015, Eddie et al., 2015). We have evaluated mouse oviductal lines (MOE) for the presence of NOTCH3 and found that the MOE PTEN^{shRNA} and MOE PTEN^{shRNA}/p53^{R273H} lines expressed little to no observable NOTCH3 ICD on western blot (Figure 7.3). We have since lentivirally infected the MOE PTEN^{shRNA}/p53^{R273H} line with *Notch3* intracellular domain generating a MOE PTEN^{shRNA}/p53^{R273H}/Notch3IC line and a PTEN^{shRNA}/p53^{R273H}/Control line. These lines were infected in a similar manner with same constructs as the ID8 IP2 luciferase line. On flow cytometry, Notch3IC infected lines were found to be GFP positive indicating successful infection (data not shown). These lines can therefore be tested to see if Notch3 signaling will show a similar effect on adhesion to collagens *in vitro* that we see in ID8 IP2. We also have human fallopian derived tumorigenic lines from the Dr. Ronny Drapkin laboratory at the University of Pennsylvania (developed at Dana-Farber Cancer Institute) and human (patient tumor/ascites derived) ovarian cancer lines that can be tested as well to demonstrate consistency between the human and mouse (Karst et al., 2011, Karst and Drapkin, 2012). Assessing human derived lines would verify that NOTCH3 effects are also similar for human and mouse derived lines, confirming translation to human disease.

A

Figure 7.3

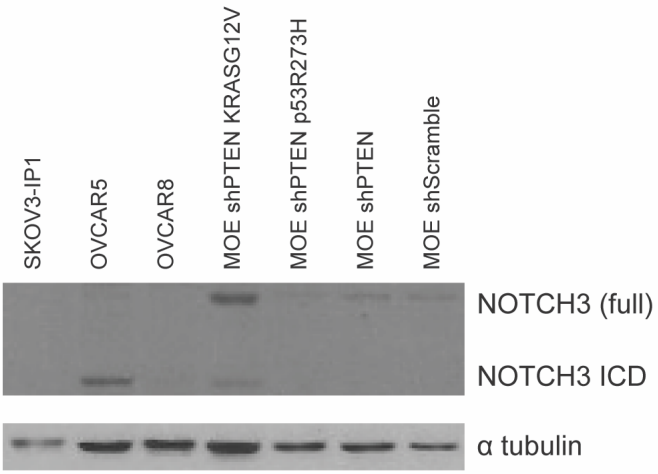

Figure 7.3 Fallopian derived tumorigenic cell lines express varying levels of NOTCH3. (A) Mouse oviductal epithelial derived cell lines were assessed for the presence of NOTCH3 protein. We observed little to no NOTCH3 intracellular domain present on western blot for MOE PTEN^{shRNA}p53^{R273H}. We therefore chose this line to potentially confirm results of Notch3 signal activation in a fallopian derived line.

In our previous experiments, we modeled the increase of Notch3 signaling by introducing the Notch3 ICD which may induce supra-physiological levels of Notch signaling. Conversely, it is possible that this level of signaling may be relevant to that seen in human ovarian cancer, that is it may resemble oncogenic Notch signaling. However, human patient samples generally show increase in *NOTCH3* copy number or upregulation of full length NOTCH3 protein, which may have different properties. Therefore, one could further explore the effects of the Notch3 pathway in the ID8 IP2 line, in particular by examining the effect of overexpressing full length Notch3 (Chapter 4, Figure A4.1) to determine if activation generates similar results as the Notch3 ICD in increasing adhesion to collagens. One could confirm the ability of these lines to signal with ligand interaction, and determine if the full length NOTCH3 has a similar effect to the introduction of ICD. This would prove useful as ovarian cancers often upregulate full length *NOTCH3*, and would be a more physiologic representation of patient ovarian cancer. We could also investigate if *Notch3* has the same effect as upregulation of *MAML*. It was found in The Cancer Genome Atlas (TCGA) study that not only *NOTCH3* was correlated with ovarian cancers, but other parts of the *NOTCH3* pathway including *MAML1, MAML2, MAML3, JAG1, and JAG2* (Cancer Genome Atlas Research, 2011). Therefore, it would be interesting to show that overexpression of *Maml* in our ID8 IP2 line also generated a similar effect on adhesion to extracellular matrix as *Notch3*. We have acquired a pFLAG-CMV-2 MAML1 construct which contains the human *MAML1* sequence with an N-terminal FLAG-tag from the Dr. Kostandin Pajcini laboratory at the University of Illinois at Chicago, which could allow us to investigate whether overexpression of *MAML* has a similar effect to overexpression of *Notch3.*

An important consideration for interpreting the results is the question of how significant is the trend toward increased peritoneal wall burden caused by Notch3 signal activation. Our analysis did not show this to be significantly changed but a strong trend was detected. One could replicate *in vivo* tumor cell implantation experiments and obtain higher numbers of mice to see if significance is obtained for this measurement. This would involve assessing for an increase of peritoneal wall and ovary tumor burden with Notch3 expression measured by IVIS in early stages of disease. In addition, we could assess metastatic spread *in vivo* from an orthotopic bursal injection model to examine spread from a primary to metastatic sites. This would be done by evaluating total bioluminescent tumor burden or the number of tumor seeds in the peritoneal wall. Both of these types of analysis should be done with a sufficient number of mice to

determine if there is a significant difference between Notch3IC and Control. This would allow us to evaluate the spread from the primary site and not just from the peritoneal environment, and may even reveal a more significant difference.

Experiments further investigating direct attachment to the ECM of ID8 IP2 luc Notch3IC compared to Control may support the hypothesis of Notch3IC promoting peritoneal adhesion presented in this thesis. Attachment of ID8 IP2 lines to *ex vivo* omental explants in culture would determine if ovarian cancer cells attach better to target peritoneal tissue (Khan et al., 2010, Clark et al., 2013). Experiments evaluating cells in a 3-dimensional *in vitro* model, consisting of fibroblasts in a collagen I layer with an overlay of a mesothelial cell layer, may be used to evaluate the attachment of Notch3IC compared to Control, which would model attachment to exposed ECM under the mesothelium (Kenny et al., 2009). These 3D cultures can be evaluated histologically to determine if there is a preference for Notch3IC cells to attach to collagen I. The *in vitro* 3D models have the added advantage of replacing the need for additional lengthy mouse experiments for depth examination of tumor seeds. We can evaluate cells to determine if Notch3IC will seed at a higher ratio than Control on omentum or will attach better in the 3D model.

There may be a role for *Notch3* in allowing the survival of non-adherent cells in the peritoneal fluid that involves adhesion pathway genes upregulated by Notch3 activation. This is plausible since it has been demonstrated that integrin signaling and ECM in the ascites and within spheroids can lead to survival signaling for ovarian cancer cells (Brown et al., 2015, Taddei et al., 2012, Sodek et al., 2012). We could explore anoikis resistance of Notch3IC cells by culturing cells in non-adherent conditions and subsequently assessing cell survival.

There is evidence that spheroid cancer cells demonstrate reduced proliferation, which assists these cancer cells in chemotherapy resistance (Sodek et al., 2012). This may explain our observation that Notch3IC lines subjected to FACS for selection of high Notch3 expressing cells displayed reduced proliferation compared to Control (Appendix Chapter 4). The reduction in proliferative ability of these cells may assist with chemotherapy resistance by reducing proliferation. Spheroid formation itself may shield cells within the spheroids from access to chemotherapy, helping cells evade death (Sodek et al., 2012). It has been shown ovarian cancer cells resist chemotherapy in spheroids better than the same cells in monolayer (L'Esperance et al., 2008). As discussed previously, spheroids may more easily form in Notch3

expressing tumors due to the change in adhesion and ECM pathways (Lengyel, 2010, Sodek et al., 2012). This hypothesis would fit with our data demonstrating high Notch3 populations of ID8 IP2 cells proliferate less, but there is still a reduction in survival in Notch3 expressing versus Control injected mice *in vivo*. We may want to repeat our *in vitro* platinum therapy experiments with ID8 IP2 Notch3IC and Control spheroids, to prove whether Notch3 influences chemotherapy resistance by spheroid formation of ovarian cancer cells, since our previous experiments only assessed cisplatin treatment of monolayers. We could assess taxane therapy as well, since the literature suggests Notch signaling is related to taxane resistance as well (Groeneweg et al., 2014a, Kang et al., 2015, Jeong et al., 2017, Hu et al., 2014).

Lastly, we may expand our studies by evaluating other pathways influenced by *Notch3* from our RNA-Seq data. Other pathways were identified that may be contributing to the increased ascites accumulation and reduced survival we observed in our *in vivo* studies. For example, pathways involving immune signaling were detected in the DAVID pathway analysis (Chapter 5), including enrichment in cytokine-cytokine receptor interaction and TGFβ signaling pathways (adj p = 2.57E-04, adj p = 3.66E-02, respectively). As previously mentioned, immune signaling enhances ovarian cancer cell attachment to metastatic sites on the peritoneal lining by retraction of mesothelial cells and exposure of the ECM (Sodek et al., 2012). Chemokines and cytokines have been shown to be upregulated in epithelial ovarian cancers, and their signaling has been implicated in cell motility and tumor angiogenesis (Freedman et al., 2004). TGFβ in particular has been linked to endothelial cell chemotaxis, adhesion of tumor cells, and immune suppression (Freedman et al., 2004, Sodek et al., 2012). Another gene significantly upregulated in our data that was identified in enhanced immune related pathways was the cytokine IL6 (log_2 fold change 2.173330651, adj p = 8.16E-03), which has been implicated in poor patient survival, tumor cell adhesion, tumor cell proliferation, and inhibition of immune cells in ovarian cancer (Freedman et al., 2004, Lane et al., 2011). We could therefore explore experiments evaluating the presence of some of these cytokines in our Notch3 ID8 IP2 cells and Control, and then determine if there is an effect on tumor burden, ascites accumulation, and microvascular density *in vivo* when targeting these cytokines. Thus, there are other promising pathways we identified that are influenced by *Notch3* that could be further investigated for their role in ovarian cancer progression and metastasis.

Implications to HGSC clinical disease and therapeutics

We have shown Notch3 signaling influences adhesion of ovarian cancer cells to collagens I and IV. This may influence the initial development of metastases to the peritoneum in high grade serous ovarian cancer. It is thought that focusing on early, low-burden ovarian cancer detection is optimal, as treatment could initiate before extensive tumor spread (Cho and Shih Ie, 2009, Kurman et al., 2008). This is an important goal as current poor survival is associated with late stage detection of ovarian cancer and remaining macroscopic tumors post cytoreduction (Cho and Shih Ie, 2009, Kurman et al., 2008). This could include detecting low volume of disease associated with initial development of tumors and recurrent HGSC. Notch3 may be effecting this earlier stage of metastatic spread as demonstrated by our *in vivo* data analysis. The role of Notch3 in upregulating adhesion and ECM pathways that we have shown may affect initiation of tumor seeds. Upregulation of these adhesion and ECM pathways may even influence survival of ovarian cancer cells in the peritoneal environment before they eventually form metastases, and is consistent with studies described earlier in this chapter.

Notch3 and integrin α1β1 may provide potential biomarkers for the detection of early disease or the beginnings of recurrent disease in patients. Evidence suggests evaluating circulating tumor DNA for genetic alterations in cancer, including ovarian cancers, may improve the detection and monitoring of disease progression (Bettegowda et al., 2014, Haber and Velculescu, 2014, Phallen et al., 2017). Because of the unique nature of ovarian cancer, tumor DNA may be accessible via ascites samples as well. Tumor DNA encoding either Notch3 or specific integrins may indicate early active metastasis or recurring disease. Assessment of tumor DNA could indicate which patients may benefit from potential therapeutic targeting of the adhesion and therefore the metastatic process in HGSC.

Targeting of integrins that are upregulated by Notch3, such as the integrin dimer α1β1, may assist in reducing recurrent metastasis. Unfortunately, integrin inhibitors that have been developed for clinical use target integrins αvβ3, αvβ5, α5β1, and the αv and α2 subunits of dimers (Tucker, 2006, Avraamides et al., 2008). Some integrin β1 antibodies have been effectively used to block function in ovarian cancer, and even reduce tumor burden in a mouse model of breast cancer (Park et al., 2006a, Casey et al., 2001, Casey and Skubitz, 2000). However, integrin β1 blocking antibodies have not yet been tested in the clinic. Since many integrin inhibitors have been able to be used clinically, it is quite plausible these integrin β1 inhibiting antibodies may eventually be able to be used in the clinic. Moreover, the naturally occurring collagen IV

derived anti-angiogenic molecule arresten is believed to function through integrin α1β1 inhibition and may provide a therapeutic strategy for inhibition of ovarian cancer cell metastatic adhesion (Nyberg et al., 2005, Colorado et al., 2000). In addition, since arresten is an endogenous inhibitor of angiogenesis, further benefit may be observed on survival as is seen for the FDA approved combination treatment of ovarian cancers with the anti-angiogenic agent bevacizumab along with chemotherapy (McClung and Wenham, 2016, Monk et al., 2017, Aghajanian et al., 2012, Pujade-Lauraine et al., 2014, Coleman et al., 2017).

The use of Notch signaling inhibitors could potentially be employed in the clinic. γ -secretase inhibitors (GSI) have previously been used in clinical setting to inhibit Notch signaling. These would only target canonical Notch signaling, and Notch3 may be acting canonically and/or non-canonically. It is at least likely that integrins are, however, upregulated by canonical signaling, as it has been shown that Notch1 interacts directly with the enhancers/promoters of integrin genes, so it is plausible Notch3 may as well (Hass et al., 2015). It is therefore possible that integrins are a direct target of Notch signaling. GSIs have been used in the clinic but do cause toxicity to the gastrointestinal tract and are not specific to Notch signaling, giving them the potential for off target effects as well (Capaccione and Pine, 2013, Groeneweg et al., 2014b). DLL4 inhibitors have been used clinically to target tumor angiogenesis, but may not be as useful in the context of Notch3 pathway upregulated ovarian cancers since the major ligand interaction appears to be with JAGGED1 (Bellavia et al., 2008, Choi et al., 2008, Chen et al., 2010, Steg et al., 2011, Capaccione and Pine, 2013). The Kitajewski lab has developed Notch “decoys” that utilize the EGF-like repeats of Notch1 and can specifically block Jagged signaling, but these have not yet made it to the clinic (Kangsamaksin et al., 2015). The Kitajewski lab is, however, working on these inhibitors, and has even developed a Notch3 variant capable of blocking Jagged interaction as well (Kitajewski lab unpublished data, data not shown).

Conclusion

High grade serous ovarian cancer is such a deadly disease because of its ability to quickly metastasize before the detection of disease, and its ability to easily recur after therapy and disseminate into the abdominal cavity again. Metastasis in ovarian cancer occurs through shedding of cells and spheroids through from the primary tumor, and dissemination primarily through the peritoneal fluid or ascites accumulation to secondary sites on the peritoneal lining of the wall and organs. Cancer metastasis is

commonly thought to be a function of proliferation and stem-like characteristics of cells that can grow large tumor seeds. Ovarian cancer, however, is characterized by the high quantity of disseminated disease affecting many areas of the peritoneum. Our studies reveal insight into the important step of adhesion in metastasis, allowing attachment of these cancer cells to metastatic sites for the subsequent development of lesions. We have shown Notch3 signaling can upregulate integrin protein in an ovarian cancer model, ID8 IP2, and that Notch3 active lines compared to Notch3 negative lines preferentially adhere to collagen I, an abundant component of the peritoneum to which ovarian cancer cells are known to attach. Our insight into the mechanism of ovarian cancer metastasis may allow us to better understand how to target this high-volume disease.

REFERENCES

Aghajanian, C., Blank, S. V., Goff, B. A., Judson, P. L., Teneriello, M. G., Husain, A., Sovak, M. A., Yi, J. and Nycum, L. R. (2012) 'OCEANS: A Randomized, Double-Blind, Placebo-Controlled Phase III Trial of Chemotherapy With or Without Bevacizumab in Patients With Platinum-Sensitive Recurrent Epithelial Ovarian, Primary Peritoneal, or Fallopian Tube Cancer', *Journal of Clinical Oncology,* 30(17), pp. 2039-2045.

Ahmed, A. A., Etemadmoghadam, D., Temple, J., Lynch, A. G., Riad, M., Sharma, R., Stewart, C., Fereday, S., Caldas, C., Defazio, A., Bowtell, D. and Brenton, J. D. (2010) 'Driver mutations in TP53 are ubiquitous in high grade serous carcinoma of the ovary', *J Pathol,* 221(1), pp. 49-56.

Albini, A., Iwamoto, Y., Kleinman, H. K., Martin, G. R., Aaronson, S. A., Kozlowski, J. M. and McEwan, R. N. (1987) 'A rapid in vitro assay for quantitating the invasive potential of tumor cells', *Cancer Res,* 47(12), pp. 3239-45.

Andersen, P., Uosaki, H., Shenje, L. T. and Kwon, C. (2012) 'Non-canonical Notch signaling: emerging role and mechanism', *Trends Cell Biol,* 22(5), pp. 257-65.

Anglesio, M. S., Wiegand, K. C., Melnyk, N., Chow, C., Salamanca, C., Prentice, L. M., Senz, J., Yang, W., Spillman, M. A., Cochrane, D. R., Shumansky, K., Shah, S. P., Kalloger, S. E. and Huntsman, D. G. (2013) 'Type-specific cell line models for type-specific ovarian cancer research', *PLoS One,* 8(9), pp. e72162.

Avraamides, C. J., Garmy-Susini, B. and Varner, J. A. (2008) 'Integrins in angiogenesis and lymphangiogenesis', *Nat Rev Cancer,* 8(8), pp. 604-17.

Ayaz, F. and Osborne, B. A. (2014) 'Non-canonical notch signaling in cancer and immunity', *Front Oncol,* 4, pp. 345.

Barbolina, M. V., Moss, N. M., Westfall, S. D., Liu, Y., Burkhalter, R. J., Marga, F., Forgacs, G., Hudson, L. G. and Stack, M. S. (2009) 'Microenvironmental regulation of ovarian cancer metastasis', *Cancer Treat Res,* 149, pp. 319-34.

Beatus, P., Lundkvist, J., Oberg, C. and Lendahl, U. (1999) 'The notch 3 intracellular domain represses notch 1-mediated activation through Hairy/Enhancer of split (HES) promoters', *Development,* 126(17), pp. 3925-35.

Beatus, P., Lundkvist, J., Oberg, C., Pedersen, K. and Lendahl, U. (2001) 'The origin of the ankyrin repeat region in Notch intracellular domains is critical for regulation of HES promoter activity', *Mech Dev,* 104(1-2), pp. 3-20.

Beaufort, C. M., Helmijr, J. C., Piskorz, A. M., Hoogstraat, M., Ruigrok-Ritstier, K., Besselink, N., Murtaza, M., van, I. W. F., Heine, A. A., Smid, M., Koudijs, M. J., Brenton, J. D., Berns, E. M. and

Helleman, J. (2014) 'Ovarian cancer cell line panel (OCCP): clinical importance of in vitro morphological subtypes', *PLoS One,* 9(9), pp. e103988.

Bellavia, D., Checquolo, S., Campese, A. F., Felli, M. P., Gulino, A. and Screpanti, I. (2008) 'Notch3: from subtle structural differences to functional diversity', *Oncogene,* 27(38), pp. 5092-8.

Berns, E. M. and Bowtell, D. D. (2012) 'The changing view of high-grade serous ovarian cancer', *Cancer Res,* 72(11), pp. 2701-4.

Berridge, M. V., Herst, P. M. and Tan, A. S. (2005) 'Tetrazolium dyes as tools in cell biology: new insights into their cellular reduction', *Biotechnol Annu Rev,* 11, pp. 127-52.

Bettegowda, C., Sausen, M., Leary, R. J., Kinde, I., Wang, Y., Agrawal, N., Bartlett, B. R., Wang, H., Luber, B., Alani, R. M., Antonarakis, E. S., Azad, N. S., Bardelli, A., Brem, H., Cameron, J. L., Lee, C. C., Fecher, L. A., Gallia, G. L., Gibbs, P., Le, D., Giuntoli, R. L., Goggins, M., Hogarty, M. D., Holdhoff, M., Hong, S. M., Jiao, Y., Juhl, H. H., Kim, J. J., Siravegna, G., Laheru, D. A., Lauricella, C., Lim, M., Lipson, E. J., Marie, S. K., Netto, G. J., Oliner, K. S., Olivi, A., Olsson, L., Riggins, G. J., Sartore-Bianchi, A., Schmidt, K., Shih I, M., Oba-Shinjo, S. M., Siena, S., Theodorescu, D., Tie, J., Harkins, T. T., Veronese, S., Wang, T. L., Weingart, J. D., Wolfgang, C. L., Wood, L. D., Xing, D., Hruban, R. H., Wu, J., Allen, P. J., Schmidt, C. M., Choti, M. A., Velculescu, V. E., Kinzler, K. W., Vogelstein, B., Papadopoulos, N. and Diaz, L. A., Jr. (2014) 'Detection of circulating tumor DNA in early- and late-stage human malignancies', *Sci Transl Med,* 6(224), pp. 224ra24.

Borggrefe, T. and Oswald, F. (2009) 'The Notch signaling pathway: transcriptional regulation at Notch target genes', *Cell Mol Life Sci,* 66(10), pp. 1631-46.

Boussios, S., Zarkavelis, G., Seraj, E., Zerdes, I., Tatsi, K. and Pentheroudakis, G. (2016) 'Non-epithelial Ovarian Cancer: Elucidating Uncommon Gynaecological Malignancies', *Anticancer Res,* 36(10), pp. 5031-5042.

Bowtell, D. D. (2010) 'The genesis and evolution of high-grade serous ovarian cancer', *Nat Rev Cancer,* 10(11), pp. 803-8.

Bowtell, D. D., Bohm, S., Ahmed, A. A., Aspuria, P. J., Bast, R. C., Jr., Beral, V., Berek, J. S., Birrer, M. J., Blagden, S., Bookman, M. A., Brenton, J. D., Chiappinelli, K. B., Martins, F. C., Coukos, G., Drapkin, R., Edmondson, R., Fotopoulou, C., Gabra, H., Galon, J., Gourley, C., Heong, V., Huntsman, D. G., Iwanicki, M., Karlan, B. Y., Kaye, A., Lengyel, E., Levine, D. A., Lu, K. H., McNeish, I. A., Menon, U., Narod, S. A., Nelson, B. H., Nephew, K. P., Pharoah, P., Powell, D. J., Jr., Ramos, P., Romero, I. L., Scott, C. L., Sood, A. K., Stronach, E. A. and Balkwill, F. R. (2015) 'Rethinking ovarian cancer II: reducing mortality from high-grade serous ovarian cancer', *Nat Rev Cancer,* 15(11), pp. 668-79.

Brown, C. W., Brodsky, A. S. and Freiman, R. N. (2015) 'Notch3 overexpression promotes anoikis resistance in epithelial ovarian cancer via upregulation of COL4A2', *Mol Cancer Res,* 13(1), pp. 78-85.

Burkholder, T., Foltz, C., Karlsson, E., Linton, C. G. and Smith, J. M. (2012) 'Health Evaluation of Experimental Laboratory Mice', *Curr Protoc Mouse Biol,* 2, pp. 145-165.

Byrne, A. T., Ross, L., Holash, J., Nakanishi, M., Hu, L., Hofmann, J. I., Yancopoulos, G. D. and Jaffe, R. B. (2003) 'Vascular endothelial growth factor-trap decreases tumor burden, inhibits ascites, and causes dramatic vascular remodeling in an ovarian cancer model', *Clin Cancer Res,* 9(15), pp. 5721-8.

Cancer Genome Atlas Research, N. (2011) 'Integrated genomic analyses of ovarian carcinoma', *Nature,* 474(7353), pp. 609-15.

Capaccione, K. M. and Pine, S. R. (2013) 'The Notch signaling pathway as a mediator of tumor survival', *Carcinogenesis,* 34(7), pp. 1420-30.

Casey, R. C., Burleson, K. M., Skubitz, K. M., Pambuccian, S. E., Oegema, T. R., Jr., Ruff, L. E. and Skubitz, A. P. (2001) 'Beta 1-integrins regulate the formation and adhesion of ovarian carcinoma multicellular spheroids', *Am J Pathol,* 159(6), pp. 2071-80.

Casey, R. C. and Skubitz, A. P. (2000) 'CD44 and beta1 integrins mediate ovarian carcinoma cell migration toward extracellular matrix proteins', *Clin Exp Metastasis,* 18(1), pp. 67-75.

Chen, X., Stoeck, A., Lee, S. J., Shih Ie, M., Wang, M. M. and Wang, T. L. (2010) 'Jagged1 expression regulated by Notch3 and Wnt/beta-catenin signaling pathways in ovarian cancer', *Oncotarget,* 1(3), pp. 210-8.

Chen, X., Thiaville, M. M., Chen, L., Stoeck, A., Xuan, J., Gao, M., Shih Ie, M. and Wang, T. L. (2012) 'Defining NOTCH3 target genes in ovarian cancer', *Cancer Res,* 72(9), pp. 2294-303.

Cheng, W., Liu, J., Yoshida, H., Rosen, D. and Naora, H. (2005) 'Lineage infidelity of epithelial ovarian cancers is controlled by HOX genes that specify regional identity in the reproductive tract', *Nat Med,* 11(5), pp. 531-7.

Cheon, D. J., Tong, Y., Sim, M. S., Dering, J., Berel, D., Cui, X., Lester, J., Beach, J. A., Tighiouart, M., Walts, A. E., Karlan, B. Y. and Orsulic, S. (2014) 'A collagen-remodeling gene signature regulated by TGF-beta signaling is associated with metastasis and poor survival in serous ovarian cancer', *Clin Cancer Res,* 20(3), pp. 711-23.

Cheung, H. W., Cowley, G. S., Weir, B. A., Boehm, J. S., Rusin, S., Scott, J. A., East, A., Ali, L. D., Lizotte, P. H., Wong, T. C., Jiang, G., Hsiao, J., Mermel, C. H., Getz, G., Barretina, J., Gopal, S., Tamayo, P., Gould, J., Tsherniak, A., Stransky, N., Luo, B., Ren, Y., Drapkin, R., Bhatia, S. N., Mesirov, J. P., Garraway, L. A., Meyerson, M., Lander, E. S., Root, D. E. and Hahn, W. C. (2011) 'Systematic investigation of genetic vulnerabilities across cancer cell lines reveals lineage-specific dependencies in ovarian cancer', *Proc Natl Acad Sci U S A,* 108(30), pp. 12372-7.

Cho, K. R. and Shih Ie, M. (2009) 'Ovarian cancer', *Annu Rev Pathol,* 4, pp. 287-313.

Cho, S., Sun, Y., Soisson, A. P., Dodson, M. K., Peterson, C. M., Jarboe, E. A., Kennedy, A. M. and Janat-Amsbury, M. M. (2013) 'Characterization and evaluation of pre-clinical suitability of a syngeneic orthotopic mouse ovarian cancer model', *Anticancer Res,* 33(4), pp. 1317-24.

Choi, J. H., Park, J. T., Davidson, B., Morin, P. J., Shih Ie, M. and Wang, T. L. (2008) 'Jagged-1 and Notch3 juxtacrine loop regulates ovarian tumor growth and adhesion', *Cancer Res,* 68(14), pp. 5716-23.

Clark, R., Krishnan, V., Schoof, M., Rodriguez, I., Theriault, B., Chekmareva, M. and Rinker-Schaeffer, C. (2013) 'Milky spots promote ovarian cancer metastatic colonization of peritoneal adipose in experimental models', *Am J Pathol,* 183(2), pp. 576-91.

Coleman, R. L., Brady, M. F., Herzog, T. J., Sabbatini, P., Armstrong, D. K., Walker, J. L., Kim, B. G., Fujiwara, K., Tewari, K. S., O'Malley, D. M., Davidson, S. A., Rubin, S. C., DiSilvestro, P., Basen-Engquist, K., Huang, H., Chan, J. K., Spirtos, N. M., Ashfaq, R. and Mannel, R. S. (2017) 'Bevacizumab and paclitaxel-carboplatin chemotherapy and secondary cytoreduction in recurrent, platinum-sensitive ovarian cancer (NRG Oncology/Gynecologic Oncology Group study GOG-0213): a multicentre, open-label, randomised, phase 3 trial', *Lancet Oncol,* 18(6), pp. 779-791.

Colorado, P. C., Torre, A., Kamphaus, G., Maeshima, Y., Hopfer, H., Takahashi, K., Volk, R., Zamborsky, E. D., Herman, S., Sarkar, P. K., Ericksen, M. B., Dhanabal, M., Simons, M., Post, M., Kufe, D. W., Weichselbaum, R. R., Sukhatme, V. P. and Kalluri, R. (2000) 'Anti-angiogenic cues from vascular basement membrane collagen', *Cancer Res,* 60(9), pp. 2520-6.

Cont, N. T., Ferrero, A., Peccatori, F. A., D'Alonzo, M., Codacci-Pisanelli, G., Colombo, N. and Biglia, N. (2015) 'Medical treatment of early stage and rare histological variants of epithelial ovarian cancer', *Ecancermedicalscience,* 9, pp. 584.

Crum, C. P., Drapkin, R., Miron, A., Ince, T. A., Muto, M., Kindelberger, D. W. and Lee, Y. (2007) 'The distal fallopian tube: a new model for pelvic serous carcinogenesis', *Curr Opin Obstet Gynecol,* 19(1), pp. 3-9.

Day, C. P., Carter, J., Weaver Ohler, Z., Bonomi, C., El Meskini, R., Martin, P., Graff-Cherry, C., Feigenbaum, L., Tuting, T., Van Dyke, T., Hollingshead, M. and Merlino, G. (2014) '"Glowing head" mice: a genetic tool enabling reliable preclinical image-based evaluation of cancers in immunocompetent allografts', *PLoS One,* 9(11), pp. e109956.

Domcke, S., Sinha, R., Levine, D. A., Sander, C. and Schultz, N. (2013) 'Evaluating cell lines as tumour models by comparison of genomic profiles', *Nat Commun,* 4, pp. 2126.

Dubeau, L. (2008) 'The cell of origin of ovarian epithelial tumours', *Lancet Oncol,* 9(12), pp. 1191-7.

Dubeau, L. and Drapkin, R. (2013) 'Coming into focus: the nonovarian origins of ovarian cancer', *Ann Oncol,* 24 Suppl 8, pp. viii28-viii35.

Dull, T., Zufferey, R., Kelly, M., Mandel, R. J., Nguyen, M., Trono, D. and Naldini, L. (1998) 'A third-generation lentivirus vector with a conditional packaging system', *J Virol,* 72(11), pp. 8463-71.

Eddie, S. L., Quartuccio, S. M., E, O. h., Moyle-Heyrman, G., Lantvit, D. D., Wei, J. J., Vanderhyden, B. C. and Burdette, J. E. (2015) 'Tumorigenesis and peritoneal colonization from fallopian tube epithelium', *Oncotarget,* 6(24), pp. 20500-12.

Ehebauer, M. T., Chirgadze, D. Y., Hayward, P., Martinez Arias, A. and Blundell, T. L. (2005) 'High-resolution crystal structure of the human Notch 1 ankyrin domain', *Biochem J,* 392(Pt 1), pp. 13-20.

Endsley, M. P., Moyle-Heyrman, G., Karthikeyan, S., Lantvit, D. D., Davis, D. A., Wei, J. J. and Burdette, J. E. (2015) 'Spontaneous Transformation of Murine Oviductal Epithelial Cells: A Model System to Investigate the Onset of Fallopian-Derived Tumors', *Front Oncol,* 5, pp. 154.

Fathalla, M. F. (1971) 'Incessant ovulation--a factor in ovarian neoplasia?', *Lancet,* 2(7716), pp. 163.

Fathalla, M. F. (2013) 'Incessant ovulation and ovarian cancer - a hypothesis re-visited', *Facts Views Vis Obgyn,* 5(4), pp. 292-7.

Finn, W. F. and Javert, C. T. (1949) 'Primary and metastatic cancer of the fallopian tube', *Cancer,* 2(5), pp. 803-14.

Freedman, R. S., Deavers, M., Liu, J. and Wang, E. (2004) 'Peritoneal inflammation - A microenvironment for Epithelial Ovarian Cancer (EOC)', *J Transl Med,* 2(1), pp. 23.

Frgala, T., Kalous, O., Proffitt, R. T. and Reynolds, C. P. (2007) 'A fluorescence microplate cytotoxicity assay with a 4-log dynamic range that identifies synergistic drug combinations', *Mol Cancer Ther,* 6(3), pp. 886-97.

Fukunaga, M., Nomura, K., Ishikawa, E. and Ushigome, S. (1997) 'Ovarian atypical endometriosis: its close association with malignant epithelial tumours', *Histopathology,* 30(3), pp. 249-55.

Garcia-Olmo, D. C., Samos, J., Picazo, M. G., Fernandez-Miguel, G., Toboso, I. and Garcia-Olmo, D. (2008) 'Loss of a reporter gene for green fluorescent protein during tumor progression suggests the recruitment of host cells in rats with experimentally induced colon cancer', *Histol Histopathol,* 23(10), pp. 1205-11.

Garson, K., Gamwell, L. F., Pitre, E. M. and Vanderhyden, B. C. (2012) 'Technical challenges and limitations of current mouse models of ovarian cancer', *J Ovarian Res,* 5(1), pp. 39.

Gerber, S. A., Rybalko, V. Y., Bigelow, C. E., Lugade, A. A., Foster, T. H., Frelinger, J. G. and Lord, E. M. (2006) 'Preferential attachment of peritoneal tumor metastases to omental immune aggregates and possible role of a unique vascular microenvironment in metastatic survival and growth', *Am J Pathol,* 169(5), pp. 1739-52.

Gotwals, P. J., Chi-Rosso, G., Lindner, V., Yang, J., Ling, L., Fawell, S. E. and Koteliansky, V. E. (1996) 'The alpha1beta1 integrin is expressed during neointima formation in rat arteries and mediates collagen matrix reorganization', *J Clin Invest,* 97(11), pp. 2469-77.

Greenaway, J., Moorehead, R., Shaw, P. and Petrik, J. (2008) 'Epithelial-stromal interaction increases cell proliferation, survival and tumorigenicity in a mouse model of human epithelial ovarian cancer', *Gynecol Oncol,* 108(2), pp. 385-94.

Groeneweg, J. W., DiGloria, C. M., Yuan, J., Richardson, W. S., Growdon, W. B., Sathyanarayanan, S., Foster, R. and Rueda, B. R. (2014a) 'Inhibition of notch signaling in combination with Paclitaxel reduces platinum-resistant ovarian tumor growth', *Front Oncol,* 4, pp. 171.

Groeneweg, J. W., Foster, R., Growdon, W. B., Verheijen, R. H. and Rueda, B. R. (2014b) 'Notch signaling in serous ovarian cancer', *J Ovarian Res,* 7, pp. 95.

Gupta, N., Xu, Z., El-Sehemy, A., Steed, H. and Fu, Y. (2013) 'Notch3 induces epithelial-mesenchymal transition and attenuates carboplatin-induced apoptosis in ovarian cancer cells', *Gynecol Oncol,* 130(1), pp. 200-6.

Haber, D. A. and Velculescu, V. E. (2014) 'Blood-based analyses of cancer: circulating tumor cells and circulating tumor DNA', *Cancer Discov,* 4(6), pp. 650-61.

Hass, M. R., Liow, H. H., Chen, X., Sharma, A., Inoue, Y. U., Inoue, T., Reeb, A., Martens, A., Fulbright, M., Raju, S., Stevens, M., Boyle, S., Park, J. S., Weirauch, M. T., Brent, M. R. and Kopan, R. (2015) 'SpDamID: Marking DNA Bound by Protein Complexes Identifies Notch-Dimer Responsive Enhancers', *Mol Cell,* 59(4), pp. 685-97.

Hori, K., Sen, A. and Artavanis-Tsakonas, S. (2013) 'Notch signaling at a glance', *J Cell Sci,* 126(Pt 10), pp. 2135-40.

Hu, L., Hofmann, J., Zaloudek, C., Ferrara, N., Hamilton, T. and Jaffe, R. B. (2002) 'Vascular endothelial growth factor immunoneutralization plus Paclitaxel markedly reduces tumor burden and ascites in athymic mouse model of ovarian cancer', *Am J Pathol,* 161(5), pp. 1917-24.

Hu, W., Liu, T., Ivan, C., Sun, Y., Huang, J., Mangala, L. S., Miyake, T., Dalton, H. J., Pradeep, S., Rupaimoole, R., Previs, R. A., Han, H. D., Bottsford-Miller, J., Zand, B., Kang, Y., Pecot, C. V., Nick, A. M., Wu, S. Y., Lee, J. S., Sehgal, V., Ram, P., Liu, J., Tucker, S. L., Lopez-Berestein, G., Baggerly, K. A., Coleman, R. L. and Sood, A. K. (2014) 'Notch3 pathway alterations in ovarian cancer', *Cancer Res,* 74(12), pp. 3282-93.

Hughes, C. S., Postovit, L. M. and Lajoie, G. A. (2010) 'Matrigel: a complex protein mixture required for optimal growth of cell culture', *Proteomics,* 10(9), pp. 1886-90.

Humphries, J. D., Byron, A. and Humphries, M. J. (2006) 'Integrin ligands at a glance', *J Cell Sci,* 119(Pt 19), pp. 3901-3.

Hynes, R. O. (1992) 'Integrins: versatility, modulation, and signaling in cell adhesion', *Cell,* 69(1), pp. 11-25.

Hynes, R. O. (2002) 'Integrins: bidirectional, allosteric signaling machines', *Cell,* 110(6), pp. 673-87.

Iwanicki, M. P., Davidowitz, R. A., Ng, M. R., Besser, A., Muranen, T., Merritt, M., Danuser, G., Ince, T. A. and Brugge, J. S. (2011) 'Ovarian cancer spheroids use myosin-generated force to clear the mesothelium', *Cancer Discov,* 1(2), pp. 144-57.

Jeong, J. Y., Kang, H., Kim, T. H., Kim, G., Heo, J. H., Kwon, A. Y., Kim, S., Jung, S. G. and An, H. J. (2017) 'MicroRNA-136 inhibits cancer stem cell activity and enhances the anti-tumor effect of paclitaxel against chemoresistant ovarian cancer cells by targeting Notch3', *Cancer Lett,* 386, pp. 168-178.

Jung, J. G., Stoeck, A., Guan, B., Wu, R. C., Zhu, H., Blackshaw, S., Shih Ie, M. and Wang, T. L. (2014) 'Notch3 interactome analysis identified WWP2 as a negative regulator of Notch3 signaling in ovarian cancer', *PLoS Genet,* 10(10), pp. e1004751.

Jung, S. G., Kwon, Y. D., Song, J. A., Back, M. J., Lee, S. Y., Lee, C., Hwang, Y. Y. and An, H. J. (2010) 'Prognostic significance of Notch 3 gene expression in ovarian serous carcinoma', *Cancer Sci,* 101(9), pp. 1977-83.

Kang, H., Jeong, J. Y., Song, J. Y., Kim, T. H., Kim, G., Huh, J. H., Kwon, A. Y., Jung, S. G. and An, H. J. (2015) 'Notch3-specific inhibition using siRNA knockdown or GSI sensitizes paclitaxel-resistant ovarian cancer cells', *Mol Carcinog*.

Kangsamaksin, T., Murtomaki, A., Kofler, N. M., Cuervo, H., Chaudhri, R. A., Tattersall, I. W., Rosenstiel, P. E., Shawber, C. J. and Kitajewski, J. (2015) 'NOTCH decoys that selectively block DLL/NOTCH or JAG/NOTCH disrupt angiogenesis by unique mechanisms to inhibit tumor growth', *Cancer Discov,* 5(2), pp. 182-97.

Karst, A. M. and Drapkin, R. (2012) 'Primary culture and immortalization of human fallopian tube secretory epithelial cells', *Nat Protoc,* 7(9), pp. 1755-64.

Karst, A. M., Levanon, K. and Drapkin, R. (2011) 'Modeling high-grade serous ovarian carcinogenesis from the fallopian tube', *Proc Natl Acad Sci U S A,* 108(18), pp. 7547-52.

Kenny, H. A., Dogan, S., Zillhardt, M., A, K. M., Yamada, S. D., Krausz, T. and Lengyel, E. (2009) 'Organotypic models of metastasis: A three-dimensional culture mimicking the human peritoneum and omentum for the study of the early steps of ovarian cancer metastasis', *Cancer Treat Res,* 149, pp. 335-51.

Kenny, H. A., Krausz, T., Yamada, S. D. and Lengyel, E. (2007) 'Use of a novel 3D culture model to elucidate the role of mesothelial cells, fibroblasts and extra-cellular matrices on adhesion and invasion of ovarian cancer cells to the omentum', *Int J Cancer,* 121(7), pp. 1463-72.

Kenny, H. A., Nieman, K. M., Mitra, A. K. and Lengyel, E. (2011) 'The first line of intra-abdominal metastatic attack: breaching the mesothelial cell layer', *Cancer Discov,* 1(2), pp. 100-2.

Keshelava, N., Frgala, T., Krejsa, J., Kalous, O. and Reynolds, C. P. (2005) 'DIMSCAN: a microcomputer fluorescence-based cytotoxicity assay for preclinical testing of combination chemotherapy', *Methods Mol Med,* 110, pp. 139-53.

Khan, S. M., Funk, H. M., Thiolloy, S., Lotan, T. L., Hickson, J., Prins, G. S., Drew, A. F. and Rinker-Schaeffer, C. W. (2010) 'In vitro metastatic colonization of human ovarian cancer cells to the omentum', *Clin Exp Metastasis,* 27(3), pp. 185-96.

Kleinman, H. K. and Martin, G. R. (2005) 'Matrigel: basement membrane matrix with biological activity', *Semin Cancer Biol,* 15(5), pp. 378-86.

Kofler, N. M., Cuervo, H., Uh, M. K., Murtomaki, A. and Kitajewski, J. (2015) 'Combined deficiency of Notch1 and Notch3 causes pericyte dysfunction, models CADASIL, and results in arteriovenous malformations', *Sci Rep,* 5, pp. 16449.

Kopan, R. and Ilagan, M. X. (2009) 'The canonical Notch signaling pathway: unfolding the activation mechanism', *Cell,* 137(2), pp. 216-33.

Korch, C., Spillman, M. A., Jackson, T. A., Jacobsen, B. M., Murphy, S. K., Lessey, B. A., Jordan, V. C. and Bradford, A. P. (2012) 'DNA profiling analysis of endometrial and ovarian cell lines reveals misidentification, redundancy and contamination', *Gynecol Oncol,* 127(1), pp. 241-8.

Ksiazek, K., Mikula-Pietrasik, J., Korybalska, K., Dworacki, G., Jorres, A. and Witowski, J. (2009) 'Senescent peritoneal mesothelial cells promote ovarian cancer cell adhesion: the role of oxidative stress-induced fibronectin', *Am J Pathol,* 174(4), pp. 1230-40.

Kurman, R. J., Vang, R., Junge, J., Hannibal, C. G., Kjaer, S. K. and Shih Ie, M. (2011) 'Papillary tubal hyperplasia: the putative precursor of ovarian atypical proliferative (borderline) serous tumors, noninvasive implants, and endosalpingiosis', *Am J Surg Pathol,* 35(11), pp. 1605-14.

Kurman, R. J., Visvanathan, K., Roden, R., Wu, T. C. and Shih Ie, M. (2008) 'Early detection and treatment of ovarian cancer: shifting from early stage to minimal volume of disease based on a new model of carcinogenesis', *Am J Obstet Gynecol,* 198(4), pp. 351-6.

L'Esperance, S., Bachvarova, M., Tetu, B., Mes-Masson, A. M. and Bachvarov, D. (2008) 'Global gene expression analysis of early response to chemotherapy treatment in ovarian cancer spheroids', *BMC Genomics,* 9, pp. 99.

Lane, D., Matte, I., Rancourt, C. and Piche, A. (2011) 'Prognostic significance of IL-6 and IL-8 ascites levels in ovarian cancer patients', *BMC Cancer,* 11, pp. 210.

Langdon, S. P. (2004) 'Isolation and culture of ovarian cancer cell lines', *Methods Mol Med,* 88, pp. 133-9.

Langdon, S. P., Lawrie, S. S., Hay, F. G., Hawkes, M. M., McDonald, A., Hayward, I. P., Schol, D. J., Hilgers, J., Leonard, R. C. and Smyth, J. F. (1988) 'Characterization and properties of nine human ovarian adenocarcinoma cell lines', *Cancer Res,* 48(21), pp. 6166-72.

Lardelli, M., Dahlstrand, J. and Lendahl, U. (1994) 'The novel Notch homologue mouse Notch 3 lacks specific epidermal growth factor-repeats and is expressed in proliferating neuroepithelium', *Mech Dev,* 46(2), pp. 123-36.

Lardelli, M., Williams, R., Mitsiadis, T. and Lendahl, U. (1996) 'Expression of the Notch 3 intracellular domain in mouse central nervous system progenitor cells is lethal and leads to disturbed neural tube development', *Mech Dev,* 59(2), pp. 177-90.

Laury, A. R., Perets, R., Piao, H., Krane, J. F., Barletta, J. A., French, C., Chirieac, L. R., Lis, R., Loda, M., Hornick, J. L., Drapkin, R. and Hirsch, M. S. (2011) 'A comprehensive analysis of PAX8 expression in human epithelial tumors', *Am J Surg Pathol,* 35(6), pp. 816-26.

Leinster, D. A., Kulbe, H., Everitt, G., Thompson, R., Perretti, M., Gavins, F. N., Cooper, D., Gould, D., Ennis, D. P., Lockley, M., McNeish, I. A., Nourshargh, S. and Balkwill, F. R. (2012) 'The peritoneal tumour microenvironment of high-grade serous ovarian cancer', *J Pathol,* 227(2), pp. 136-45.

Leitinger, B. and Hohenester, E. (2007) 'Mammalian collagen receptors', *Matrix Biol,* 26(3), pp. 146-55.

Lengyel, E. (2010) 'Ovarian cancer development and metastasis', *Am J Pathol,* 177(3), pp. 1053-64.

Lengyel, E., Burdette, J. E., Kenny, H. A., Matei, D., Pilrose, J., Haluska, P., Nephew, K. P., Hales, D. B. and Stack, M. S. (2014) 'Epithelial ovarian cancer experimental models', *Oncogene,* 33(28), pp. 3619-33.

Lewellen, K. A., Metzinger, M. N., Liu, Y. and Stack, M. S. (2016) 'Quantitation of Intra-peritoneal Ovarian Cancer Metastasis', *J Vis Exp,* (113).

Liu, Z., Yun, R., Yu, X., Hu, H., Huang, G., Tan, B. and Chen, T. (2016) 'Overexpression of Notch3 and pS6 Is Associated with Poor Prognosis in Human Ovarian Epithelial Cancer', *Mediators Inflamm,* 2016, pp. 5953498.

Lu, K. H., Patterson, A. P., Wang, L., Marquez, R. T., Atkinson, E. N., Baggerly, K. A., Ramoth, L. R., Rosen, D. G., Liu, J., Hellstrom, I., Smith, D., Hartmann, L., Fishman, D., Berchuck, A., Schmandt, R., Whitaker, R., Gershenson, D. M., Mills, G. B. and Bast, R. C., Jr. (2004) 'Selection of potential markers for epithelial ovarian cancer with gene expression arrays and recursive descent partition analysis', *Clin Cancer Res,* 10(10), pp. 3291-300.

Martinez, R. L. M. C. and Naranjo, J. D. (2010) 'A pretest for choosing between logrank and wilcoxon tests in the two-sample problem', *METRON,* 68(2), pp. 111-125.

Matulonis, U. A., Sood, A. K., Fallowfield, L., Howitt, B. E., Sehouli, J. and Karlan, B. Y. (2016) 'Ovarian cancer', *Nat Rev Dis Primers,* 2, pp. 16061.

McAuliffe, S. M., Morgan, S. L., Wyant, G. A., Tran, L. T., Muto, K. W., Chen, Y. S., Chin, K. T., Partridge, J. C., Poole, B. B., Cheng, K. H., Daggett, J., Jr., Cullen, K., Kantoff, E., Hasselbatt, K., Berkowitz, J., Muto, M. G., Berkowitz, R. S., Aster, J. C., Matulonis, U. A. and Dinulescu, D. M. (2012) 'Targeting Notch, a key pathway for ovarian cancer stem cells, sensitizes tumors to platinum therapy', *Proc Natl Acad Sci U S A,* 109(43), pp. E2939-48.

McClung, E. C. and Wenham, R. M. (2016) 'Profile of bevacizumab in the treatment of platinum-resistant ovarian cancer: current perspectives', *Int J Womens Health,* 8, pp. 59-75.

Mendrick, D. L., Kelly, D. M., duMont, S. S. and Sandstrom, D. J. (1995) 'Glomerular epithelial and mesangial cells differentially modulate the binding specificities of VLA-1 and VLA-2', *Lab Invest,* 72(3), pp. 367-75.

Mitra, A. K., Davis, D. A., Tomar, S., Roy, L., Gurler, H., Xie, J., Lantvit, D. D., Cardenas, H., Fang, F., Liu, Y., Loughran, E., Yang, J., Sharon Stack, M., Emerson, R. E., Cowden Dahl, K. D., M, V. B., Nephew, K. P., Matei, D. and Burdette, J. E. (2015) 'In vivo tumor growth of high-grade serous ovarian cancer cell lines', *Gynecol Oncol,* 138(2), pp. 372-7.

Miyake, S., Sakurai, T., Okumura, K. and Yagita, H. (1994) 'Identification of collagen and laminin receptor integrins on murine T lymphocytes', *Eur J Immunol,* 24(9), pp. 2000-5.

Mohr, O. L. (1919) 'Character Changes Caused by Mutation of an Entire Region of a Chromosome in Drosophila', *Genetics,* 4(3), pp. 275-82.

Monk, B. J., Huh, W. K., Rosenberg, J. A. and Jacobs, I. (2017) 'Will bevacizumab biosimilars impact the value of systemic therapy in gynecologic cancers?', *Gynecologic Oncology Research and Practice,* 4(1), pp. 7.

Moser, T. L., Pizzo, S. V., Bafetti, L. M., Fishman, D. A. and Stack, M. S. (1996) 'Evidence for preferential adhesion of ovarian epithelial carcinoma cells to type I collagen mediated by the alpha2beta1 integrin', *Int J Cancer,* 67(5), pp. 695-701.

Mumm, J. S. and Kopan, R. (2000) 'Notch signaling: from the outside in', *Dev Biol,* 228(2), pp. 151-65.

Nakayama, J., Raines, T. A., Lynch, K. R. and Slack-Davis, J. K. (2015) 'Decreased peritoneal ovarian cancer growth in mice lacking expression of lipid phosphate phosphohydrolase 1', *PLoS One,* 10(3), pp. e0120071.

Nakayama, K., Nakayama, N., Jinawath, N., Salani, R., Kurman, R. J., Shih Ie, M. and Wang, T. L. (2007) 'Amplicon profiles in ovarian serous carcinomas', *Int J Cancer,* 120(12), pp. 2613-7.

Naora, H. and Montell, D. J. (2005) 'Ovarian cancer metastasis: integrating insights from disparate model organisms', *Nat Rev Cancer,* 5(5), pp. 355-66.

Niedbala, M. J., Crickard, K. and Bernacki, R. J. (1985) 'Interactions of human ovarian tumor cells with human mesothelial cells grown on extracellular matrix. An in vitro model system for studying tumor cell adhesion and invasion', *Exp Cell Res,* 160(2), pp. 499-513.

Nik, N. N., Vang, R., Shih Ie, M. and Kurman, R. J. (2014) 'Origin and pathogenesis of pelvic (ovarian, tubal, and primary peritoneal) serous carcinoma', *Annu Rev Pathol,* 9, pp. 27-45.

Nowell, C. S. and Radtke, F. (2017) 'Notch as a tumour suppressor', *Nat Rev Cancer,* 17(3), pp. 145-159.

Ntziachristos, P., Lim, J. S., Sage, J. and Aifantis, I. (2014) 'From fly wings to targeted cancer therapies: a centennial for notch signaling', *Cancer Cell,* 25(3), pp. 318-34.

Nyberg, P., Xie, L. and Kalluri, R. (2005) 'Endogenous inhibitors of angiogenesis', *Cancer Res,* 65(10), pp. 3967-79.

Ong, C. T., Cheng, H. T., Chang, L. W., Ohtsuka, T., Kageyama, R., Stormo, G. D. and Kopan, R. (2006) 'Target selectivity of vertebrate notch proteins. Collaboration between discrete domains and CSL-binding site architecture determines activation probability', *J Biol Chem,* 281(8), pp. 5106-19.

Orsulic, S., Li, Y., Soslow, R. A., Vitale-Cross, L. A., Gutkind, J. S. and Varmus, H. E. (2002) 'Induction of ovarian cancer by defined multiple genetic changes in a mouse model system', *Cancer Cell,* 1(1), pp. 53-62.

Park, C. C., Zhang, H., Pallavicini, M., Gray, J. W., Baehner, F., Park, C. J. and Bissell, M. J. (2006a) 'Beta1 integrin inhibitory antibody induces apoptosis of breast cancer cells, inhibits growth, and distinguishes malignant from normal phenotype in three dimensional cultures and in vivo', *Cancer Res,* 66(3), pp. 1526-35.

Park, J. T., Chen, X., Trope, C. G., Davidson, B., Shih Ie, M. and Wang, T. L. (2010) 'Notch3 overexpression is related to the recurrence of ovarian cancer and confers resistance to carboplatin', *Am J Pathol,* 177(3), pp. 1087-94.

Park, J. T., Li, M., Nakayama, K., Mao, T. L., Davidson, B., Zhang, Z., Kurman, R. J., Eberhart, C. G., Shih Ie, M. and Wang, T. L. (2006b) 'Notch3 gene amplification in ovarian cancer', *Cancer Res,* 66(12), pp. 6312-8.

Park, J. T., Shih Ie, M. and Wang, T. L. (2008) 'Identification of Pbx1, a potential oncogene, as a Notch3 target gene in ovarian cancer', *Cancer Res,* 68(21), pp. 8852-60.

Perets, R., Wyant, G. A., Muto, K. W., Bijron, J. G., Poole, B. B., Chin, K. T., Chen, J. Y., Ohman, A. W., Stepule, C. D., Kwak, S., Karst, A. M., Hirsch, M. S., Setlur, S. R., Crum, C. P., Dinulescu, D. M. and Drapkin, R. (2013) 'Transformation of the fallopian tube secretory epithelium leads to high-grade serous ovarian cancer in Brca;Tp53;Pten models', *Cancer Cell,* 24(6), pp. 751-65.

Phallen, J., Sausen, M., Adleff, V., Leal, A., Hruban, C., White, J., Anagnostou, V., Fiksel, J., Cristiano, S., Papp, E., Speir, S., Reinert, T., Orntoft, M. W., Woodward, B. D., Murphy, D., Parpart-Li, S., Riley, D., Nesselbush, M., Sengamalay, N., Georgiadis, A., Li, Q. K., Madsen, M. R., Mortensen, F. V., Huiskens, J., Punt, C., van Grieken, N., Fijneman, R., Meijer, G., Husain, H., Scharpf, R. B., Diaz, L. A., Jr., Jones, S., Angiuoli, S., Orntoft, T., Nielsen, H. J., Andersen, C. L. and Velculescu, V. E. (2017) 'Direct detection of early-stage cancers using circulating tumor DNA', *Sci Transl Med,* 9(403).

Piek, J. M., van Diest, P. J., Zweemer, R. P., Jansen, J. W., Poort-Keesom, R. J., Menko, F. H., Gille, J. J., Jongsma, A. P., Pals, G., Kenemans, P. and Verheijen, R. H. (2001) 'Dysplastic changes in prophylactically removed Fallopian tubes of women predisposed to developing ovarian cancer', *J Pathol,* 195(4), pp. 451-6.

Pradeep, S., Kim, S. W., Wu, S. Y., Nishimura, M., Chaluvally-Raghavan, P., Miyake, T., Pecot, C. V., Kim, S. J., Choi, H. J., Bischoff, F. Z., Mayer, J. A., Huang, L., Nick, A. M., Hall, C. S., Rodriguez-Aguayo, C., Zand, B., Dalton, H. J., Arumugam, T., Lee, H. J., Han, H. D., Cho, M. S., Rupaimoole, R., Mangala, L. S., Sehgal, V., Oh, S. C., Liu, J., Lee, J. S., Coleman, R. L., Ram, P., Lopez-Berestein, G., Fidler, I. J. and Sood, A. K. (2014) 'Hematogenous metastasis of ovarian cancer: rethinking mode of spread', *Cancer Cell,* 26(1), pp. 77-91.

Pujade-Lauraine, E., Hilpert, F., Weber, B., Reuss, A., Poveda, A., Kristensen, G., Sorio, R., Vergote, I., Witteveen, P., Bamias, A., Pereira, D., Wimberger, P., Oaknin, A., Mirza, M. R., Follana, P., Bollag, D. and Ray-Coquard, I. (2014) 'Bevacizumab Combined With Chemotherapy for Platinum-Resistant Recurrent Ovarian Cancer: The AURELIA Open-Label Randomized Phase III Trial', *Journal of Clinical Oncology,* 32(13), pp. 1302-1308.

Puls, L. E., Duniho, T., Hunter, J. E., Kryscio, R., Blackhurst, D. and Gallion, H. (1996) 'The prognostic implication of ascites in advanced-stage ovarian cancer', *Gynecol Oncol,* 61(1), pp. 109-12.

Radtke, F. and Raj, K. (2003) 'The role of Notch in tumorigenesis: oncogene or tumour suppressor?', *Nat Rev Cancer,* 3(10), pp. 756-67.

Radtke, F., Schweisguth, F. and Pear, W. (2005) 'The Notch 'gospel'', *EMBO Rep,* 6(12), pp. 1120-5.

Rahman, M. T., Nakayama, K., Rahman, M., Katagiri, H., Katagiri, A., Ishibashi, T., Ishikawa, M., Iida, K., Nakayama, S., Otsuki, Y. and Miyazaki, K. (2012) 'Notch3 overexpression as potential therapeutic target in advanced stage chemoresistant ovarian cancer', *Am J Clin Pathol,* 138(4), pp. 535-44.

Resta, L., Russo, S., Colucci, G. A. and Prat, J. (1993) 'Morphologic precursors of ovarian epithelial tumors', *Obstet Gynecol,* 82(2), pp. 181-6.

Roby, K. F., Taylor, C. C., Sweetwood, J. P., Cheng, Y., Pace, J. L., Tawfik, O., Persons, D. L., Smith, P. G. and Terranova, P. F. (2000) 'Development of a syngeneic mouse model for events related to ovarian cancer', *Carcinogenesis,* 21(4), pp. 585-91.

Rosen, D. G., Yang, G., Liu, G., Mercado-Uribe, I., Chang, B., Xiao, X. S., Zheng, J., Xue, F. X. and Liu, J. (2009) 'Ovarian cancer: pathology, biology, and disease models', *Front Biosci (Landmark Ed),* 14, pp. 2089-102.

Sawada, K., Radjabi, A. R., Shinomiya, N., Kistner, E., Kenny, H., Becker, A. R., Turkyilmaz, M. A., Salgia, R., Yamada, S. D., Vande Woude, G. F., Tretiakova, M. S. and Lengyel, E. (2007) 'c-Met overexpression is a prognostic factor in ovarian cancer and an effective target for inhibition of peritoneal dissemination and invasion', *Cancer Res,* 67(4), pp. 1670-9.

Schneider, C. A., Rasband, W. S. and Eliceiri, K. W. (2012) 'NIH Image to ImageJ: 25 years of image analysis', *Nat Methods,* 9(7), pp. 671-5.

Shah, M. M., Zerlin, M., Li, B. Y., Herzog, T. J., Kitajewski, J. K. and Wright, J. D. (2013) 'The role of Notch and gamma-secretase inhibition in an ovarian cancer model', *Anticancer Res,* 33(3), pp. 801-8.

Shen, Y., Shen, R., Ge, L., Zhu, Q. and Li, F. (2012) 'Fibrillar type I collagen matrices enhance metastasis/invasion of ovarian epithelial cancer via beta1 integrin and PTEN signals', *Int J Gynecol Cancer,* 22(8), pp. 1316-24.

Sher, I., Adham, S. A., Petrik, J. and Coomber, B. L. (2009) 'Autocrine VEGF-A/KDR loop protects epithelial ovarian carcinoma cells from anoikis', *Int J Cancer,* 124(3), pp. 553-61.

Shih Ie, M. and Kurman, R. J. (2004) 'Ovarian tumorigenesis: a proposed model based on morphological and molecular genetic analysis', *Am J Pathol,* 164(5), pp. 1511-8.

Shih Ie, M., Nakayama, K., Wu, G., Nakayama, N., Zhang, J. and Wang, T. L. (2011) 'Amplification of the ch19p13.2 NACC1 locus in ovarian high-grade serous carcinoma', *Mod Pathol,* 24(5), pp. 638-45.

Shimizu, K., Chiba, S., Saito, T., Kumano, K., Hamada, Y. and Hirai, H. (2002) 'Functional diversity among Notch1, Notch2, and Notch3 receptors', *Biochem Biophys Res Commun,* 291(4), pp. 775-9.

Siegel, R. L., Miller, K. D. and Jemal, A. (2017) 'Cancer Statistics, 2017', *CA Cancer J Clin,* 67(1), pp. 7-30.

Silva, E. G. (2016) 'The Origin of Epithelial Neoplasms of the Ovary: An Alternative View', *Adv Anat Pathol,* 23(1), pp. 50-7.

Sodek, K. L., Murphy, K. J., Brown, T. J. and Ringuette, M. J. (2012) 'Cell-cell and cell-matrix dynamics in intraperitoneal cancer metastasis', *Cancer Metastasis Rev,* 31(1-2), pp. 397-414.

Sorensen, E. W., Gerber, S. A., Sedlacek, A. L., Rybalko, V. Y., Chan, W. M. and Lord, E. M. (2009) 'Omental immune aggregates and tumor metastasis within the peritoneal cavity', *Immunol Res,* 45(2-3), pp. 185-94.

Steg, A. D., Katre, A. A., Goodman, B., Han, H. D., Nick, A. M., Stone, R. L., Coleman, R. L., Alvarez, R. D., Lopez-Berestein, G., Sood, A. K. and Landen, C. N. (2011) 'Targeting the notch ligand JAGGED1 in both tumor cells and stroma in ovarian cancer', *Clin Cancer Res,* 17(17), pp. 5674-85.

Steinbauer, M., Guba, M., Cernaianu, G., Kohl, G., Cetto, M., Kunz-Schughart, L. A., Geissler, E. K., Falk, W. and Jauch, K. W. (2003) 'GFP-transfected tumor cells are useful in examining early metastasis in vivo, but immune reaction precludes long-term tumor development studies in immunocompetent mice', *Clin Exp Metastasis,* 20(2), pp. 135-41.

Symowicz, J., Adley, B. P., Gleason, K. J., Johnson, J. J., Ghosh, S., Fishman, D. A., Hudson, L. G. and Stack, M. S. (2007) 'Engagement of collagen-binding integrins promotes matrix metalloproteinase-9-dependent E-cadherin ectodomain shedding in ovarian carcinoma cells', *Cancer Res,* 67(5), pp. 2030-9.

Taddei, M. L., Giannoni, E., Fiaschi, T. and Chiarugi, P. (2012) 'Anoikis: an emerging hallmark in health and diseases', *J Pathol,* 226(2), pp. 380-93.

Takebe, N., Nguyen, D. and Yang, S. X. (2014) 'Targeting notch signaling pathway in cancer: clinical development advances and challenges', *Pharmacol Ther,* 141(2), pp. 140-9.

Tarin, D., Price, J. E., Kettlewell, M. G., Souter, R. G., Vass, A. C. and Crossley, B. (1984) 'Mechanisms of human tumor metastasis studied in patients with peritoneovenous shunts', *Cancer Res,* 44(8), pp. 3584-92.

Tarone, R. E. and Ware, J. (1977) 'Distribution-Free Tests for Equality of Survival Distributions', *Biometrika,* 64(1), pp. 156-160.

Tenti, P., Aguzzi, A., Riva, C., Usellini, L., Zappatore, R., Bara, J., Samloff, I. M. and Solcia, E. (1992) 'Ovarian mucinous tumors frequently express markers of gastric, intestinal, and pancreatobiliary epithelial cells', *Cancer,* 69(8), pp. 2131-42.

Torre, L. A., Bray, F., Siegel, R. L., Ferlay, J., Lortet-Tieulent, J. and Jemal, A. (2015) 'Global cancer statistics, 2012', *CA Cancer J Clin,* 65(2), pp. 87-108.

Tucker, G. C. (2006) 'Integrins: molecular targets in cancer therapy', *Curr Oncol Rep,* 8(2), pp. 96-103.

Ullman-Cullere, M. H. and Foltz, C. J. (1999) 'Body condition scoring: a rapid and accurate method for assessing health status in mice', *Lab Anim Sci,* 49(3), pp. 319-23.

Vaughan, S., Coward, J. I., Bast, R. C., Jr., Berchuck, A., Berek, J. S., Brenton, J. D., Coukos, G., Crum, C. C., Drapkin, R., Etemadmoghadam, D., Friedlander, M., Gabra, H., Kaye, S. B., Lord, C. J., Lengyel, E., Levine, D. A., McNeish, I. A., Menon, U., Mills, G. B., Nephew, K. P., Oza, A. M., Sood, A. K., Stronach, E. A., Walczak, H., Bowtell, D. D. and Balkwill, F. R. (2011) 'Rethinking ovarian cancer: recommendations for improving outcomes', *Nat Rev Cancer,* 11(10), pp. 719-25.

White, E. A., Kenny, H. A. and Lengyel, E. (2014) 'Three-dimensional modeling of ovarian cancer', *Adv Drug Deliv Rev,* 79-80, pp. 184-92.

Wiegand, K. C., Shah, S. P., Al-Agha, O. M., Zhao, Y., Tse, K., Zeng, T., Senz, J., McConechy, M. K., Anglesio, M. S., Kalloger, S. E., Yang, W., Heravi-Moussavi, A., Giuliany, R., Chow, C., Fee, J., Zayed, A., Prentice, L., Melnyk, N., Turashvili, G., Delaney, A. D., Madore, J., Yip, S., McPherson, A. W., Ha, G., Bell, L., Fereday, S., Tam, A., Galletta, L., Tonin, P. N., Provencher, D., Miller, D., Jones, S. J., Moore, R. A., Morin, G. B., Oloumi, A., Boyd, N., Aparicio, S. A., Shih Ie, M., Mes-Masson, A. M., Bowtell, D. D., Hirst, M., Gilks, B., Marra, M. A. and Huntsman, D. G. (2010) 'ARID1A mutations in endometriosis-associated ovarian carcinomas', *N Engl J Med,* 363(16), pp. 1532-43.

Witz, C. A., Montoya-Rodriguez, I. A., Cho, S., Centonze, V. E., Bonewald, L. F. and Schenken, R. S. (2001) 'Composition of the extracellular matrix of the peritoneum', *J Soc Gynecol Investig,* 8(5), pp. 299-304.

Wolf, C. R., Hayward, I. P., Lawrie, S. S., Buckton, K., McIntyre, M. A., Adams, D. J., Lewis, A. D., Scott, A. R. and Smyth, J. F. (1987) 'Cellular heterogeneity and drug resistance in two ovarian adenocarcinoma cell lines derived from a single patient', *Int J Cancer,* 39(6), pp. 695-702.

Xing, D. and Orsulic, S. (2006) 'A mouse model for the molecular characterization of brca1-associated ovarian carcinoma', *Cancer Res,* 66(18), pp. 8949-53.

Zhang, J., Yin, X. J., Xu, C. J., Ning, Y. X., Chen, M., Zhang, H., Chen, S. F. and Yao, L. Q. (2015) 'The histone deacetylase SIRT6 inhibits ovarian cancer cell proliferation via down-regulation of Notch 3 expression', *Eur Rev Med Pharmacol Sci,* 19(5), pp. 818-24.

Zhang, X., Samadi, A. K., Roby, K. F., Timmermann, B. and Cohen, M. S. (2012) 'Inhibition of cell growth and induction of apoptosis in ovarian carcinoma cell lines CaOV3 and SKOV3 by natural withanolide Withaferin A', *Gynecol Oncol,* 124(3), pp. 606-12.

APPENDIX

Table A4.1 Primers for semiquantitative RT-PCR for *Notch* receptor and ligand genes.

Gene	Forward Primer 5' to 3'	Reverse Primer 5' to 3'	Product Size
Notch1	CTC ACC TGG TGC AGA CCC AG	GCA CCT GTA GCT GGT GGC TG	345 bp
Notch2	CAG TGT GCC ACA GGT TTC ACT G	GCA TAT ACA GCG GAA ACC ATT CAC	454 bp
Notch3	CGC CTG AGA ATG ATC ACT GCT TC	TCA CCC TTG GCC ATG TTC TTC	345 bp
Notch4	GGT GAC ACC CCT GAT GTC AG	AGC CTG GCA GCC AGC ATC	381 bp
Jag1	GCT TGG ATC TGT TGC TTG GTG AC	ACT TTC CAA GTC TCT GTT GTC CTG	384 bp
Dll1	CTA CAC GGG CAG GAA CTG CAG	CGC CTT CTT GTT GGT GTT CTT G	445 bp
Dll4	CGG GTC ATC TGC AGT GAC AAC	AGT TGA GAT CTT GGT CAC AAA ACA G	346 bp
Actb	CGA GGC CCA GAG CAA GAG AG	CTC GTA GAT GGG CAC AGT GTG	334 bp

Table A4.2 Primers for RT-qPCR for *Notch3* and downstream target genes.

Gene	Forward Primer 5' to 3'	Reverse Primer 5' to 3'
Notch3	CGC CTG AGA ATG ATC ACT GCT TC	TCA CCC TTG GCC ATG TTC TTC
Hey1	ACG AGA ATG GAA ACT TGA GTT C	AAC TCC GAT AGT CCA TAG CAA G
HeyL	CAG GAT TCT TTG ATG CCC GAG	GAC AGG GCT GGG CAC TCT TC
Hes1	CCC AAC GCA GTG TCA CCT TC	TAC AAA GGC GCA ATC CAA TAT G
Actb	CGA GGC CCA GAG CAA GAG AG	CTC GTA GAT GGG CAC AGT GTG

Tables A4.1 and A4.2. Notch pathway primer sequences for primers used in Semiquantitative RT-PCR and RT-qPCR experiments. Notch 1, 3, and 4 receptor sequences target the intracellular domain. **(A4.1)** Primer sequences for Notch receptors and ligands for RT-PCR. PCR product sizes have been included to compare to images in Figure 4.1. **(A4.2)** Primer sequences for RT-qPCR.

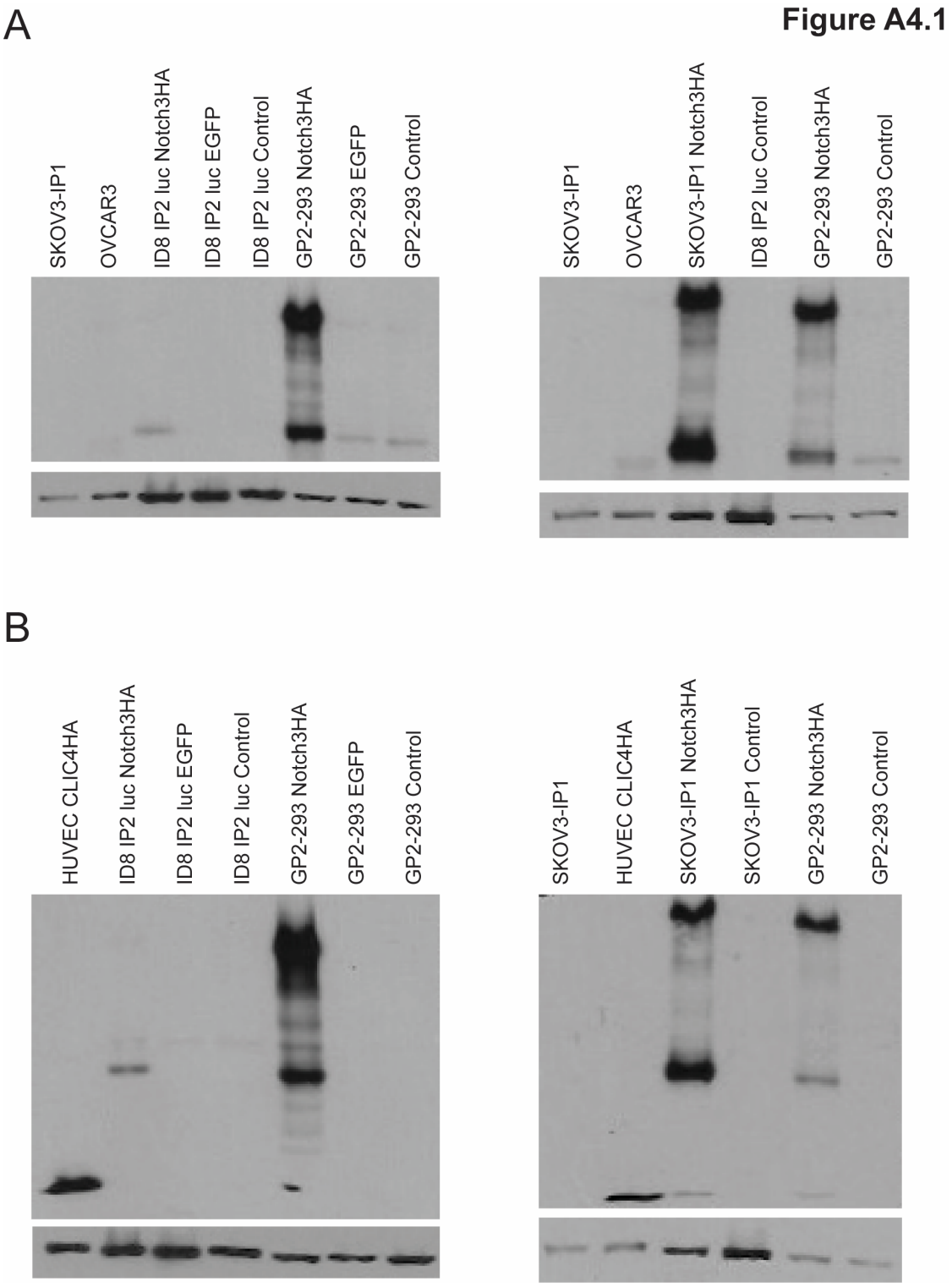

Figure A4.1 NOTCH3 is present in ovarian cancer cell lines that are retrovirally infected with full length Notch3HA. (A) Western blot of NOTCH3 expression in retroviral packaging transfected GP2-293 lines, infected ID8 IP2 luc mouse ovarian surface epithelial line (left panel), and SKOV3-IP1 human epithelial adenocarcinoma ascites (right panel). **(B)** Expression of ectopic NOTCH3 detected by staining western blot with HA antibody to recognize the C-terminal HA tag on NOTCH3. Expression is shown for both ID8 IP2 luc and SKOV3-IP1.

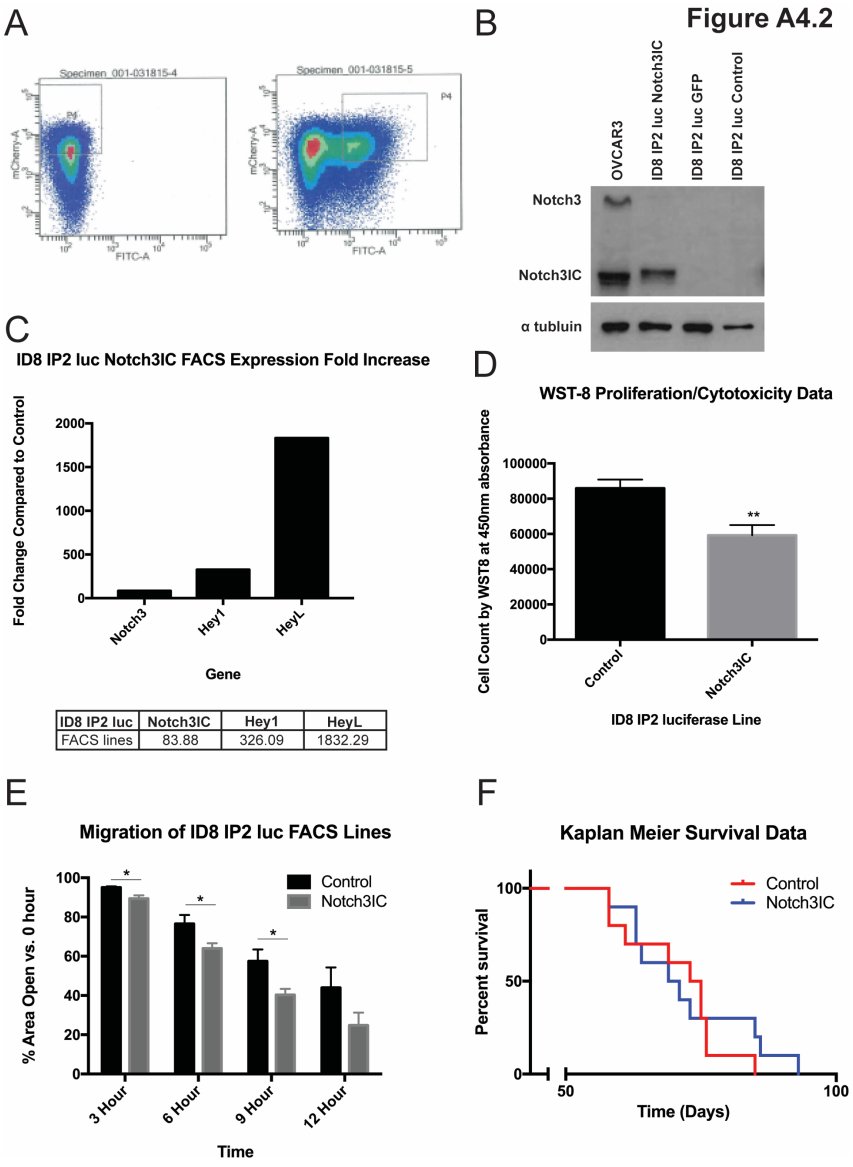

Figure A4.2 Properties of ID8 IP2 luc Notch3IC and Control subjected to FACS display different phenotypes than for non-sorted populations of lentivirally infected cells. (A) FACS sorting of ID8 IP2 luc based on mCherry positivity for Control (mCherry-A) and GFP positivity for Notch3IC (FITC-A). The P4 square indicates cells collected from the sort. **(B)** Western blot showing the NOTCH3 expression of the lentiviral infected ID8 IP2 luc lines subjected to FACS. NOTCH3 intracellular domain is seen in the Notch3IC line but not Control or cells infected by virus generated from a pCCL GFP plasmid construct. OVCAR3 is a known high NOTCH3 expressing human ovarian cancer line. **(C)** RT-qPCR from one set of triplicates demonstrating the Notch3IC line subjected to FACS displays an increase in *Notch3* and downstream *Hey* target transcripts. The table shows the same data of ID8 IP2 luc Notch3IC line transcript fold increase compared to Control. **(D)** FACS Notch3IC cells display a significant decrease in viability compared to Control p = 0.0022, Welch's t-test). Two experiments of sextuplicate were analyzed. **(E)** Migration of FACS ID8 IP2 luc Notch3IC demonstrate a significantly increased capacity to migrate in a Scratch wounding assay at 3, 6 and 9 hours post monolayer disruption (p = 0.018, p = 0.041, and p = 0.038 respectively, Student's t-test). Two experiments of triplicates were analyzed. **(F)** Survival data displaying no significant difference between ID8 IP2 luc Notch3IC and Control injected mice (Log-rank p = 0.5794, Gehan-Breslow-Wilcoxon p = 0.9098). Data is shown from 10 Notch3IC and 10 Control tumor bearing mice.

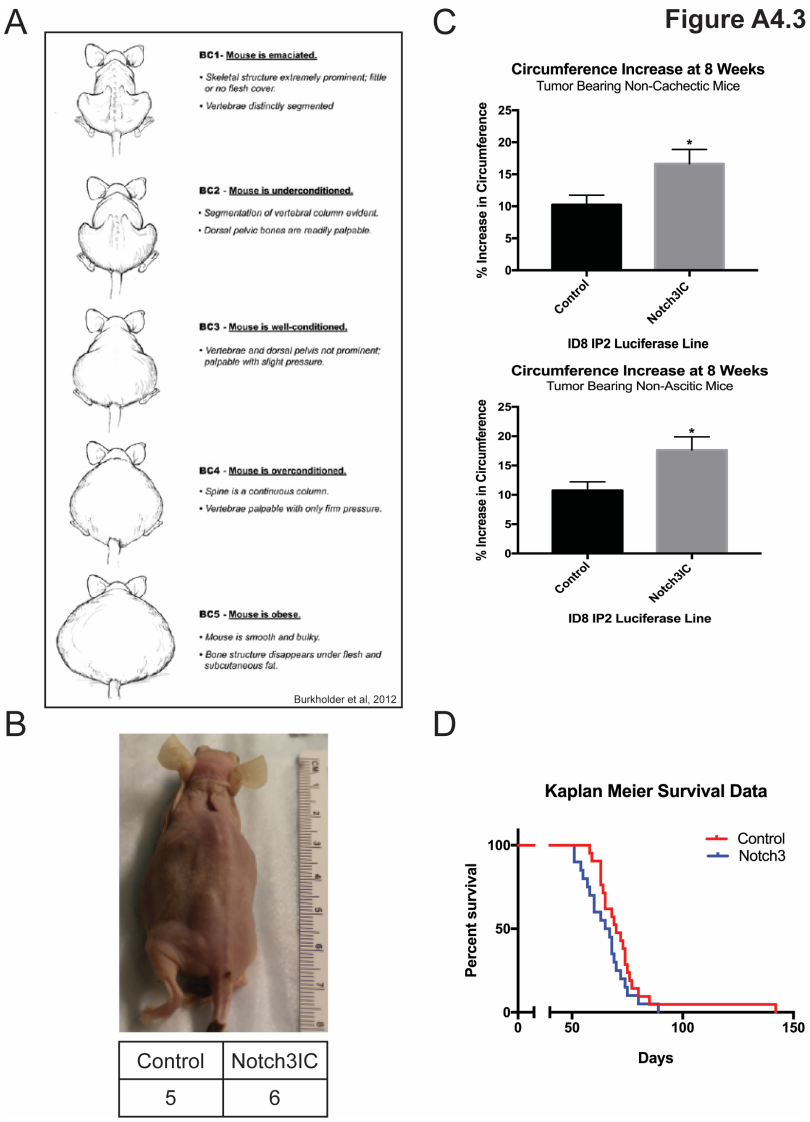

Figure A4.3 Cachexia criteria and *in vivo* data analysis excluding cachectic tumor bearing mice. **(A)** Body condition score criteria. Cachexia was determined by criteria for underconditioned and emaciated mice. Image from (Burkholder et al., 2012). **(B)** Example image of a cachectic tumor bearing mouse at sacrifice. The table at bottom shows the number of Control and Notch3IC mice euthanized due to cachexia which were including in the Chapter 4 *in vivo* analysis. This data demonstrates that cachexia was not specific to either group. **(C)** The top graph demonstrates the percent increase in circumference specifically in the non-cachectic subset of the mice previously analyzed in figure 4.4B. 57 total mice were analyzed (29 Control, 28 Notch3IC). The bottom graph shows analysis for all mice that did not bear ascites. A proportion of the mice were sacrificed at the same 8-week time point; therefore, some of the mice that did not develop ascites may have eventually developed cachexia if allowed to survive to an endpoint defined as BC1, BC2, or ≥25% increase in circumference for other mice included in the study. Since cachexia was defined for remaining mice as having developed cachexia at all, and not necessarily by the 8 week time point, this analysis includes all potential cachectic mice as well. 54 total mice were analyzed (28 Control, 29 Notch3IC). In both cases, Notch3IC mice display a significant increase in circumference compared to Control ($p = 0.0217$, $p = 0.0142$, Welch's t-test). **(D)** Kaplan Meier survival data analysis for all non-cachectic tumor bearing mice. A total of 41 mice were analyzed (21 Control, 20 Notch3IC). The median survival for Control mice was 70 days compared to Notch3IC mice at 66 days. The mean survival was 73 days for Control and 65 days for Notch3IC. There was no significant difference in the survival between Notch3IC and Control tumor bearing mice when cachectic animals were excluded ($p = 0.1405$ Log Rank, $p = 0.0629$ Gehan-Breslow-Wilcoxon).

Figure A4.4

A

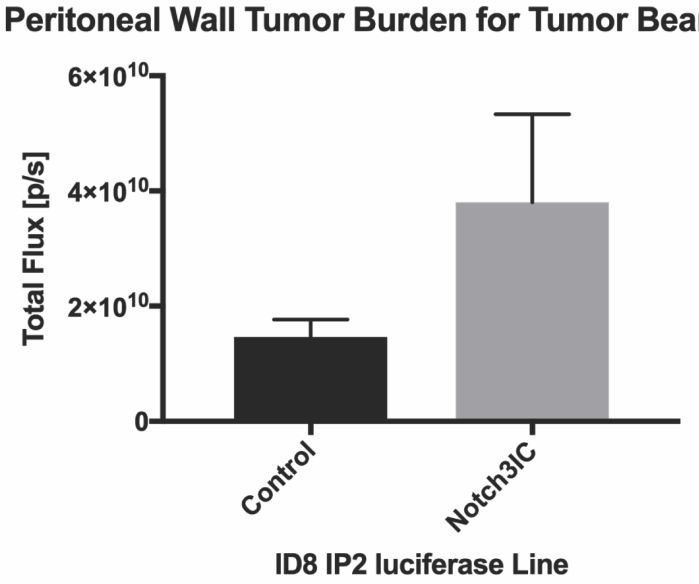

B

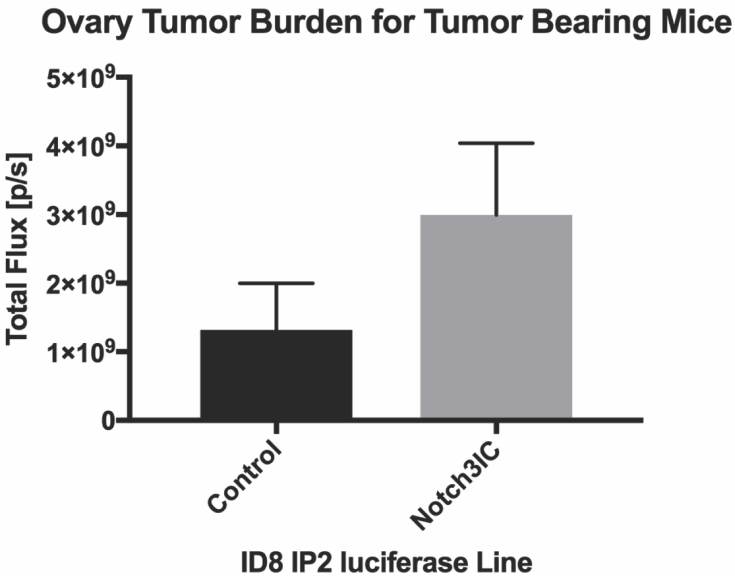

Figure A4.4 Peritoneal wall tumor burden, and right ovary and uterine horn tumor burden in mice sacrificed at 8 weeks does not show a significant difference between Notch3IC and Control despite higher levels of Notch3IC bioluminescent signal. (A) Peritoneal wall tumor burden measured by IVIS spectrum bioluminescent at the 8 week endpoint for Notch3IC and Control tumor bearing mice ($p = 0.1686$, Welch's t-test). **(B)** Tumor burden by bioluminescent signal of the right ovary and right uterine horn combined for Notch3IC and Control tumor bearing mice ($p = 0.2015$, Welch's t-test).

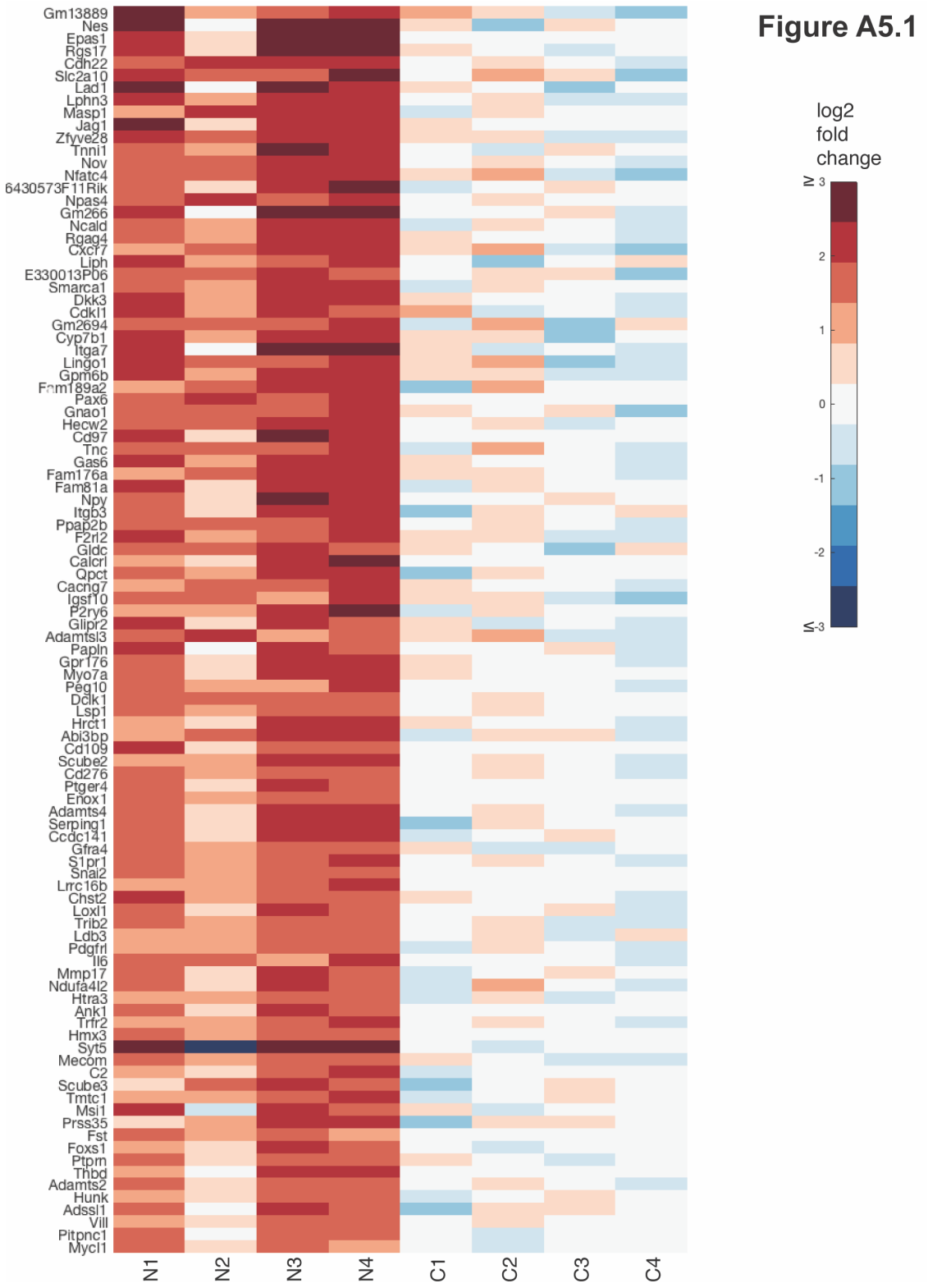

Figure A5.1 Selected list of the most upregulated genes in Notch3IC compared to Control ID8 IP2 luciferase. Heat map of genes upregulated in Notch3IC cells, with threshold criteria of adjusted $p < 0.1$ and average $\log_2$ fold change ≥ 2. Samples are listed from left to right in the following order: Notch3IC Set # 1, Notch3IC Set #2, Notch3IC set #3, Notch3IC Set #4, Control Set #1, Control Set #2, Control Set #3, Control Set #4.

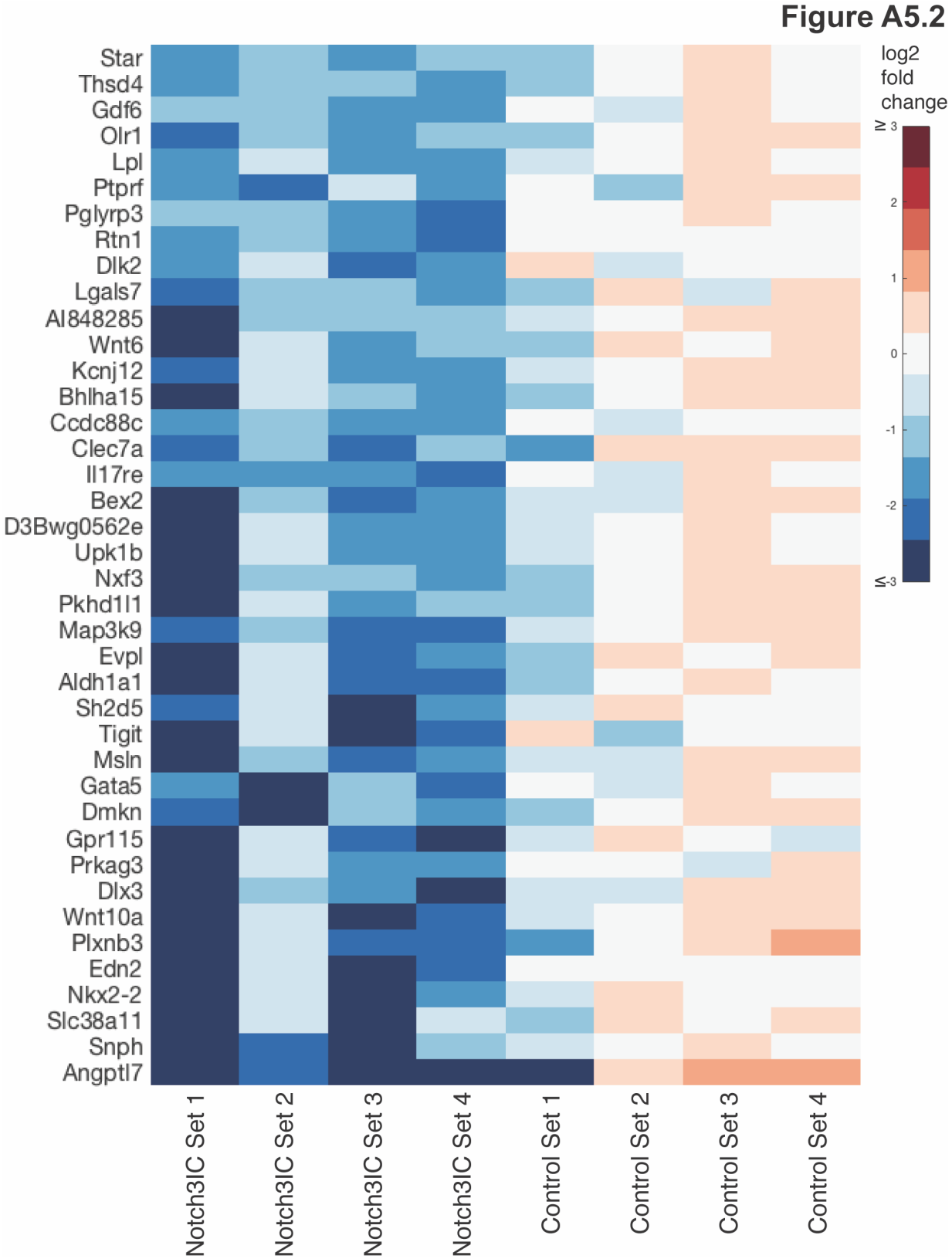

Figure 5.2 Selected list of the most highly downregulated genes in Notch3IC compared to Control ID8 IP2 luciferase. Heat map showing genes downregulated with a threshold of adjusted $p < 0.1$ and average $\log_2$ fold change ≤ -2.

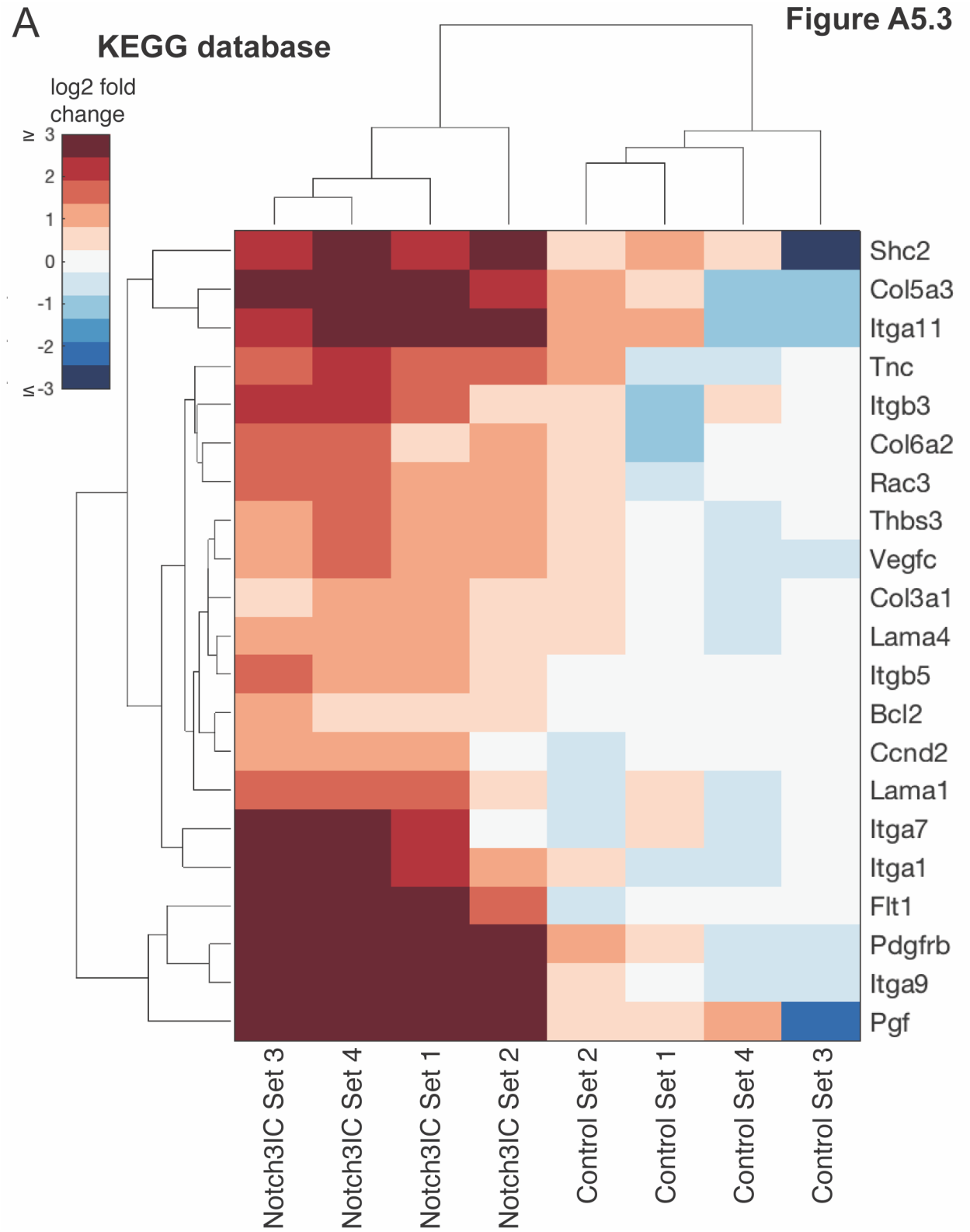
A
KEGG database
Figure A5.3
log2 fold change
≥ 3
2
1
0
-1
-2
≤ -3
Shc2
Col5a3
Itga11
Tnc
Itgb3
Col6a2
Rac3
Thbs3
Vegfc
Col3a1
Lama4
Itgb5
Bcl2
Ccnd2
Lama1
Itga7
Itga1
Flt1
Pdgfrb
Itga9
Pgf
Notch3IC Set 3
Notch3IC Set 4
Notch3IC Set 1
Notch3IC Set 2
Control Set 2
Control Set 1
Control Set 4
Control Set 3

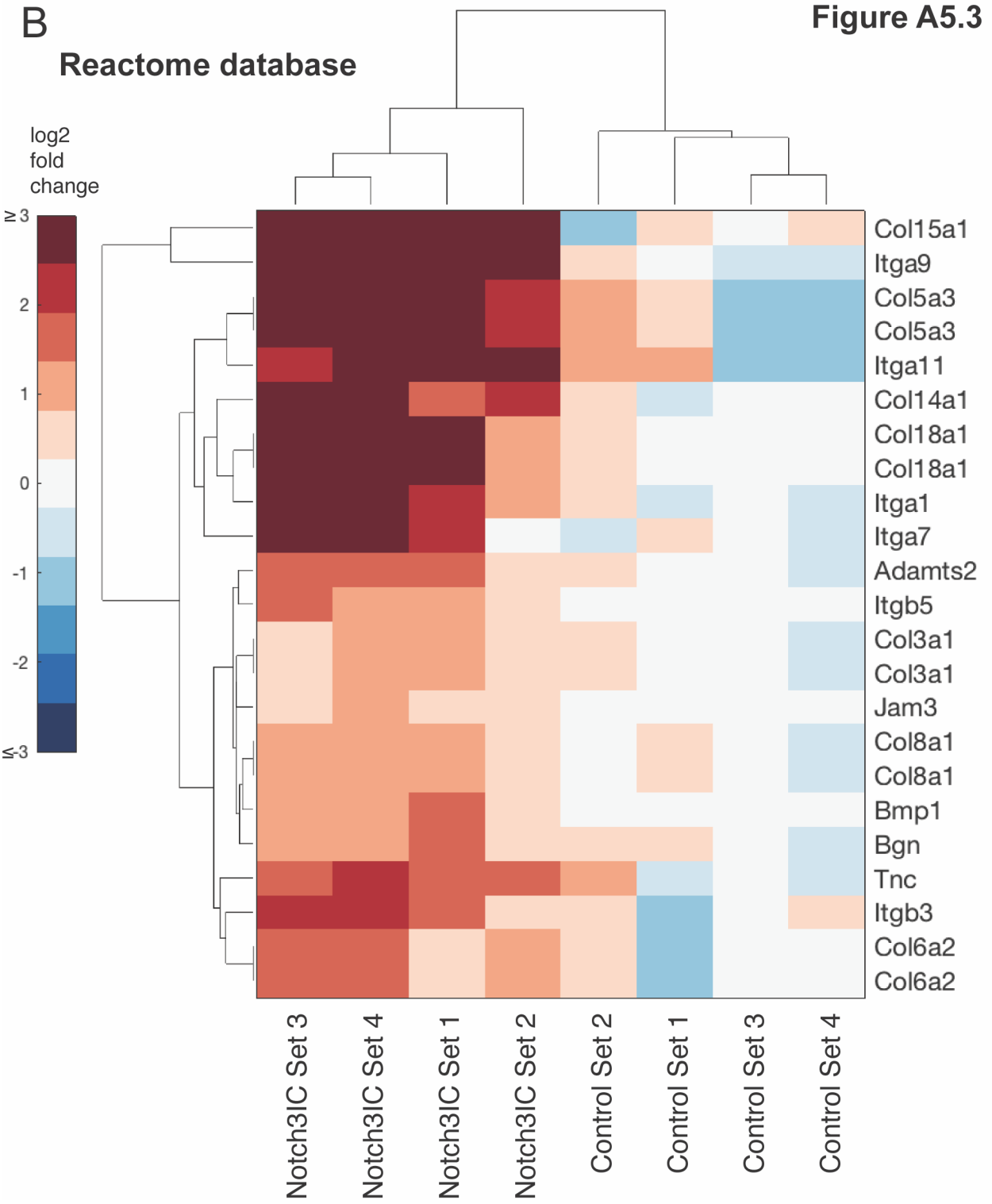
B
Reactome database
log2
fold
change
≥ 3
2
1
0
-1
-2
≤-3
Col15a1
Itga9
Col5a3
Col5a3
Itga11
Col14a1
Col18a1
Col18a1
Itga1
Itga7
Adamts2
Itgb5
Col3a1
Col3a1
Jam3
Col8a1
Col8a1
Bmp1
Bgn
Tnc
Itgb3
Col6a2
Col6a2
Notch3IC Set 3
Notch3IC Set 4
Notch3IC Set 1
Notch3IC Set 2
Control Set 2
Control Set 1
Control Set 3
Control Set 4

Figure A5.3

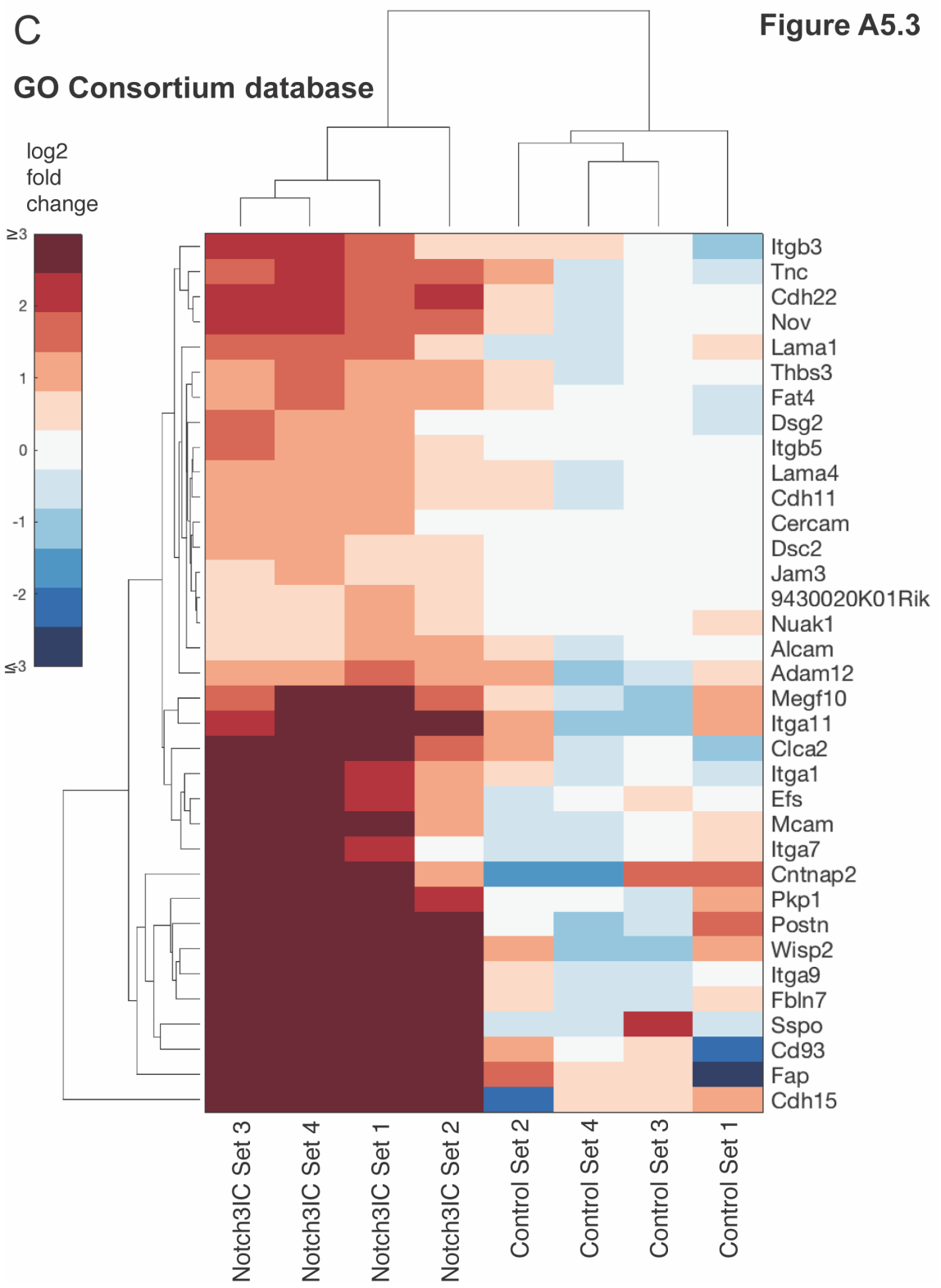

Figure A5.3 Significantly upregulated genes in adhesion and ECM pathways identified by DAVID pathway analysis show many integrin and collagen genes among others. This heat map displays upregulated genes (p >0.1, and > log2 fold) matched to significantly enriched adhesion and extracellular matrix pathways in DAVID pathway analysis by database. **(A)** Kyoto Encyclopedia of Genes and Genomes (KEGG) **(B)** Reactome **(C)** Gene Ontology Consortium (GO).

Pathway Database	Pathway Name	Gene Count	p Value	Fold Enrichment
KEGG	mmu00533:Glycosaminoglycan biosynthesis - keratan sulfate	3	6.23E-03	24.51
KEGG	mmu04390:Hippo signaling pathway	5	3.27E-02	4.06
REACTOME	Keratan sulfate biosynthesis	3	1.88E-02	13.88
GO TERM	GO:0032332~positive regulation of chondrocyte differentiation	4	5.37E-04	24.60
GO TERM	GO:0071312~cellular response to alkaloid	3	1.86E-03	45.09
GO TERM	GO:0014824~artery smooth muscle contraction	3	2.31E-03	40.59
GO TERM	GO:0030324~lung development	6	2.45E-03	6.39
GO TERM	GO:0010628~positive regulation of gene expression	10	2.83E-03	3.37

Table A5.1 DAVID pathway enrichment analysis of downregulated genes identified by RNA-Seq analysis of Notch3IC compared to Control. DAVID analysis representing the top significantly enriched pathways ($p < 0.05$) for each database assessed. Genes assessed in this pathway analysis had $p < 0.1$ and more than a $\log_2$ fold reduction in Notch3IC compared to Control ($\log_2 \leq -1$).

Pathway Database	Pathway Name	Gene Count	p Value	Fold Enrichment
GO TERM	GO:0007156~homophilic cell adhesion via plasma membrane adhesion molecules	6	7.06E-03	4.98
GO TERM	GO:0007155~cell adhesion	10	9.56E-03	2.79
GO TERM	GO:0007159~leukocyte cell-cell adhesion	3	1.44E-02	16.23
GO TERM	GO:0016337~single organismal cell-cell adhesion	4	4.62E-02	4.96
GO TERM	GO:0022614~membrane to membrane docking	2	3.62E-02	54.11

Table A5.2 Adhesion pathways found to be downregulated in pathway analysis are related to cell to cell adhesion despite upregulation of many adhesion pathways. Since we focused on the change in upregulated adhesion genes from the pathway analysis, this table displays the enriched pathways related to adhesion that were composed of selected downregulated genes. Genes identified within these pathways include those listed in table A5.3.

Gene	log2 Fold Change	Adj p Value
Mpzl2	-1.62	5.39E-06
Pdpn	-1.22	1.85E-04
Tinagl1	-1.40	1.93E-04
Itga3	-1.27	3.66E-04
Esam	-1.66	2.91E-03
Pcdh9	-1.04	3.55E-03
Msln	-2.61	4.12E-03
Ezr	-1.39	1.25E-02
Icam1	-1.04	1.28E-02
Tigit	-2.73	3.34E-02
Ptprf	-2.18	4.07E-02
Olr1	-2.22	4.16E-02
Plxnb3	-2.50	9.94E-02
Celsr1	-1.19	9.96E-02

Table A5.3 Genes identified in downregulated pathways related to adhesion. Genes with $p < 0.1$ and more than a 1 $\log_2$ fold reduction in Notch3IC compared to Control identified in pathways considered enriched by DAVID analysis (see Table A5.2).

Pathway Name	Gene Count	Normalized Enrichement	NOM p-val
LIM_MAMMARY_LUMINAL_MATURE_DN	32	2.04	0
KEGG_LONG_TERM_DEPRESSION	21	2.03	0
MULLIGHAN_NPM1_MUTATED_SIGNATURE_2_UP	21	2.01	0
RADMACHER_AML_PROGNOSIS	21	1.97	1.28E-03
KEGG_ALZHEIMERS_DISEASE	23	1.94	1.22E-03
REACTOME_PLATELET_HOMEOSTASIS	23	1.93	0
BROWNE_HCMV_INFECTION_30MIN_UP	16	1.91	1.32E-03
REACTOME_SIGNALING_BY_NOTCH	23	1.90	0
YAO_TEMPORAL_RESPONSE_TO_PROGESTERONE_CLUSTER_14	41	1.89	1.16E-03
KEGG_CALCIUM_SIGNALING_PATHWAY	58	1.84	1.08E-03
MULLIGHAN_NPM1_SIGNATURE_3_UP	68	1.81	0
MULLIGHAN_NPM1_MUTATED_SIGNATURE_1_UP	54	1.80	0
KEGG_OLFACTORY_TRANSDUCTION	16	1.80	5.28E-03
KEGG_LONG_TERM_POTENTIATION	19	1.79	7.73E-03
HOSHIDA_LIVER_CANCER_SURVIVAL_UP	27	1.79	4.76E-03
LINDGREN_BLADDER_CANCER_CLUSTER_1_UP	17	1.73	1.05E-02
SERVITJA_LIVER_HNF1A_TARGETS_UP	33	1.73	9.56E-03
BOQUEST_STEM_CELL_UP	84	1.73	0
NABA_COLLAGENS	29	1.73	2.37E-03
REACTOME_NEUROTRANSMITTER_RECEPTOR_BINDING_AND_ DOWNSTREAM_TRANSMISSION_IN_THE_POSTSYNAPTIC_CELL	36	1.72	8.17E-03

Table A5.4 GSEA top enriched pathways show a variety of pathways which includes a pathway related to collagen genes. This table represents the top 20 pathways determined by GSEA pathway analysis of $\log_2$ fold change for all analyzed genes.

Pathway Name	Gene Count	NOM p-val	Fold Enrichment
HESS_TARGETS_OF_HOXA9_AND_MEIS1_DN	16	0	-2.07
GAJATE_RESPONSE_TO_TRABECTEDIN_UP	16	3.85E-03	-2.06
REACTOME_CELL_JUNCTION_ORGANIZATION	26	1.10E-02	-1.84
REACTOME_RNA_POL_I_PROMOTER_OPENING	19	1.99E-02	-1.83
REACTOME_MEIOTIC_RECOMBINATION	21	9.01E-03	-1.79
GOZGIT_ESR1_TARGETS_UP	35	6.85E-03	-1.70
GOLDRATH_HOMEOSTATIC_PROLIFERATION	36	1.64E-02	-1.69
KYNG_DNA_DAMAGE_BY_GAMMA_AND_UV_RADIATION	27	1.70E-02	-1.68
REACTOME_RNA_POL_I_RNA_POL_III_AND_MITOCHONDRIAL_ TRANSCRIPTION	22	1.03E-02	-1.68
HOLLMANN_APOPTOSIS_VIA_CD40_UP	35	2.55E-02	-1.66
CHIARADONNA_NEOPLASTIC_TRANSFORMATION_KRAS_CDC25_UP	16	2.03E-02	-1.66
MCCLUNG_COCAINE_REWARD_5D	18	1.38E-02	-1.64
REACTOME_CELL_CELL_JUNCTION_ORGANIZATION	21	3.29E-02	-1.62
KANG_IMMORTALIZED_BY_TERT_UP	23	1.98E-02	-1.61
BOYLAN_MULTIPLE_MYELOMA_PCA3_UP	17	2.44E-02	-1.61
REACTOME_PHASE_II_CONJUGATION	15	4.12E-02	-1.61
KIM_MYCN_AMPLIFICATION_TARGETS_DN	17	2.89E-02	-1.59
NING_CHRONIC_OBSTRUCTIVE_PULMONARY_DISEASE_DN	28	1.84E-02	-1.58
COULOUARN_TEMPORAL_TGFB1_SIGNATURE_UP	24	2.91E-02	-1.58
REACTOME_RNA_POL_I_TRANSCRIPTION	21	5.91E-02	-1.51

Table A5.5 Top enriched pathways identified by GSEA analysis of downregulated genes show similarity to adhesion pathways significantly enriched in DAVID analysis for Notch3 intracellular domain regulated genes. The table shows top the 20 pathways enriched from GSEA assessment of genes with adjusted $p < 0.1$ and average $\log_2$ fold change ≤ -1 for Notch3IC compared to Control. While enriched adhesion pathways identified by GSEA are similar to adhesion pathways identified by DAVID, these pathways were ranked higher among enriched pathways in GSEA assessment.

Gene	Rank in Gene List	Rank Metric Score	Enrichment Score	Core Enrichment
Col16a1	6	9.23	0.172	Yes
Col19a1	71	4.48	0.238	Yes
Col6a1	72	4.42	0.321	Yes
Col15a1	100	3.89	0.386	Yes
Col2a1	209	2.84	0.408	Yes
Col6a5	298	2.41	0.427	Yes
Col24a1	434	1.94	0.424	Yes
Col4a2	499	1.82	0.440	Yes
Col6a3	543	1.75	0.460	Yes
Col8a2	772	1.39	0.419	Yes
Col4a3	774	1.39	0.445	Yes
Col27a1	839	1.30	0.451	Yes
Col4a1	861	1.28	0.469	Yes
Col6a6	898	1.24	0.481	Yes
Col6a2	959	1.17	0.486	Yes
Col20a1	1008	1.13	0.493	Yes
Col5a2	1107	1.03	0.484	Yes
Col18a1	1128	1.01	0.497	Yes
Col1a2	1156	0.99	0.507	Yes
Col28a1	1188	0.96	0.516	Yes
Col23a1	1311	0.87	0.497	No
Col8a1	1498	0.75	0.456	No
Col3a1	1594	0.70	0.442	No
Col13a1	1810	0.59	0.390	No
Col11a1	1905	0.56	0.372	No
Col11a2	1939	0.54	0.373	No
Col5a1	2465	-0.69	0.231	No
Col7a1	2920	-1.10	0.119	No
Col4a5	3212	-1.61	0.063	No

Table A5.6 Collagen genes are found to be enriched in GSEA analysis of Notch3 intracellular domain regulated genes. Chart displaying each collagen gene in the pathway for enrichment in the significantly enriched pathway NABA_COLLAGENS. Genes are listed by rank in the pathway determined by the GSEA algorithm.

Figure A5.4

A

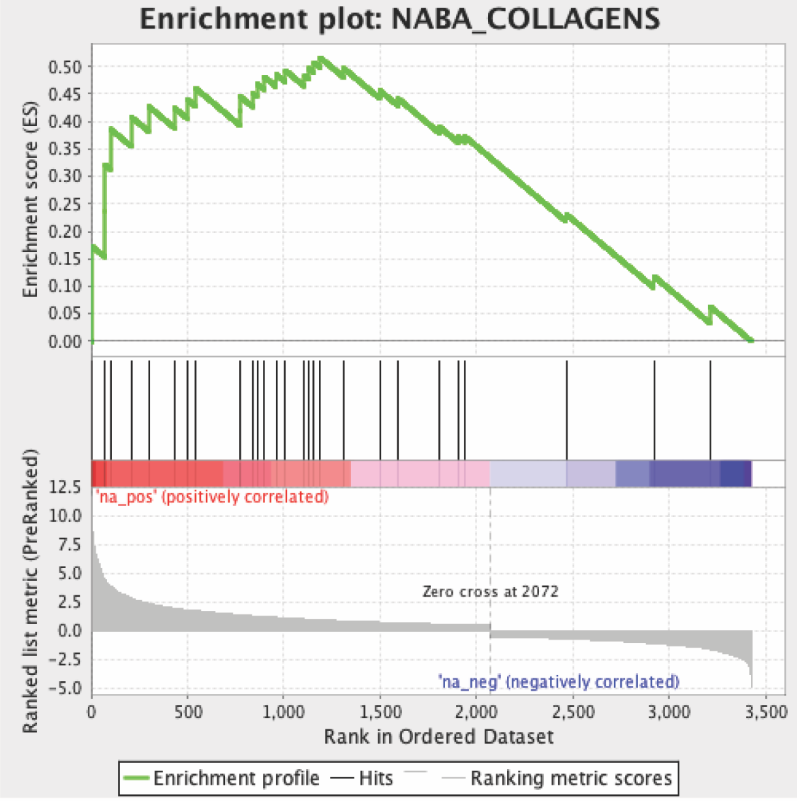

B

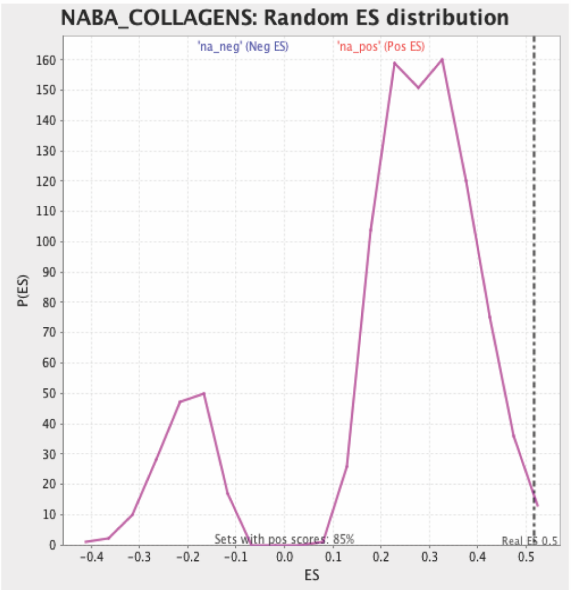

Figure A5.4 GSEA assessment identifies the NABA_COLLAGENS pathway as enriched in RNA-Seq analysis of Notch3 intracellular domain regulated genes. From pathway analysis of $\log_2$ fold change of genes the NABA_COLLAGENS pathway was the most significantly upregulated adhesion pathway. This figure shows the graphs generated in the pathway analysis for comparison of RNA-Seq data from GSEA for NABA_COLLAGENS. **(A)** Image displays the enrichment plot **(B)** Panel shows the enrichment score distribution of the genes in this pathway generated by GSEA

A

Figure A6.1

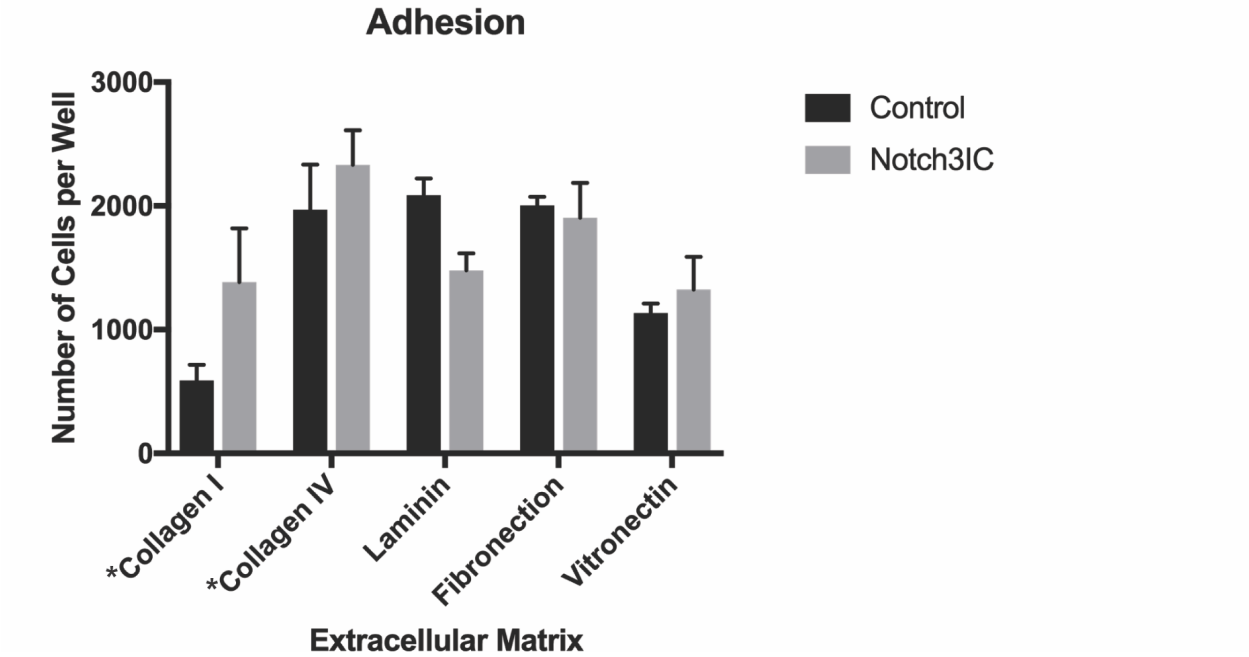

Figure A6.1 ID8 IP2 luciferase lines are differentially adherent to distinct extracellular matrices.
(A) Average counts of cells adhered to plates coated with the indicated ECM using 3 sets of ID8 IP2 luciferase Notch3IC and Control infected cells. Averages for each cell line (a biological replicate) were generated from 3-4 experiments of triplicates, and averages for the 3 biological replicates were plotted. Laminin, fibronectin, and vitronectin experiments were completed by plating $2x10^4$ cells per well, and cells were allowed to adhere for 30 minutes. Collagen I and collagen IV, designated with asterisks, were completed by seeding $2x10^4$ cells per well which were allowed to adhere for a total of 90 minutes. This increase in seeding time was designed to compensate for the overall lower levels of adherence to collagen substrates and achieve a constant of approximately 5% adherence of the originally added cells.

Figure A6.2

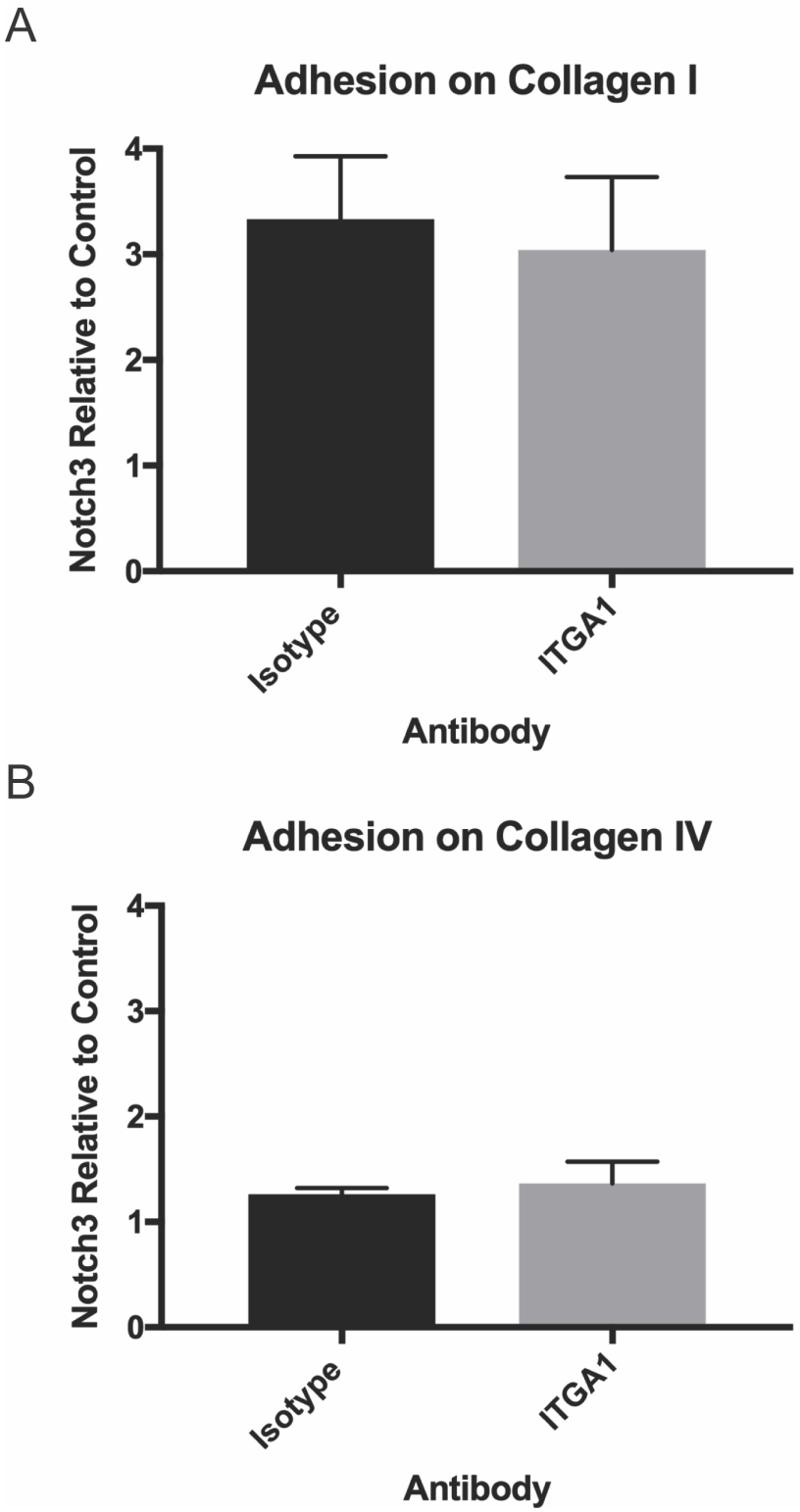

Figure A6.2 ITGA1 antibody blocking does not affect adhesion to collagens I and IV.
(A) The ratio of Notch3IC cells adhered to collagen I compared to Control is similar for cells treated with ITGA1 blocking antibody versus isotype control, indicating that the increased adhesion of Notch3IC cells is not altered by blocking ITGA1 ($p = 0.7652$, Welch's t-test). Cells were treated with 10μg/mL of ITGA1 antibody or isotype control antibody. **(B)** IGTA1 blocking antibody also does not significantly alter the ratios of adherent cells on collagen IV ($p = 0.6686$, Welch's t-test)